

**WATER DEFLUORIDATION USING RAW, MODIFIED AND COMBINED
SULPHONATED POLYSTYRENE, CHICKEN FEATHERS AND FISH SCALES**

BY

NASIEBANDA ROSELYNE

**A THESIS SUBMITTED IN PARTIAL FULFILLMENT OF THE
REQUIREMENTS FOR THE AWARD OF THE DEGREE OF DOCTOR OF
PHILOSOPHY IN THE SCHOOL OF SCIENCE OF
UNIVERSITY OF ELDORET, KENYA**

MAY, 2021

DECLARATION

Declaration by the candidate

This thesis is my original work and has not been submitted for any academic award in any institution; and shall not be reproduced in part or full, or in any format without prior written permission from the author and/or University of Eldoret.

Signed.....

Date.....

ROSELYNE NASIEBANDA
SC/PHD/003/15

Declaration by the Supervisors

We confirm that the work reported in this thesis was carried out by the candidate under our supervision and it has been submitted with our approval as university supervisors:

Signature.....

Date.....

DR. ENOS W. WAMBU
Inorganic and physical chemistry, Department of Chemistry and Biochemistry
University of Eldoret.

Signature.....

Date.....

PROF. JOHN L. KITUYI
Inorganic and physical chemistry, Department of Chemistry and Biochemistry University of
Eldoret.

DEDICATION

I dedicate this work to my mum Consolata N. Wafula who has been my source of inspiration for hard work.

ABSTRACT

Adequate fluoride intake is necessary in developing health bones and teeth and for the prevention of dental caries. Too much fluoride intake, however, leads to dental, skeletal and soft tissue damage, an irreversible condition that has no cure; prevention is the only remedy for this menace. Today fluorosis remains an important clinical and public health problem in many parts of the world. In Kenya native fluorosis has been problematic for several years and as a result there is a serious concern over the destiny of fluoride (F) in the environment especially the ground and sources of water underground, especially in areas associated with the Great Rift Valley and the Central Highlands. People get exposed to excessive fluoride through food, soil and water. However, drinking water with excessive fluoride remains the primary pathway of human exposure to hazardous levels of fluoride from the environment. Providing water, with optimal fluoride concentration is, therefore one of the ways by which the future generation can be protected against the disease. Defluoridation is the conventional and widely tested method for supplying safe water to the fluorosis affected communities. In the current study a number of low cost materials, which included sulphonated polystyrene (SPS), fish scales and chicken feathers single and combined forms were investigated for fluoride adsorption. These materials were ground and tested for fluoride removal in water using both simulated solutions and natural high Fluoride water from Lake Elementaita. The adsorbents were also modified using solutions containing Ca^{2+} , Mg^{2+} and Al^{3+} ions. Characterization of the adsorbents was done by use of FTIR and SEM. The fluoride adsorption properties of the adsorbents were then assessed with respect to changes in adsorbent dosage, contact time, agitation rate, solution pH, temperature and initial fluoride concentration. Batch and column tests were carried out using natural high-fluoride water in order to assess the efficacy of the adsorbents to adsorb fluoride. Solution parameters and chemical composition of the adsorbents were found to control fluoride adsorption onto the adsorbents. According to the batch tests, aluminium modified feathers showed the highest maximum fluoride adsorption capacities of 285 mg/g. The fish scales had a capacity of 133 mg/g, while SPS had 22 mg/g fluoride adsorption and combined adsorbents 34 mg/g. The fluoride adsorption equilibrium data for the adsorbents were fitted by the Giles, the Langmuir and the Freundlich isotherms. The Al feathers, SPS and fish scales showed a similarity with the C isotherm classification by Giles, while the combined adsorbents curve showed a resemblance with the S Giles classification of isotherms. Basing on the Langmuir and Freundlich isotherms, fluoride adsorption onto the adsorbents was therefore based on mixed reactions. However, the SPS did not fit on both the Langmuir and Freundlich isotherms. Additionally, the fluoride adsorption data for the adsorbents were correlated to pseudo-first order, pseudo second order and Weber-Morris intraparticle diffusion kinetic models. For the pseudo first-order plots were found linear with good correlation coefficients (>0.9) indicating the applicability of pseudo first-order model in this study. However, the correlation coefficient (R^2) values for pseudo second-order adsorption model had high values; hence the adsorption kinetics of fluoride onto the adsorbents could be better described by pseudo second order model. The fluoride adsorption onto the adsorbents described by Weber-Morris intraparticle diffusion model, had all the R^2 values greater than 0.9. The fluoride adsorption data based on the column experiments were analyzed using the Thomas model. The adsorbent were regenerated using 1 M NaOH. The adsorbents showed good fluoride adsorption capacities and they could be utilized as low cost adsorbents to defluoridate high fluoride drinking waters and help to alleviate endemic fluorosis

TABLE OF CONTENTS

DECLARATION	II
DEDICATION	III
ABSTRACT.....	IV
TABLE OF CONTENTS	V
LIST OF TABLES	X
LIST OF FIGURES	XI
ABBREVIATIONS AND ACRONYMS.....	XIII
ACKNOWLEDGEMENTS	XV
CHAPTER ONE	1
INTRODUCTION	1
1.1 Background.....	1
1.2 Statement of the problem	4
1.3 Justification of the study.....	5
1.4 Objectives of the study	6
1.4.1 General objective	6
1.4.2 Specific objectives	7
1.5 Research questions	8
1.6 Significance of the study	8
CHAPTER TWO	9
LITERATURE REVIEW	9
2.1 Fluoride contamination of water in Kenya	9
2.2. Fluorosis and other health effects the case of Kenya.....	10
2.3 Flouride remediation strategies	11
2.3.1 An overview of water defluoridation methods	11
2.3.2 Adsorption technology.....	12
2.3.3 Biosorption.....	16
2.3.4 Effect of adsorption parameters on fluoride adsorption	17
2.3.6 Sorption equilibrium	22
2.3.7 Kinetics and thermodynamics.....	31
2.3.7.1 Pseudo-First Order Kinetic Model.....	32
2.3.7.2 Pseudo-Second Order Kinetic Model	33
2.3.7.2 Weber and Morris Intra-particle Diffusion Model	34

2.3.7.3 Elovich Kinetic Model.....	35
2.3.8 Transport within a bed packed with porous adsorbent	36
2.3.8.1 Pore Diffusion.....	38
2.3.8.2 Solid Diffusion.....	40
2.3.8.3 Reaction Kinetics.....	40
2.3.8.4 External Mass Transfer.....	40
2.3.8.5 Fluid Mixing and Flow through a Fixed Bed	41
2.3.9 Use of low cost adsorbents in fluoride removal from water.....	42
2.3.9.1 Fluoride removal by nonliving biomass	45
2.3.10 Water defluoridation by Fish scales.....	53
2.3.11 Water defluoridation by Keratin and its derivatives.....	56
2.3.11.1 Extraction of keratins and fabrication of material	57
2.3.11.2 Mechanisms of pollutant removal.....	59
2.3.12 Water defluoridation by modified polystyrene wastes	60
2.3.13 Water defluoridation by use of combined adsorbents	61
2.4 Analytical techniques	62
2.4.1 Fourier Transform Infrared Spectroscopy (FT-IR).....	62
2.4.1.1 Introduction.....	62
2.4.1.2 IR Frequency Range and Spectrum Presentation	62
2.4.1.3 Samples and sample preparation.....	64
2.4.1.4 Limitations, accuracy and detection limits	65
2.4.1.5 Theory of Infrared Absorption.....	65
2.4.1.6 Fourier Transform Spectrometers.....	68
2.4.1.7 A typical operating procedure for FTIR Spectrometer	72
2.4.1.8 FT-IR advantages.....	73
2.4.1.9 General Uses and application of FT-IR	74
2.4.3 Ion selective electrodes.....	75
2.4.4 Scanning electron microscopy	78
CHAPTER THREE.....	81
MATERIALS AND METHODS	81
3.1 Chemicals, equipment and Materials	81
3.1.1 Chemicals.....	81
3.1.2 Instruments.....	81
3.1.3 Materials	82
3.2 adsorbent characterization.....	84
3.3 Batch experiments	84
3.3.1 Optimization of mass	84
3.3.2 Optimization of time.....	85
3.3.3 Optimization of agitation rate	85

3.3.4 Optimization of pH	85
3.3.5 Optimization temperature	85
3.3.6 The effect of fluoride concentration	85
3.4 Equilibrium analyses	86
3.5 Kinetics and thermodynamic analyses	86
3.6 Regeneration tests.....	86
3.7 Data Analysis.....	87
CHAPTER FOUR	88
RESULTS AND DISCUSION.....	88
4.1 Chemical characterization of adsorbents	88
4.2 Effect of modification	96
4.2.1 On fish scales.....	96
4.2.2 On feathers.....	97
4.2.3 On sulphonated polystyrene	98
4.2.4 Combined adsorbent.....	99
4.3 Optimization of adsorption parameters	99
4.3.1 Effect of change in mass of adsorbent	99
4.3.2 Effect of change in adsorption contact time.....	102
4.3.3 The effect of change of agitation rate on adsorption	104
4.3.4 Effect of change in fluoride solution pH	106
4.3.5 Effect of change in solution temperature	109
4.3.6 Effect of adsorbate concentration	111
4.4 Equilibrium Analysis.....	114
4.4.1 The Giles isotherm.....	114
4.4.2 Langmuir isotherm.....	116
4.4.3 Freundlich isotherm	119
4.5 Adsorption kinetics.....	122
4.5.1 Pseudo First order kinetic model	122
4.5.2 Pseudo Second order kinetic model.....	125
4.5.3 Weber and Morris Intra-particle Diffusion Model	127
4.6 Adsorption Thermodynamics	129
4.7 Fluoride removal from natural high-fluoride water	132
4.7.1 Batch tests	132
4.7.2 Column water defluoridation using combined adsorbent	134
4.8 Regeneration tests.....	137
CHAPTER FIVE	139
CONCLUSIONS AND RECOMMENDATIONS.....	139
5.1 Conclusions	139

5.2 Recommendations 141

REFERENCES.....142

APPENDICES.....156

Appendix I Similarity report.....156

LIST OF TABLES

Table 2.1:	Physical adsorption and chemisorption typical characteristics.....	13
Table 2.2:	Removal of fluoride by using different adsorbents and its optimal parameters.....	44
Table 2.3:	Interaction of surface groups of biomaterials with halide ions.....	45
Table 2.4:	Cost comparison of different adsorbents.....	52
Table 4.1:	IR data for chicken feathers.....	93
Table 4.2:	Effect of modification on fish scales.....	96
Table 4.3:	Effect of modification on feathers.....	97
Table 4.4:	Effect of modification on sulphonated polystyrene.....	98
Table 4.5:	Langmuir isotherm constants for the adsorption of fluoride onto adsorbents.....	118
Table 4.6:	Freundlich Isotherm constants for the adsorption of fluoride onto adsorbents.....	120
Table 4.7:	Kinetics constants for Pseudo-first order fluoride adsorption onto adsorbents.....	123
Table 4.8:	Kinetics constants for Pseudo-second order fluoride adsorption onto adsorbents.....	126
Table 4.9:	Kinetics constants for Weber and Morris intra-particle diffusion model fluoride adsorption onto adsorbents.....	128
Table 4.10:	Thermodynamic parameters for the uptake of fluoride by the adsorbents.....	131

LIST OF FIGURES

Figure 2.1:	A summary of defluoridation processes.....	12
Figure 2.2:	Lennard Jones potential mathematical illustration.....	14
Figure 2.3:	The four main types of isotherms.....	24
Figure 2.4:	General illustration of transfer locations in porous packed beds.....	37
Figure 2.5:	Schematic of pore diffusion resistance combination.....	39
Figure 2.6:	Fluoride removal mechanisms of chitin and chitosan.....	47
Figure 2.7:	Lignocellulosic plant structure.....	51
Figure 2.8:	Fluoride removal by neem oil phenolic resin treated lignocellulosic materials.....	53
Figure 2.9:	Chemical structures of chitin, chitosan and cellulose.....	55
Figure 2.10:	Reaction mechanisms of keratin extraction.....	58
Figure 2.11:	Major vibrational modes of a nonlinear group CH_2	67
Figure 2.12:	Simplified optical layout of a typical FT-IR spectrometer.....	69
Figure 2.13:	Schematic diagram of the Nicolet Magna FT-IR spectrometer.....	72
Figure 2.14:	A commercial solid-state fluoride ISE.....	77
Figure 4.1:	FTIR spectra for the adsorbents before and after defluoridation.....	88
Figure 4.2:	SEM images for the adsorbents before and after defluoridation.....	94
Figure 4.3:	Effect of change in dosage on fluoride adsorption onto the adsorbents.....	101
Figure 4.4:	Effect of contact time on fluoride adsorption onto the adsorbents.....	103
Figure 4.5:	Effect of agitation rate on fluoride adsorption onto the adsorbents.....	105
Figure 4.6:	Effect of change in solution pH on fluoride adsorption onto the adsorbents.....	107
Figure 4.7:	Effect of change in temperature on fluoride adsorption onto the adsorbents.....	110

Figure 4.8:	Effect of change in initial adsorbate concentration on fluoride adsorption onto the adsorbents.....	112
Figure 4.9:	The Giles isotherms for the adsorbents.....	115
Figure 4.10:	Langmuir isotherm plots for the adsorption of fluoride onto the adsorbents.....	117
Figure 4.11:	Freundlich isotherms for fluoride adsorption onto the adsorbents.....	121
Figure 4.12:	Time profile for fluoride adsorption onto the adsorbents showing Pseudo-first order plot.....	124
Figure 4.13:	Time profile for fluoride adsorption onto the adsorbents showing Pseudo.second order plot.....	125
Figure 4.14:	Time profile for fluoride adsorption onto the adsorbents showing Weber-Morris intraparticle.....	127
Figure 4.15:	Regression of Van't Hoff's plot for fluoride adsorption onto the adsorbents.....	130
Figure 4.16:	Fluoride removal from natural high-fluoride water using the adsorbents..	132
Figure 4.17:	Breakthrough curve of combined adsorbents.....	135
Figure 4.18:	Thomas plots for fluoride removal from water using combined adsorbents.....	136
Figure 4.19:	Regeneration tests for combined adsorbents.....	137

ABBREVIATIONS AND ACRONYMS

AES	Auger electron microscopy
AC	Activated charcoal
AlF	Aluminium modified feathers
b	Langmuir thermodynamic equilibrium constant'
C	Weber-Moris intercept
COCA	Copper oxide-coated aluminum
C _o	Initial adsorbate concentration
C _e	Equilibrium adsorbate concentration
C _y	Effluent adsorbate concentration at a particular volume
DCE	Dichloroethane
DDW	Doubly de-ionized water
DTGS	Deuterated triglycine sulphate
EXD	Energy dispersive X-ray
EPMA	Electron Probe micro-analysis
ΔH^*a	Activation enthalpy
HMOCA	Hydrous manganese-coated alumina
IAST	Ideal adsorbed solution theory
ISE	Ion selective electrode
IUPAC	International union of Pure and Applied chemistry
FT-IR	Fourier Transform Infrared Spectroscopy
K _{1,ads}	First order adsorption rate constant
K _{2,ads}	Second order adsorption rate constant
K _r	Freundlich adsorption constant

K_{Th}	Thomas adsorption rate constant
$K_{w,1}$	Weber-Moris intraparticle constant in the initial stages
$K_{w,2}$	Weber-Moris intraparticle constant in the later stages
MCT	Mercury cadmium telluride
m	Adsorption batch adsorbent mass
n	Freundlich intensity parameter
PS	Polystyrene
q_e	Equilibrium adsorption
q_m	Langmuir maximum adsorption capacity
q_t	Amount of adsorption per unit time
q_{Th}	Thomas maximum adsorption capacity
r_L	Langmuir dimensionless parameter
SAM	Scanning Auger Microscopy
SEM	Scanning electron microscopy
SEMPA	Scanning electrode microscopy with polarization analysis
TiSAB	Total ionic strength adjustment buffer
V_t	Break through volume
WHO	World health organization

ACKNOWLEDGEMENTS

This thesis project received funding from European Union's Horizon 2020 Research and Innovation Programme under Grant Agreement No. 690378. I, however sincerely thank my supervisors Dr. Enos. W. Wambu and Prof John. L. Kituyi for the tireless support they have given me throughout this work. Their guidance, advice and being physically available is greatly appreciated. In addition, am grateful for the assistance and encouragement I received from the technicians of chemistry department Mr. Antony Odero, Mr. Froebel Karani and Mrs. Magret Maina. In addition special thanks to Allan Rajway of Technical University Nairobi, for analysis of samples by FT-IR. Thanks very much for supporting me and being there for me whenever I needed your help.

CHAPTER ONE

INTRODUCTION

1.1 Background

Adequate consumption of fluoride is important for the growth of healthy bones and teeth and for dental caries prevention. Excessive ingestion of fluoride however contributes to fluorosis of the dental, skeletal and soft tissue (Piddennavar & Krishnappa, 2013). The relation between excess fluoride in water and endemic enamel mottling sparked much research into fluoride-related physiology and pathology of the hard tissue (Ole *et al.*, 1996). Since fluorosis is an irreversible disease, and has no cure; the only treatment for this threat is prevention. Fluorosis is still a significant clinical and public health concern worldwide. The total number of cases of fluorosis is estimated to be about 32 per cent worldwide. (Kumar & Gopal, 2000). People get exposed to excessive fluoride through food, soil and water. However, drinking water with excessive fluoride remains the primary pathway of human exposure to hazardous levels of fluoride from the environment.

Since fluoride is extremely harmful to humans, there is an immediate need to treat water polluted with fluoride and make it safe for human consumption. The maximum acceptable concentration of fluoride in drinking water is 1.5 mg / L according to the World Health Organization (WHO) (Puthenveedu *et al.*, 2012). Providing water with optimal concentration of fluoride is therefore one of the ways by which the future generation can be protected against the disease. Provision of safe water can be accomplished by harvesting rain water, diluting high fluoride water, transporting safe water from other regions, identifying

alternative sources of safe water and preventing industrial fluorosis. Both these methods, however, have drawbacks ranging from high costs and poor availability of rainwater and scanty natural, safe sources of water.

Defluoridation is the standard and widely validated technique for supplying clean water to the populations affected by fluorosis. The most widely used fluoride removal methods are based on ion exchange, precipitation, distillation, electrochemical defluoridation, reverse osmosis and adsorption (Piddennavar & Krishnappa, 2013). Several researchers have studied water defluorination through the use of chemical precipitation using alum, iron, lime and magnesium compounds and calcium phosphate (Mariappan and Vasudevan 2011). Usage of chemical precipitation needs desalination when the total dissolved solids reach 1500 mg / L and softening of precipitation when the raw hardness is 200-600 mg / L. On the other hand, large quantities of aluminum required to remove fluoride and the need for careful pH management of treated water make aluminum unfit for fluoride removal and high residual aluminum was recorded in aluminum-treated water (Piddennavar & Krishnappa, 2013). The use of precipitation, distillation, ion exchange, membrane technology, electro dialysis and reverse osmosis to remove fluoride from water is limited by high costs, energy requirements and technical complexities (Wambu *et al.*, 2011).

Adsorption involves the passage of contaminated water through an adsorbent bed, upon which fluoride removal by physical, ion-exchange or surface chemical reaction with adsorbent takes place. Plant materials have the ability to remove fluoride from water. The

application of these materials as defluoridating agents is therefore possible. Previous work has been conducted on the application of plant materials for fluoride removal from water (Puthenveedu *et al.*, 2012). Since an adsorption device is of simple design, low sludge production and low maintenance costs, the process of adsorption tends to have more benefits compared to other methods of removing pollutants from water and wastewater. Its versatility and simplicity makes adsorption to be widely accepted protocol to remove pollutants from water. The most common adsorbents employed include activated carbon, bone char, aluminium oxide, silicon dioxide, some adsorbents and several of natural and synthetic organic polymers (Piddennavar & Krishnappa, 2013).

In rural India UNICEF introduced the application of adsorption techniques for domestic defluoridation based on activated alumina (Mariappan & Vasudevan, 2011). However, fluoride adsorption on alumina occurs only at different pH ranges and requires pre- and repeated actuation of alumina which makes the technique uneconomical (Piddennavar & Krishnappa, 2013). Bone char fluoride removal is a process that involves the swapping and surface assimilation of ions in solution between fluoride and apatite carbonate comprising bone char. The bone char, however, nurtures bacteria therefore insanitary, also the possibility to decide without routine fluoride analysis, if the substance is depleted and the fluoride adsorption has stopped (Larsen & Pearce, 2002).

Chitin and chitosan are some of the alternative fluoride removal materials commonly used, but their removal performance is lower than existing fluoride removal techniques

(Sanghratna & Tanvir, 2015). Nonetheless, these biomasses can easily be found and have various specific substituents that could be altered to enhance improve their fluoride removal efficacy. Several researchers investigated the improvement of these bio matter by infusing them with metal ions or covering them with silicon dioxide to improve the water fluoride adsorption performance. From the structure chitosan has an amino group which forms coordination bonds with metal ion resulting to increase in fluoride removal from water. However, these materials are readily available and have multiple forms of functional groups that could be changed to increase their performance in fluoride removal. (Suvendu *et al.*, 2018).

In the current study a number of low cost materials, which included sulphonated polystyrene, fish scales and chicken feathers were investigated for fluoride adsorption. The preparation of the materials included, sulphonating the polystyrene, the fish scales and feathers were ground and tested for fluoride removal in water using both simulated solutions and natural contaminated water. A combination of fish scales, aluminium modified feathers and sulphonated polystyrene were also used for defluoridation. The materials were then further chemically modified to improve their fluoride removal.

1.2 Statement of the problem

In Kenya native fluorosis has been problematic for several years and as a result there is a serious concern over the destiny of fluoride (F) in the environment especially the ground and sources of water underground, especially in areas of the Great Rift Valley and the Central

Highlands. More so, quick increase in population and variation in the amount of rainfall in many parts of Kenya have resulted in quality water scarcity, causing people to use second rate water sources for their necessity. The main water supply for the countryside populations in Kenya are rivers, streams, springs, and wells in areas with good supply of water and boreholes in arid and semi-arid regions. Availability of piped water is restricted to urban areas. Communities in countryside use water from various sources without remedy, and analysis of water quality on regular basis is hardly done due to lack of access in many rural areas as a result of poor infrastructure. Water defluoridation previously by use of magnesium oxide, bone charcoal, clay pot chips has not been able to combat fluorosis in Kenya (Wambu, 2015). Consequently there is need to develop more ways which will ensure quality water is available to the affected communities in Kenya. Studies on use of combined adsorbents are minimal and therefore this study used the low cost adsorbents singly and also combined them in order to determine their fluoride adsorption capacities in combined form.

1.3 Justification of the study

In accordance to the 2008 United Nations report on Millennium Development Goals, more than 50 % of world's population faces water rarity (United Nations, 2008). About 1.2 billion people in this category experience physical water scarcity but a bigger proportion of 1.6 billion others cannot access water because of lack of investment in water infrastructure or insufficient human capacity to satisfy the demand of water in areas where the population cannot afford to use an adequate source of water. The latter conditions are prevalent in South-

Eastern Asia and Sub-Saharan Africa, where large proportions of the communities in rural areas suffer financial water acute water shortage (Wambu, 2015).

In Kenya, research shows the presence of high levels of fluoride in the water sources and as a result there is limited amount of quality water in the affected areas (Gaciri & Davies, 1993). The presence of high levels of fluoride in groundwater in parts of the Rift Valley poses a serious health threat to people that rely on these untreated waters for domestic use. Contamination of water with fluoride necessitates the development of efficient and low-cost technologies for the removal of fluoride from water. One of the aims of vision 2030 in Kenya is provision of high quality life for all citizens; therefore provision of quality water to communities affected by high fluoride water contributes to realizing of the vision 2030. Most agricultural by-products have high fluoride removal capacities in their raw and modified forms; however, there is need to study the capacities of combined raw and modified adsorbents, as well as further elucidate interactions between mixed adsorbents with fluoride (Opeolu *et al.*, 2010). It is for this reason that this study concerns adsorptive removal of fluoride from contaminated water, namely to modification, studying of properties, and application of mixtures of sulphonated polystyrene, whole chicken feathers and fish scales. The materials are easily available and affordable.

1.4 Objectives of the study

1.4.1 General objective

To investigate and design a water defluoridation protocol based on use of sulphonated polystyrene, feathers and fish scales as low cost adsorbents singly and also combined.

1.4.2 Specific objectives

- i. To prepare, combine and chemically modify adsorbents from polystyrene, chicken feathers, and fish scales in order to use them for defluoridation of contaminated water.
- ii. To characterize the adsorbents using FTIR and SEM to determine the functional groups and surface morphology before and after fluoride adsorption
- iii. To investigate the effect of pH, initial fluoride concentrations, temperature, contact time, rate of agitation, and adsorbent dosage on the fluoride uptake capacities of the adsorbents
- iv. To analyze the fluoride adsorption data for the adsorbents based on Giles, Langmuir and Freundlich isotherms so as to quantify the adsorptivity of the ion.
- v. To analyze the fluoride adsorption data for the adsorbents based on pseudo-first, pseudo-second and Weber Morris intra-particle diffusion kinetics models so as to elucidate the principle adsorption mechanism
- vi. To analyze the fluoride adsorption data for the adsorbents based on Thomas model so as to evaluate the feasibility of practical use of this adsorption protocol in water defluoridation and sustainable cleaning

1.5 Research questions

- i. Can polystyrene, chicken feathers, and fish scales be prepared, combined and chemically modified in order to use them for defluoridation of contaminated water?
- ii. How does the functional groups in the adsorbents affect fluoride adsorption?
- iii. What is the effect of pH, initial fluoride concentrations, temperature, contact time, rate of agitation, and adsorbent dosage on the fluoride uptake capacities of the adsorbents?
- iv. Will the fluoride adsorption data for the adsorbents fit on Giles, Langmuir and Freundlich isotherms?
- v. Will the fluoride adsorption data for the adsorbents be described pseudo-first, pseudo-second and Weber Morris intra-particle diffusion kinetics?

Can the adsorbents be used water defluoridation and sustainable cleaning?

1.6 Significance of the study

The results from this work have provided information on utilization of fish scales, chicken feathers and sulphonated polystyrene singly and combined as adsorbents for effective defluoridation of high fluoride water. This will reduce environmental pollution by such waste and improve the water quality. The results will help the affected communities to use locally available waste material to obtain clean and safe water for use. With seminars on the use of these waste materials defluoridation will become a reality for the affected communities.

CHAPTER TWO

LITERATURE REVIEW

2.1 Fluoride contamination of water in Kenya

Documentation on the occurrence of fluoride in water and its hazardous effects in Kenya begun in nineteen thirties. A research was carried out on the occurrence and distribution of fluoride in ground waters of Kenya. The results show a higher percentage of the samples (61.4%) had fluoride ion concentrations above 1.0 mg/L, whilst 19.5% had above 5.0 mg/L. The levels of fluoride were found to be above the WHO limits substantially in the country, especially in the Nairobi, Rift Valley, Eastern and Central Provinces which contain approximately 59.5% of Kenya's population. This study showed that virtually all regions of the country are prone to the negative effects of excess fluoride in water (Nair *et al.*, 1984).

According to Gikunju *et al.*, (1995) in their determination of water fluoride in Molo division of the Rift Valley in Nakuru District of Kenya gave the results as follows. The average fluoride concentration was 0.28 ± 0.03 mg/L. the samples were collected from streams, tap water, boreholes, dams, and rain water with percentages of 62.5%, 15.0%, 10.0%, 10.0% and 2.5% respectively, fluoride levels were between 0.06 to 2 mg/L This and other studies demonstrate ground water sources in the areas of the rift valley are most affected. Wambu and Muthakia, (2011) have reported high levels of water fluoride in Gilgil area Nakuru county. Recent studies have identified fluoride levels in water in Nakuru County at 4.744 mg / L (Ochieng, 2013).

Furthermore, according to Kahama *et al.*, (1997), who analyzed fluoride levels in cow's milk, vegetables and water? The results show that fluoride levels in drinking water from different boreholes were high, varying from 2.0-20.9 mg/L. Milk fluoride levels in samples from seven localities ranged from 0.05-0.22 mg/L (mean) and an individual animal range of 0.02-0.34 mg/L. Vegetables had fluoride levels between 7.9-59.3 mg/L with an exception of one with 296.6 mg/L. The soils in which the vegetables are grown had over 1000 mg/L. This being a landscape formed by the process of faulting and volcanic activity, the dust from Lake Elementaita also had high fluoride concentration of 2300 mg/L.

2.2. Fluorosis and other health effects the case of Kenya

Dental fluorosis is a condition ranging from a hardly noticeable appearance to a marked discolouring or severe pitting of the teeth. The principal cause is a high level of fluoride in or close to the enamel that is growing (Whitford, 1997). Therefore, dental fluorosis can grow in children but not in adults. Dental fluorosis in adults is a result of excessive exposure to fluoride while the adult was an infant or teenager. A research conducted to illustrate the contribution of drinking water to dental fluorosis in Njoro District, Nakuru County, Kenya, found that 48.3% of children in the region had mild to serious dentistry (Moturi *et al.*, 2002). Manji *et al.* (1986) who examined enamel changes among children in Machakos, Kenya, reported that the prevalence and frequency of enamel changes in each type of tooth increased from the lowest to the highest region in F⁻.

An assessment on endemic fluorosis was carried out in Kenya (Mwaniki *et al.*, 1994). The findings of such an examination based on mothers' responses from two affected groups

showed that unacceptable dental fluorosis was not seen as a major health issue relative to other infectious diseases. Research on dental fluorosis in Kenya's drinking water from Molo region with 2 ppm fluoride showed that: 100 percent incidence of dental fluorosis; 92 percent of all teeth had 4 or higher TFI score; and 50 percent of children had pitting or more severe damage to enamel in at least half of their teeth. The fluorotic changes showed extremity of bilateral symmetry (Manji *et al.*, 1986).

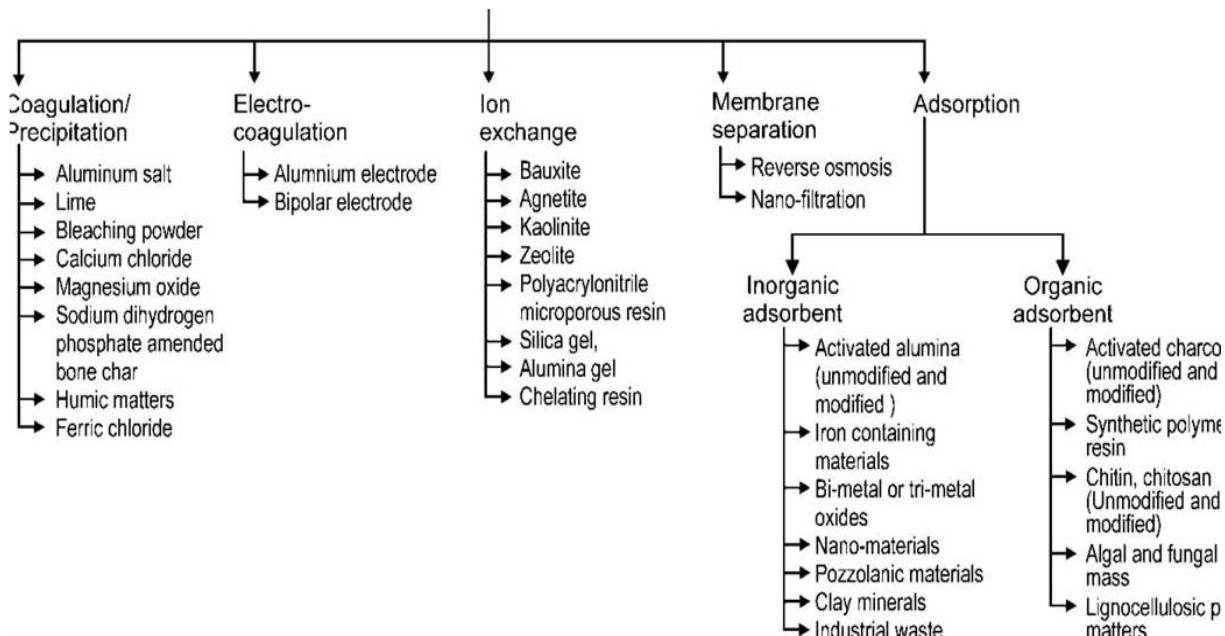
Native skeletal fluorosis is well developed and is reported to happen in far too many parts of the globe, including India, China, and northern, eastern, central, and southern Africa, with different frequencies. It's often mainly associated with drinking water having exceedingly high concentrations of fluoride, although it is also theoretically associated with exposure to other sources of fluoride like high fluoride coal. A number of different factors are involved are environment, combined with water intake, dietary intake, and nutrition, along with new sources of fluoride as well as proximity to other substances that cause changes in the body's fluoride uptake. Severe skeletal fluorosis, linked to higher levels of exposure, can sometimes arise from chronic inflammation of the osteosclerosis, ligamentous and tendinous calcification, and extreme bone deformation.

2.3 Fluoride remediation strategies

2.3.1 An overview of water defluoridation methods

Innovations for fluoride removal encompass precipitation, distillation, ion exchange, membrane processing, reverse osmosis and electro dialysis (Nath & Dutta, 2010). Of this kind approaches would not be used reliably due to “high production costs, high requirements

for energy and technical expertise and shortfalls of some of them, particularly at low contamination rates (Wambu & Muthakia 2011). Through use of natural and affordable adsorbent materials and other modified substances which seem to be resilient to community interests would become a suitable solution for water defluoridation. A summary of defluoridation processes is shown in Figure 2.1 below.



(Source: Suvendu *et al.*, 2018).

Figure 2.1: Defluoridation processes.

2.3.2 Adsorption technology

Adsorption technique works by adsorption of fluoride ions to an active agent's surface (Piddennavar & Krishnappa, 2013). Adsorption has been found to be among the most powerful fluoride removal approaches in water supply relative to all other fluoride removal methods based on the initial cost, adaptability of design and simplicity, and easy implementation and refurbishment. The biosorbent kind utilized defines how successful the methodology is. Adsorption relies on the ions in the liquid phase that migrate to the solid

surface at which they attach to the solid surface or are retained by weak intermolecular forces there. (Kavita *et al.*, 2016).

Adsorption is a chemical separation process; it consists of adhesion of a liquid, gas, or dissolved solid component (adsorbate) onto the surface of a, usually solid, material (adsorbent). Adsorption processes are classified between physical adsorption and chemisorption. Physical adsorption only involves weak intermolecular connecting the adsorbate and adsorbent; chemical bonds, on the other hand, bind the compounds in chemisorption (Ruthven, 1984). The most common differences between the types of adsorption processes are summarized in Table 2.1.

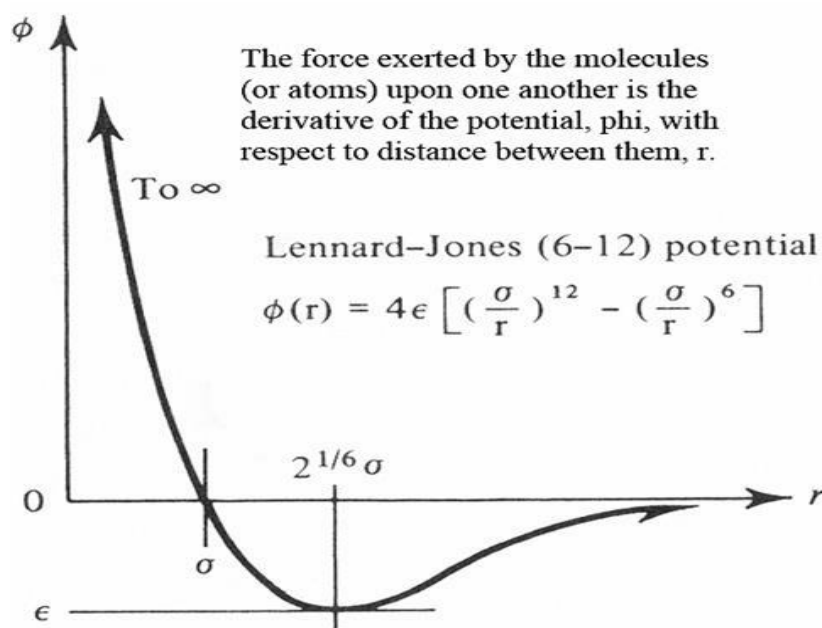
Table 2.1: Physical adsorption and chemisorption typical characteristics

Physical adsorption	Chemisorption
Low enthalpy	High enthalpy
Non specific	Highly specific
Multi-layer adsorption	Mono-layer adsorption
Rapid process	Slow process
No electron transfer present	Electron transfer/Bond formation present

(Source: Kavita *et al.*, 2016).

Physically, separation-enabling effects are intermolecular forces forces and electrostatic forces; whereas if adsorbent has an ionic structure, electrostatic interactions are particularly

important. Aqueous fluoride is a charged ion and adsorbents tested have a surface charge. Van der Waals forces are also called dispersion-repulsion energy; dispersion forces are always present and can dictate equilibrium behaviour if stronger forces are not acting on the system. The dispersion-repulsion energy between two isolated interactive molecules, neglecting the non-dominant attractive terms and higher contributions to dispersion, is described through the Lennard-Jones potential function. Equation 2.1 illustrates the function: a combination of inverse sixth-power attractive term and inverse twelfth power repulsion term (Ruthven, 1984). The equation is illustrated graphically in Figure 2.2.



(Source: Ruthven, 1984).

Figure 2.2: Lennard Jones Potential Mathematical Illustration

$$\phi_{LJ} = 4\epsilon \left(\frac{\sigma}{r}\right)^{12} - \left(\frac{\sigma}{r}\right)^6$$

Where r is the distance between the centres of the two isolated and interactive molecules in [m], ϵ is the potential well depth in [m], and σ is distance where the potential is equal to zero in [m].

In systems with a significant electric field present, electrostatic energies contribute to the energy of adsorption. Electrostatic energies may be caused by polarization, field-dipole, and field gradient-quadrupole interactions. In the case of aqueous fluoride adsorption, charged ions dissolved in a polar adsorbate are adsorbing onto a charged surface adsorbent. A significant electrostatic energy contribution is, therefore, assumed for the system. Overall potential for an ionic adsorbent can be defined as the sum of the six contributor energies, as shown in Equation 2.2 (Ruthven, 1984). For chemisorption, the bond formation energies will significantly contribute to the overall potential.

$$\Phi = \Phi_D + \Phi_R + \Phi_P + \Phi_\mu + \Phi_Q + \Phi_S$$

2.2

Where Φ is the overall surface potential, Φ_D is attractive potential, Φ_R is the repulsive potential, Φ_P is the polarisation contribution, Φ_μ is the field-dipole contribution, Φ_Q is the field gradient-quadrupole interaction contribution, and Φ_S is the sorbate-sorbate interaction contribution, all in [J/mol] (Ruthven, 1984).

Once it comes to liquid adsorption, the zero charge point can have a major impact on the electrostatic interactions between the adsorbate and adsorbent surfaces. The surface charge of natural particles, as is the case for the bone char adsorbent, is contributed to the following three operational categories: structural, adsorbed proton, and adsorbed ions; the point of

zero charge is the pH value for which one contribution to surface charge equals zero at a given temperature, pressure and aqueous solution concentration (Sposito, 1998). Depending on the charge of the adsorbate components, a solution of pH below or above the point of zero charge can either hinder or favour adsorption.

The isosteric adsorption heat is calculated by the relation Clausius-Clapeyron given in Equation 2.3. Remember that equations with partial pressure variables are suitable for gas adsorption systems, but can be applied to liquid systems by expressing partial concentration pressure by assuming ideal (Perry & Green, 2008).

$$\lambda_i = RT^2 \frac{\partial \ln p_i}{\partial T_{n_i n_j}}$$

2.3

Where λ_i is the isosteric heat of adsorption for component i in [kJ/mol], R is the gas constant in [J/Kmol], T is temperature in [K], p_i is partial pressure for component i in [Pa], and n_i is number of adsorbed moles of component i in [mol] (Perry & Green, 2008).

2.3.3 Biosorption

This method requires a biosorbent (solid phase) and an adsorbate (liquid phase) with a dissolved material that must be sorbed. As a result of the immense attraction of the sorbent to the adsorbent material, the adsorbate is attracted and collected by diverse processes. It proceeds until equilibrium exists between the amount of solid-bound sorbate species and the remaining portion of them in the solution. The sorbent degree of affinity of the sorbate stipulates its distribution between solid and liquid phases (Nilanjan *et al.*, 2007).

2.3.4 Effect of adsorption parameters on fluoride adsorption

Adsorption is affected by several factors related to the biomass, adsorbate ions and to environmental conditions and they include mass of adsorbent, contact time, agitation rate, pH, temperature, surface area and initial fluoride concentration.

The temperature affects attachment mechanisms of fluoride and adsorbent and could still have an immediate influence on the physical properties of a sorbent, if thermally conditioned before exposure, so that the sorption potential can be substantially altered. Most of the adsorption experiments are performed in laboratory settings at room temperature. When the temperature increases, sorption becomes more likely to be less preferred due to increased deprotonation or hydroxylation of the surface, resulting in more negative surface charges (Kavita *et al.*, 2016).

Adsorption rate decreases as particle size increases. In general, increasing the size of the particles from 100 to 500 microns decreases the degree of sorption from 75 to 45 per cent. Crushing of bigger particles tends to create small outlets and gaps on the particle surface of the sorbent. The smaller particle gives more locations of sorption and surface area, resulting in higher sorption (Piyush *et al.*, 2012).

Increase in agitation time results to increase in adsorption rate to a certain point after which the sorption rate remains constant (Puthenveedu *et al.*, 2012). An additional increase in the

contact time attributable to the increased amount of fluoride ions on adsorbent material sites does not maximize adsorption (Piyush *et al.*, 2012).

The adsorption process is affected by the pH of the aqueous solution. The amount of fluoride ion adsorption using biomass: *Tinospora cordifolia* was found to be optimum at pH seven and then decreased with a further rise in pH. The favorable pH for fluoride removal was defined as seven (Piyush *et al.*, 2012).). When the pH was acidic, the quantity of fluoride adsorbed marginally decreased and this may be due to the formation of weak hydrofluoric acid. Adsorption within the alkaline pH range decreased significantly, which may be attributed to the adsorption rivalry between the OH⁻ ions and F⁻ (Puthenveedu *et al.*, 2012). The optimum pH for adsorption depends on the type of adsorbent being used.

The quantity of adsorbent is a significant parameter, having an effect on efficiency and the sum of fluoride adsorbed per unit mass of adsorbent. The adsorption of fluoride increases as higher doses of the adsorbent provided more active sites for the adsorbent's growing mass. Higher dosages don't lead to the large rise in defluoridation. It reduces the net surface area due to the coinciding of the binding sites with more adsorbent amounts (Piyush *et al.*, 2012).

When the mass of the adsorbent dose rose, the level of adsorption also rose as there will be more sorbent surface and pores available for contact with adsorption at higher doses of adsorbent, leading to greater. Fluoride adsorption initially increases with the dosage but there

is no noticeable rise in adsorption beyond this dose level. Maybe this is because of the fluoride ion not adsorbing as a result of sorbent-sorbate associations (Puthenveedu *et al.*, 2012).

2.3.5 Experimental designs for adsorption tests

The various designs from which adsorption studies could be carried out include batch adsorption, continuous stirred flow or stationary set-up of columns (Vannela & Verma, 2006). Selection of the type of experimental design is important for optimizing the adsorption protocol. The batch method is widely used, since designing and running is fairly cheap and simple. A solution of known adsorbate concentration, C_j (mg/L), is contacted with a pre-determined adsorbent mass. After equilibration the final concentration, C , (milligrams per litre), of the adsorbate solution could be determined and quantity of adsorption, q_e (milligrams per gram), calculated from remaining mass equation as (Wambu & Muthakia, 2011):

$$q_e = \frac{v(C_i - C_e)}{m1000}$$

2.4

where, v is the volume of the solution (mL) and m is the mass of the adsorbent (g) used. The percentage adsorption can then be obtained as:

$$\% \text{ adsorption} = \left(1 - \frac{C_{eq}}{C_i}\right) \times 100$$

2.5

Fixed bed column reactors comprised of the appropriate size and transverse measurements of cylindrical steel, glass or plastic columns, packed with the necessary adsorbent quantity. Under certain specifications an adsorbate solution of the stated amount at accelerations operated via a regulator to the column in an up-flow or down-flow fashion. The effluent is evaluated for the residual adsorbate levels at specified time or volume intervals (Xu *et al.*, 2012) and the quantity of adsorption calculated by a mass balance statement shown below:

$$C_{ad} = (C_o - C_t)$$

2.6

Where, C_o and C_t , respectively, are the concentrations of the influents and effluents

The adsorption activity of a column system is evaluated by plotting the adsorption number (C_{ad} or uniform concentration (C_t/C_o)) as per the time or volume of the effluent solution (Malkoc & Nuhoglu, 2006). From the respective curves, the breakthrough volume (V_B); retention volume (V_R); exhaustion or equilibrium volume (V_E); and total volume (V_a) can then be determined. The Thomas expression is the most useful model for theoretical characterization of an adsorption processes in fixed bed columns. It is generally used in linearized form as (Murugan & Subramanian, 2006)

$$\ln = \left(\frac{C_o}{C} - 1 \right) = \frac{k_T q_T m}{\theta} - \frac{k_T C_o v}{\theta}$$

2.7

Where, \ln is the natural log function, C is the effluent amount in milligrams per litre, C_o is the influent amount in milligrams per litre k_T is the rate constant in litre milligrams per minute, q_T is the maximum sorption capacity in milligrams per gram of the column, m is the mass of adsorbent in grams v is the throughput volume in litres and θ is the flow rate (Umin). According to equation 2.7 the constants q_T and k_T can be computed from linear regression of $\ln = \left(\frac{C_o}{C} - 1\right)$ to v . Compliance to the Thomas model of adsorption data suggests the presence of Langmuir kinetics for the adsorption-desorption procedure and also that the speed driving force follows reversible reaction kinetics of second order (Wambu, 2015).

Stirred-flow approach incorporates elements of reactors in batch and column reactors. It retains adsorbent suspended particles as they traverse the adsorption column. The benefits of the technique would be that the rate of reaction appears independent of the effects of the porous media, and the equilibrium and kinetic parameters could be calculated using the same tool. Nonetheless, the column design should ensure that the adsorbent solution combination is appropriately balanced, and diffusion gradients are significantly lowered in the solution phase (Seyfried *et al.*, 1989).

To test the influence of solution factors such as pH, temperature, time of contact, concentrations, adsorbent doses on the efficacy of untreated, chemically modified and combined (sulphonated polystyrene, chicken feathers and fish scales) to sorb fluoride from water and to refine the fluoride adsorption protocol using these adsorbents, fluoride adsorption on adsorbents was studied on batch basis as a function of each of the solution

variables. The batch findings were then tested using natural high-fluoride water from Lake Elementaita, Nakuru County in Kenya in fixed bed column experiments.

2.3.6 Sorption equilibrium

Sorption equilibrium refers to the state of balance between the adsorbate fluid phase and adsorbate-rich solid phase (Perry & Green, 2008). Equilibrium adsorption processes are characterized by adsorption isotherms; defined as amount of adsorbate bound to adsorbent surface, as a function of either pressure in the case of gas phase adsorption or of concentration for liquid phase adsorption at constant temperature; single-component physical gas adsorption is the most studied form.

The simplest equilibrium relationship for single-component systems is the Henry isotherm; the most common and widely used isotherm models are the Langmuir, and Freundlich models (Perry & Green, 2008). A number of additional mathematical isotherm expressions, for both single and multi-component adsorption, are available in literature. Due to the complexity and expenses of modelling and testing multicomponent systems, estimations based on single component systems using molecular simulations and the Ideal Adsorbed Solution Theory (IAST) have been investigated extensively.

The IAST is a thermodynamic approach used to predict multicomponent adsorption. The theory relies on the belief that a component's partial pressure can be calculated by the product of its mole fraction and the pressure its pure component would apply at the same temperature

and spreading pressure of the multicomponent mixture (as shown mathematically in Equation 2.9, when taking γ_i as 1 due to the ideality assumption); this assumption is based on the Gibbs adsorption theory, stated in Equation 2.8 (Perry & Green, 2008). Although initially derived for gas systems, the theory was extended to dilute liquid mixtures with the following assumptions: a liquid solution is dilute, the adsorbed phase is an ideal solution, the adsorbent is thermodynamically inert, and the available surface area for all solutes is chemically uniform (Radke & Prausnitz, 1972).

$$Ad\pi = \sum_i q_i d\mu_i$$

2.8

$$p_i = \gamma_i x_i p_i^{ref}(T\pi)$$

2.9

Where A is the area in [m²], π is the thermodynamic spreading pressure in [N/m], μ_i is the chemical potential of component i in [J/mol], γ_i is the adsorbed-phase activity coefficient, x_i is component i mole fraction, q_i is the specific adsorbed amount in [mol/kg], and P_i^{ref} is the standard state in Pa.

Studies on adsorbents include mainly isotherm models and affinity distribution (selectivity) studies. The calculation of the binding properties can be achieved by applying the adsorption from the binding isotherm. It is a fact that the key hypotheses are similar in accordance with the adsorbents widely used. However, certain sign shifts and the actual meanings vary (Bunin *et al.*, 2013; Donato *et al.*, 2014).

Mainly, the Giles, Freundlich, Langmuir, and Langmuir-Freundlich (L-F) models will be discussed. Typically the isotherm selected to characterize an adsorbent's specific output is the easiest, and the most statistically important. For example, when the data is well described by a model with three different binding sites better than a model with one or two binding sites, then the tri-binding site model is always selected, unless other autonomous evidence suggests the use of another. It is advisable to check if the shift is statistically significant when approving a specific n-site fit (George *et al.*, 2014).

Giles and David (1974) proposed a general modelling of sorption isotherms, in which 4 particular cases are now used as the 4 main shapes of isotherm commonly observed (Figure 2.3)

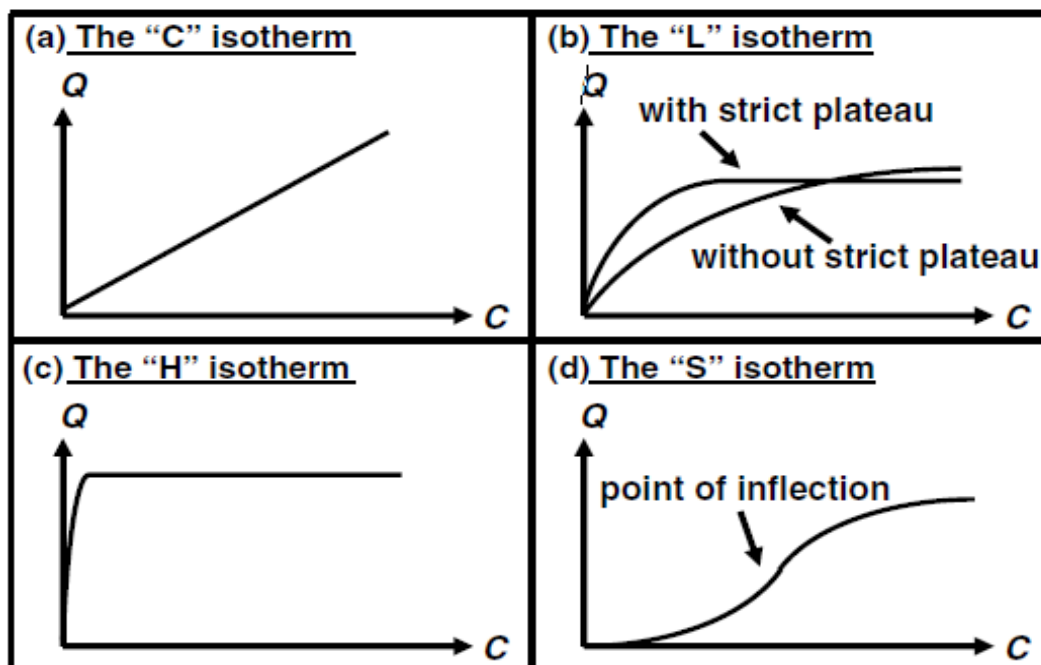


Figure 2.3: The four main types of isotherms (Source: Giles *et al.*, 1974).

The isotherm "C," the curve is a line which starts at zero (Fig. 2.3a). It indicates the relation between the amount of the compound residing in solution and being adsorbed to the solid is constant at any initial concentration. At present this ratio is referred to as "distribution coefficient" or "partition coefficient": K_d or K_p ($L\ kg^{-1}$). The isotherm "C" is often used as a user-friendly approximation explicitly for limited concentration ranges or very trace amounts as seen for low amount contaminants instead of as an accurate summary. However the versatility of this isotherm shouldn't justify its usage before testing, as it may lead to misconceptions. For instance, when the solid does have a tiny amount of adsorption sites the isotherm may be nonlinear due to a potential peak of saturation (Hinz 2001).

The isotherm "L," the relation among the amount of the residual compound in solution and adsorbed on the surface, reduces as the amount of the solute increases, forming a concave curve (Fig. 2.3b). This implies that the solid gradually becomes saturated. One typically makes two subgroups: (i) the curve hits a strict asymptotic plateau (the solid has a limited capacity for sorption), and (ii) the curve does not hit any plateau (the solid clearly shows no limited capacity for sorption). But it also seems almost impossible to tell whether an isotherm belongs to the 1st or the 2nd subgroup.

The "H" isotherm, this is indeed a special scenario of the "L" isotherm, whereby the original slope is extremely large (Fig. 2.3c). This scenario became different from all the others since the material also displays a very great connection to the solid that it is not difficult to isolate the initial slope from infinity, although it makes little sense from a thermodynamic point of view.

The isotherm "S," the curve is non-linear, and thus has a point at which the sign of the curvature changes (Fig. 2.3d). This isothermic form is always, at least, the result of two conflicting processes. The non-polar organic compounds are such common scenario: they have a low connection with clays. However as often as these compounds reach a clay surface other organic molecules are adsorbed more readily. This effect is called "collaborative adsorption," and is observed in solvents as well. Indeed the availability of a soluble ligand could provide a nonlinear isotherm for the metallic ions. The existence of ligand restrains adsorption at trace metals. The ligand has to be exhausted, and then there is automatic adsorption. The point of inflection indicates the concentration at which the adsorption overcomes difficulty (Hinz 2001).

Freundlich isotherm is a factual power outcome for non-ideal adsorption on heterogenous surfaces and multilayer adsorption and is represented via the equation:

$$B = aC^m$$

2.10

Where B represents the sum of the adsorbed contaminant in equilibrium; an is the Freundlich adsorption constant; m is the Freundlich constant representing the heterogeneousness index and varies from 0-1 (values approaching null indicate-heterogeneity and one homogeneity); C is the standard concentration of an equilibrium. From the basic mass balance equation the term B in Equation (2.10) was determined:

$$B = \frac{(C_0 - C)v}{M}$$

2.11

Where C_0 is the original concentration of pollutants, C is the quantity of pollutants at equilibrium, v represents volume of the solution and M biosorbent mass. Linearized form of equation (2.10) was obtained after obtaining logs on both sides:

$$\log B = \log(a) + M \cdot \log(C)$$

2.12

So, the logarithm of B plotted as a function of the logarithm of C was used to produce the intercept value of a and the slope of m . The Freundlich equation is based on the premise that the energy is transmitted from rapid decaying active sites. In most cases, the data provided by this model can be clarified considering that the model is a generalization of the Langmuir model applied to a heterogeneous surface with an energy distribution that corresponds to an exponential decrease. While this Freundlich theory assumes that the adsorbed solvent will increase its solution amount endlessly, the equation is suitable for highly assorted surfaces and often represents typical adsorption results throughout a limited range of concentrations (Rampey *et al.*, 2004; Umplebyli *et al.*, 2004) While the Freundlich isotherm is ideal for explaining the connection between the scale of exposure (available) and the energy of adsorption, it will not obey the elemental thermodynamic basis, because it doesn't really reduce the saturation of monolayers at higher concentrations to Henry's rule.

From the other hand, as per the Langmuir Isotherm adsorption occurs at equal positions within the substance. The langmuir isotherm formula is obtained from pure bulk-movement kinetics, suggesting chemisorption. Therefore, it is assumed that once a sample occupies a

position, there can be no further adsorption at that location, all locations are energetically the same, and there is no relationship with adsorbed molecules at adjacent surfaces. An exhaustion point should be achieved above which there can be no more adsorption (George *et al.*, 2014).

The bi-Langmuir argument predicts the imprinted substance is composed of two groups of zones. The Langmuir and bi-Langmuir models can be applied utilizing Scatchard plots for evaluating binding factors, binding affinity (K) and number of binding sites (N_t), by using general equation: $\frac{B}{C} = KN_t - KB$

$$2.13$$

Where B is the sum of adsorbed pollutant at equilibrium in mg/g; N_t is the total number of usable adsorption sites; C is template concentration of equilibrium; K is the constant of equilibrium of the Langmuir isotherm. In homogeneous systems with only one type of binding sites, the value of N_t from the x-intercept and the value of K from the slope can be obtained by plotting B/C against B. In heterogeneous structures, the scatchard plots are not linear and the simplest example here is a material with two distinct ways of adsorbent surface.

The Langmuir equation is instead generalized to a two Langmuir terms equation:

$$B = \frac{N_1 K_1 C_1}{1 + K_1 C_1} + \frac{N_2 K_2 C_2}{1 + K_2 C_2}$$

$$2.14$$

As B/C is plotted as a function of B it comprises of 2 straight lines thus it is possible to obtain 2 types of binding variables (K₁, N₁ and K₂, N₂) for the 2 classifications of functional groups inside the influenced polymer. Where the line is steeper it correlates to sites of greater affinity whereas in the flatter line the ones of less affinity were measured.

In addition, some other isotherm design that is the integration of Langmuir and Freundlich formulas, called isotherm Langmuir-Freundlich (L-F), could be used. This prototype, first defined by Sips, was implemented for the biomasses by Shimizu and Guiochon (George *et al.*, 2014). The L-F langmuir model defines a balanced relationship between the composition of a bound template (B) and the composition of the equilibrium template in solution (C) enough so (where N_t is the total number of binding sites, and K_0 is the median binding affinity):

$$B = \frac{N_t K_0^m C^m}{1 + K_0^m C^m}$$

2.15

In equation 2.10 the variable a is related to K_0 through $K_0 = 1/m$. Parameter "m" is the same as the Freundlich Isotherm heterogeneity index of site energies.

The main distinction between the L-F model as well as the Freundlich seems to be the saturation response the L-F model displays at high adsorbent concentrations. The L-F formula is much like the standard freundlich model, whenever the amount of adsorbents is minimal. At the other hand, when m reaches unity, which is representative of a totally uniform adsorbent surface (energy equivalence of all binding sites), the L-F formula transforms to the standard Langmuir equation. Thus the hybridized L-F isotherm is able to model solute adsorption on homogeneous and heterogeneous biosorbents at high and low concentrations. For such a three-parameter isotherm a linear model is not feasible but the L-F isotherm can be applied to the experimental results by using Shimizu approach (Loukidou, *et al.*, 2004), where an optimizer variable could be used to optimize the determination

coefficient (R^2) by sequentially changing the 3 appropriate parameters N_t , a and m . R^2 is calculated by inconsistency of the induced study and model-predicted bound concentration. The linear regression is widely used to evaluate the most suited isotherm for two-parameter isotherms. The linear regression is commonly used for assessing the most suitable isotherm for isotherms with 2 factors. The aim is to change the information to construct a linear graph and to obtain the variables of the isotherm while using least squares method. The idea is to transform the data to create a linear graph and use the method of least squares to find the parameters of the isotherm. Examples include Scatchard plots of binding data (Umplebyli *et al.*, 2004; Quiñones *et al.*, 2000; Umplebyli *et al.*, 2000) and linearized forms of Freundlich and Langmuir equations (Umplebyli *et al.*, 2001; Sajonz *et al.*, 1998; Andersson *et al.*, 1995; Vlatakis *et al.*, 1993).

The isotherm models are usually represented linearly. A downside arising from linearithmic ($y = a + bx$) is that it contradicts most linear regression statements. The linear regression analysis reveals, in specific, that perhaps the experimental results put along the correct line has a Gaussian pattern about their distribution. Furthermore the sample variance analysis is just like any other value of x . For some modifications, the connection between x and y is often changed. For example, when a Scatchard plot is formed, both the x -axis (which plots bound) and the y -axis (which plots bound/free) wind up with the calculated value of bound template. Despite these disadvantages, linearization methods are a good beginning for calculating starting nonlinear regression variables (George *et al.*, 2014).

To measure the adsorption capability of cheap fluoride adsorbents (sulphonated polystyrene, feathers and fish scales) and hence, evaluate the feasibility of fluoride removal from water using them and elucidate the dominant adsorption mechanisms, the empirical Langmuir isotherm and the Freundlich isotherm were applied to the fluoride adsorption data for the low cost materials. The corresponding linear plots were constructed and the adsorption equilibrium constants computed. The Giles classification of adsorption isotherms was then used to characterize the interaction of fluoride particles with the adsorbents.

2.3.7 Kinetics and thermodynamics

The process design, operation control and adsorption kinetics play a vital role when it comes to practical applications. The adsorption kinetics in a waste management are important, since they give useful insights into the reactions occurring and the dynamics of an adsorption process (Ho *et al.*, 2000). Also, the kinetics describes the solute uptake, which in turn controls the residence time of adsorbate at the solid-solution interface (Guo *et al.*, 2003). The process describes, by nature, the attachment of charged species to a coexisting bio solid surface from solution to solution. A number of independent processes can affect kinetics, which can function in series or parallel. Such sorption procedures typically fall into one of preceding broad categories: bulk diffusion, external mass transfusion (film diffusion), chemical processes (chemisorption), and intraparticle diffusion. Kinetic analysis allows the calculation of sorption rates and contributes to correct expressions characteristic of potential process parameters (Salman *et al.*, 2014).

Throughout the literature more than 25 models were published, all of which tried to clarify the kinetic actions quantitatively during adsorption. Every Kinetic adsorption model has its own drawbacks, arising from various theoretical and experimental assumptions. Although they breach fundamental assumptions, several models of adsorption have been used to study experimental data successfully (Lagergren, 1989). Specifically the following models are used mostly to define the kinetic models.

2.3.7.1 Pseudo-First Order Kinetic Model

The Lagergren rate equation (Salman et al., 2014) was the very first rate formula for liquid / solid process adsorption focus on substance capability. It is among the most frequently used adsorption rate formulas for the adsorption from a solvent liquid solution. Could be shown as:

$$\frac{dq}{dt} = K_L(q_{eq} - q_t)$$

2.16

When Equation (2.16) is intergrated for limit conditions; $t = 0$ to $t = t$, and $q_t = 0$ to $q_t = q_t$, to obtain:

$$\log \left(\frac{q_{eq}}{q_{eq} - q_t} \right) = \frac{K_L t}{2.303}$$

2.17

This is the integrated rate formula for a pseudo-first - order reaction where q_{eq} is the quantity of pollutant equilibrium concentration in milligrams per gram; q_t is the quantity of pollutant adsorbed at time t in milligrams per gram and k_L is the pseudo-first-sorption (1/s) equilibrium value. Equation (2.17) can be reorganized for a linear shape:

$$\log(q_{eq} - q_t) = \log q_{eq} - \left(\frac{K_L t}{2.303}\right)$$

2.18

The equilibrium adsorption capability, q_{eq} , has to be defined for one to apply Equation (2.18) to scientific results.

2.3.7.2 Pseudo-Second Order Kinetic Model

This kinetic model has certain assumptions in its explanation (Ho, *et al.*, 2000). Hypotheses are as follows. At the adsorption sites there is a single coat of adsorbate, the adsorption energy for every biomass is similar and does not depend on the surface distribution, adsorption takes place only at defined points and does not require interplay between adsorbed contaminants and the adsorption rate is almost insignificant in relation to the starting adsorption rate.

The equation of the Pseudo-Second Order rate could be as described as shown below:

$$\frac{dq_t}{dt} = K_s(q_{eq} - q_t)^2$$

2.19

Where K_s is the rate parameter of adsorption in grams per milligrams per second, q_{eq} is concentration of pollutant adsorbed at equilibrium in milligrams per gram, q_t is concentration of adsorbate on the surface of the adsorbent at any time, t , in milligrams per gram.

Sorting out parameters in the Equation (2.19) results to:

$$\frac{dq_t}{(q_{eq} - q_t)^2} = K_s dt$$

2.20

For limit conditions $t=0$ to $t=t$ and $q_t=0$ to $q_t=q_t$; the integration of Equation (2.20) forming:

$$\frac{1}{q_{eq}-q_t} = \frac{1}{q_{eq}} + K_s t$$

2.21

The integrated rate law for a pseudo-second order process. One can adjust Equation (2.21) to get:

$$q_t = \frac{t}{\frac{1}{K_s q_{eq}^2} + \frac{t}{q_{eq}}}$$

2.22

This has a linear form in which to:

$$\frac{t}{q_t} = \frac{1}{K_s q_{eq}^2} + \frac{t}{q_{eq}}$$

2.23

2.3.7.2 Weber and Morris Intra-particle Diffusion Model

Weber and Morris have suggested a model for intraparticle diffusion, which can be written as (Salman, *et al.*, 2014):

$$q_t = K_{id} t^{1/2} + C$$

2.24

Whereas q_t in milligrams per gram is the quantity adsorbed at time t in seconds, K_{id} in milligrams per gram per second is the intraparticle diffusion rate parameter, C is the intercept value that further provides an idea of the width of the boundary layer. A bigger intercept value means the influence on the boundary layer is stronger. The linear plots of q_t versus $t^{1/2}$ with zero intercept indicate that intra-particle determination of the total adsorption rate.

Throughout this situation, intra-particle diffusion may not be the only decisive process; in comparison to other processes such as electrostatic attraction, ion exchange will operate to various extents (Salman, *et al.*, 2014).

2.3.7.3 Elovich Kinetic Model

The Elovich formula is a widespread technique used to describe the chemisorption kinetics:

$$\frac{d_q}{d_t} = a \exp(-bq_t)$$

2.25

Where the equation variables a in milligrams per gram per second, and b in grams per milligram. The factor (a) is assumed to be the starting rate since d_q/d_t tends toward a as q tends towards zero and b is related to the extent of particle size and the bond of chemisorption. Because $q = 0$ at $t = 0$, the integrated Equation form (2.25) is:

$$q_t = \frac{1}{b} \ln(t + t_0) - \frac{1}{b} \ln t_0$$

2.26

Where $t_0 = 1/ab$. If $t \gg t_0$, Eq. (2.26) is simplified as:

$$q_t = \frac{1}{b} \ln ab + \frac{1}{b} \ln t$$

2.27

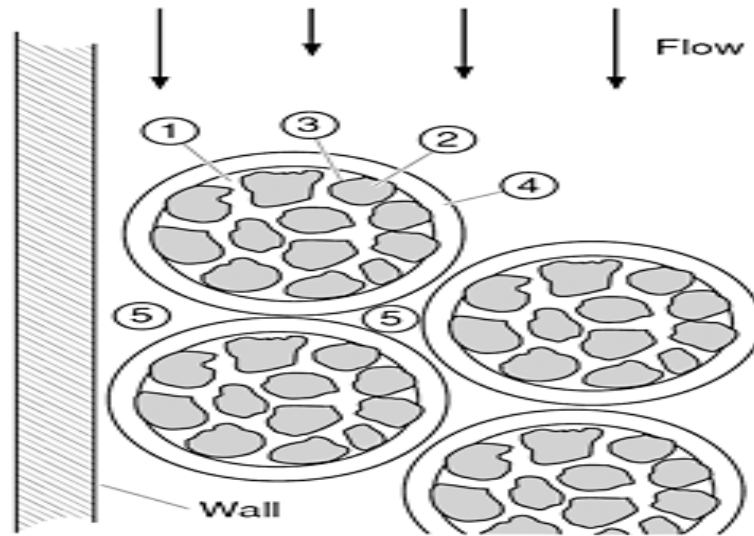
The usage of the Elovich method in the adsorption of liquids is becoming increasingly widespread (Badmus *et al.*, 2007). Once Pseudo-second order kinetic equation was tested on biosorption of lead to dried modified sludge, this was discovered that perhaps the pseudo-second order model would best represent the adsorption of lead into the sludge than the Elovich model with a correlation coefficient of 0.994, 0.726, respectively (Dabhade *et al.*,

2009). Several scientists used first- and second-order pseudo models for phenol adsorption. The pseudo-second order well described the results data with a coefficient of 0.998 for a 1000 milligrams per litre concentration while the pseudo-first order had a coefficient of 0.900 for a 100 milligrams per litre concentration (Adeogun *et al.*, 2012).

Characterization of the essence of adsorption kinetics and determination of the effective residence time of adsorbents in batch reactors in order to explain the rate of fluoride adsorption steps on low cost adsorbents; time-dependent fluoride adsorption data were studied through application of the Lagergren pseudo-first order rate law, Ho's pseudo-second order rate expression and the intraparticle adsorption kinetics of Weber Moris. The respective kinetic plots were then developed and the adsorption kinetics constants were determined.

2.3.8 Transport within a bed packed with porous adsorbent

The transport varies due to the nature and location of each transport mechanism. Figure 2.4 illustrates the different regions and types of transport that occur; they are categorized between intraparticle transport: pore diffusion, solid diffusion, reaction kinetics on adsorbent surface, and extraparticle transport and dispersion: external mass transfer, and fluid mixing (Perry & Green, 2008). Depending on the system, one or more of these processes limit the overall transport rate. In adsorption and desorption, the rate is usually limited by the transport inside porous media rather than kinetic sorption rates at the active sites (Ruthven, 1984).



(Source: Perry & Green, 2008)

Figure 2.4: General illustration of transfer locations in porous packed bed

- 1. Pore diffusion- diffusion in liquid within pores, 2. Solid diffusion- diffusion in adsorbed phase in micropores small enough that molecules do not escape surface force, 3. Reaction kinetics at phase boundary, 4. External mass transfer – bulk fluid to particle surface, 5. Fluid mixing and flow through a fixed bed in fixed bed systems.**

Intraparticle transport is assumed to be a diffusive process described by Fick's Law which, for component i , is given in Equation 2.28. This law states that, for ideal systems, diffusivity is only dependent on the concentration gradient and is independent of concentration. In real systems the driving force is the chemical potential gradient. Most transport models are based on this assumption, and on Fickian diffusivity (Perry & Green, 2008).

$$J_i = -D_i \frac{\partial c_i}{\partial x_i}$$

2.28

Where J_i is the diffusion flux in [mol/m²s], c_i is the adsorbate concentration, and \mathcal{D}_i is the diffusivity in [m²/s], all for component i .

2.3.8.1 Pore Diffusion

Occurrence of diffusion within pores is considered a diffusive process because there is either no, or very slow flow inside material pores (Ruthven, 1984). This mass transfer may be described by a combination of four different mechanisms depending on system conditions: Knudsen diffusion, an additional equivalent viscous contribution to diffusive flux, an additional molecular diffusivity contribution to diffusive flux, an additional molecular diffusivity contribution to diffusive flux, or surface diffusion. Knudsen diffusion dominates systems where the molecules' mean free path length is larger than the average pore diameter. Equivalent viscous contributions are significant when the system experiences a pressure gradient, while molecular diffusivity contributions are significant when a mixture is present in the system. Surface diffusion, lastly, is the mechanism describing diffusion in the case the molecules move in the direction of pores in the adsorbed phase (Cunningham & Williams, 1980). The four mechanisms introduced above are joined as necessary by joining molecular and Knudsen as resistances in series, and then the resulting resistance in parallel to surface and viscous resistances (as shown by Figure 2.5 when taking the diffusion coefficients as the inverse of resistance).

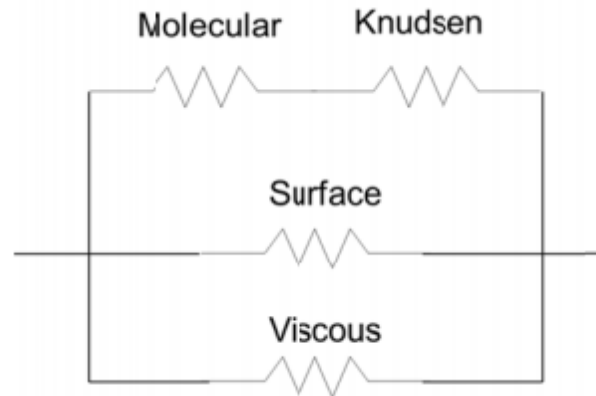


(Figure source: Ruthven, 1984).

Figure 2.5: Schematic of pore diffusion resistances combination

Less rigorously, the diffusion flux through fluid-filled pores can be described, as shown in Equation 2.29, in terms of the pore diffusion coefficient \mathcal{D}_{pi} , which corrects the diffusion coefficient to account for diffusion path and variation pores diameter through the integration of the tortuosity factor, as shown in Equation 2.30. Experimental tortuosity factors, which correct for the deviating and length or pore paths, generally fall in the range 2-6 and decrease as the particle porosity increases (Perry & Green, 2008).

$$J_{pi} = \epsilon_p \mathcal{D}_{pi} \frac{\partial c_{pi}}{\partial z}$$

2.29

$$\mathcal{D}_{pi} = D_i / \tau$$

2.30

Where J_{pi} is pore diffusion flux in [mol/m²s], \mathcal{D}_{pi} is the pore diffusivity in [m²/s], ϵ_p is the adsorbent porosity, τ is the tortuosity, and z is the bed length direction in [m].

2.3.8.2 Solid Diffusion

Fick's transport diffusivity for solid, or micropore, diffusion is described by Equation 2.31. Correcting the driving force as the chemical potential is allowed by using the corrected diffusivity, \mathcal{D}_{0i} ; Equation 2.32 shows how the corrected diffusivity is related to the diffusivity in Equation 2.31 through multiplication with the Darken correction factor.

$$J_i = -D_i \frac{\partial q_i}{\partial z}$$

2.31

$$D_i = \mathcal{D}_{0i} \frac{d \ln(p_i)}{d \ln q_i}$$

2.32

Where \mathcal{D}_{0i} is the corrected diffusivity in [m^2/s].

2.3.8.3 Reaction Kinetics

Rate equations describe interphase mass transfer in adsorption systems. Combining the general component balance for a chosen particle geometry and the relevant flux expressions (depending on the limiting transport process in the system), results to rate equations that can be solved with appropriate boundary conditions (Perry & Green, 2008).

2.3.8.4 External Mass Transfer

Avoiding rigorous analysis of hydrodynamics around particles, mass transfer around the adsorbent can be straightforwardly described in terms of a mass transfer coefficient, available from correlations in terms of the Sherwood number and the Schmidt number. Packed bed

correlations are available in Perry's Chemical Engineering Handbook (Perry & Green, 2008). The mass transfer flux on particle surface is generally described by Equation 2.33.

$$N_i = k_f(C_i - C_i^s)$$

2.33

Where N_i is the mass transfer flux between the adsorbent and bulk fluid in [mol/sm²], k_f is the coefficient of mass transfer in [m/s], c_i is the adsorbate bulk fluid concentration in [mol/m³], and c_i^s is the adsorbate concentration at the adsorbent surface [mol/m³].

2.3.8.5 Fluid Mixing and Flow through a Fixed Bed

When considering the bulk fluid flow in packed beds, the most important parameter is the pressure drop resulting from fluid flowing at a particular flow rate. The Ergun Equation for a packed bed, given by Equation 2.34, is the mathematical description of flow for a single incompressible fluid through an incompressible bed of granular solids. (Perry & Green, 2008). The Reynolds number and the bed void fraction equations necessary for the Ergun Equation are given by Equation 2.35 and Equation 2.36 respectively. At low Reynolds number the viscous forces dominate therefore the 1.75 component in the Ergun Equation becomes insignificant and pressure drop is proportional to bed void fraction, fluid viscosity and superficial velocity (Perry & Green, 2008).

$$\left(\frac{\Delta p}{L}\right) \left(\frac{d}{\rho u_s^2}\right) \left(\frac{\varepsilon_b^3}{1-\varepsilon_b}\right) = \frac{150}{Re} + 1.75$$

2.34

$$Re = \frac{d u_s \rho}{(1-\varepsilon_b) \mu}$$

2.35

$$\varepsilon_b = \frac{(V_b - V_{ad})}{V_b}$$

2.36

Where Δp is the pressure drop in [Pa], L is the bed length in [m], d is the average particle diameter in [m], ρ is the fluid density in [kg/m^3], μ the fluid viscosity in [kg/ms^2], u_s is the superficial velocity in [g/s], ε_b is the bed void fraction, and Re the Reynolds number.

The dispersion coefficient in the axial dispersion term takes into account all contributions to axial mixing in packed beds and is best determined experimentally but can be also estimated from relevant correlations. The axial dispersion term in the continuity equation is often assumed negligible but can be especially relevant for liquid flow in large beds (Perry & Green, 2008).

Adsorption of fluoride to adsorbent material typically takes place via three phases: diffusion or transmission of fluoride ions from the liquid phase to the outer surface of the adsorbent via the boundary layer covering the adsorbent molecule, referred to as external mass transport; adsorption of fluoride ions to nanoparticle surface; The adsorbed fluoride ions are likely to swap within adsorbent particles with the structural elements depending on the composition of solids, or the adsorbed fluoride ions are moved to the inner walls for porous materials (intraparticle diffusion) (Kavita *et al.*, 2016).

2.3.9 Use of low cost adsorbents in fluoride removal from water

Table 2.2 displays fluoride transfer through the use of various adsorbents and best possible parameters. Several low cost adsorbents used in this table have excellent potential to

eliminate fluoride in water supplies. Table 2.2 displays parameters such as dosage of adsorbent, pH, contact time, % adsorption of fluoride, determined by the use of several low cost adsorbents. High adsorption varies from pH of two to eight. It is evident that low-cost adsorbents in use in the adsorption mechanism deliver excellent removal ability and improve the fluoride adsorption capacity. (Kavita *et al.*, 2016).

Table 2.2: Removal of fluoride by using different adsorbents and its optimal parameters

Name of adsorbents	pH	Dosages g/L	Contact Time in minutes	Removal Percentage
Clay material	2.0	5 -10	180	40 -50
Activated dolichos lablab carbon	7.40-8.24	3	30 -75	83.6
Cynodondactylon activated carbon	Neutral	1.25	105	83.77
Granular activated carbon(GAC)& Sewage sludge(SS)	Neutral	GAC-4 SS-3	180	GAC-78, SS-88
Tea ash	6.0	0.8	60	51.3 -97.6
Pumic	7.0	20	180	74.64
Neem stem charcoal	5.0	0.1- 0.6	180	94
Bleaching powder	6.0 -10.0	73	480-540	28-90.6
Sand	6.0	12	180	10.3
Saw dust	8.0	0.15	30	80
Phyllanthus emblica	Neutral	0.75	75	82.1
Neem, Pipal, Khair	2-10	10	180	90
Electro-coagulation	Neutral		20	87
Activated charcoal	2.0	2	120	94
Neem leaves	2	10	60	90
Bark of babool	8	5	480	77.04
Bagasse Dust (BD), Bagasse Fly ash (BF), Al treated Bagasse Fly ash (ABF)	6.0	1-20	5	BD-36.8 BF-42.6 ABF-59.0, BP- 67.9 SP-84.4
SiO ₂	6.0	0.5	20	99.4
Clay-Hydroxyapatite	6.0	1.25	30	99.5
Bottom ash	6.0	70	105	83.2
Ferric poly mineral	3.32	0.2	30	90
Saw dust	7.0	2	120	70
Rice Husk	2-10	10	120	75

(Source: Kavita *et al.*, 2016).

2.3.9.1 Fluoride removal by nonliving biomass

The biosorbents obtained from biomatter and used for water treatment are creative and effective alternative methods. Biosorbent surfaces contain functional groups of NH_2 , COOH , OH , SH , and PO_4^{2-} (Table 2.3) which may bind and eliminate contaminants. Effectiveness of any adsorbent relies on its attraction to fluoride ions and the ability and accuracy of the binding sites inside the adsorbent (Suvendu *et al.*, 2018).

Table 2.3: Interactions with halide ions with surface groups of biosorbents

Functional groups	Interaction
OH	Hydrogen bonding and electrostatic motion and interchange of ions
NH_2 and PO_4^{2-}	Electrostatic forces, hydrogen bonding
COOH	Hydrogen bonding, electrostatic motion
SH	Hydrogen bonding

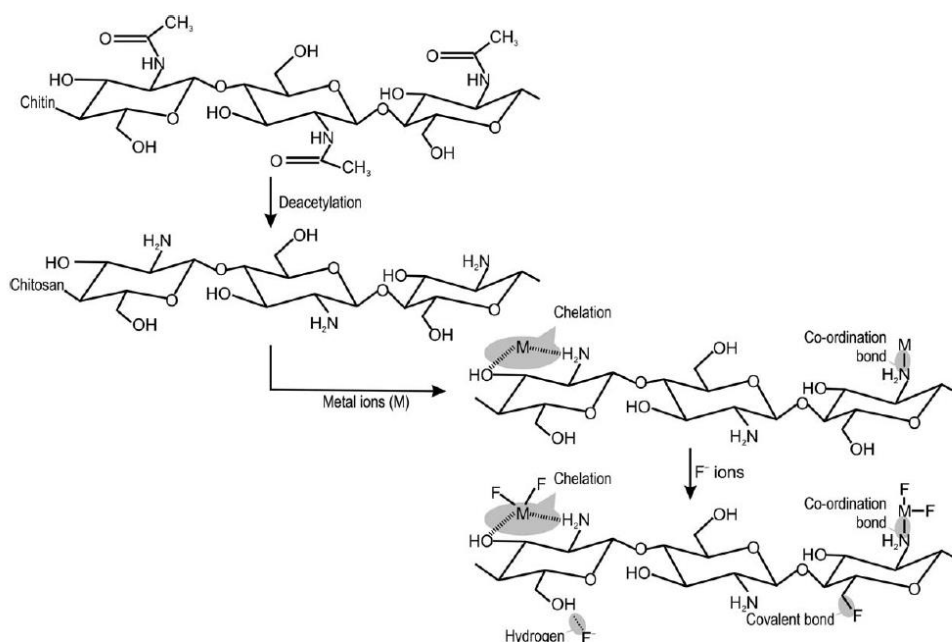
(Source: Suvendu *et al.*, 2018).

Biomasses of plants and animals have been used to prepare Activated Charcoal (AC) commonly used for water purification. This adsorbent has very high specific surface area (ranges from 500 to 1500 m^2g^{-1}), large variety of functional classes, and well-developed internal microporosity. Then AC is an appealing substitute for the alternatives available for extracting fluoride from water. AC preparation includes the pyrolysis of animal and plant biomass and the activation of many physical and chemical processes (Romanos *et al.*, 2012).

Activated charcoals were successfully used to adsorb fluoride. Nonetheless, recent AC modification research is gaining further attention to boost the efficiency and workability of the AC for fluoride removal over a broad range of sorption parameters. For the last couple of years researchers have been using metal ions and/or oxides to alter the activated charcoal. AC impregnated with aluminum ions, zirconium ions, calcium ions, and manganese oxide coated showed greater fluoride removal efficiency than their untreated counterparts. In contrast, the modifications interfere with the environment; requires a lot of energy and modified ACs only workable over a small range of pH. Furthermore, impregnated metal ions could leach into the treated water and could pose health problems if consumed (Suvendu *et al.*, 2018).

Chitin is a polymer present in the cell wall of many invertebrate fungi and exoskeletons. Chitosan prepared from chitin through deacetylation. The two adsorbents are known to adsorb fluoride, although their efficiencies in removal are less than the existing fluoride removal techniques. These materials are high in availability, and they have several functional groups that could be modified to further enhance their fluoride adsorption efficacy. Scientists have changed the biosorbents by using metal ions (Kamble *et al.*, 2007; Viswanathan & Meenakshi, 2010) or coating them with silica (Vijaya & Krishnaiah, 2009) to increase their fluoride removal efficiency from water. As shown in Figure 2.6, the amino group present within chitosan forms a coordination bond with the metal ions and helps enhance fluoride capture from the water. However, when it comes to fluoride adsorption, these biosorbents are not efficient in alkaline pH, because coordination bonds break in alkaline pH and release of metal ions. Consequently, the ability to eliminate fluoride decreases (Bernini *et al.*, 2009).

In another attempt, the researchers modified by carboxylation the hydroxyl groups of chitosan and then chelated the amino groups by adding La^{3+} (Viswanathan & Meenakshi, 2008a) or Fe^{3+} ions (Viswanathan & Meenakshi, 2008a) or Fe^{3+} ions (Viswanathan & Meenakshi, 2008b) for increasing their fluoride adsorption efficacy. Impregnated chitosan Sn (IV) has been developed in the recent past to extract fluoride from waster (Kahu *et al.*, 2017). While the efficacy of these biosorbents for fluoride removal was high, they operate in relatively narrow pH ranges, and their removal efficacy in the presence of other anions was often compromised. Sometimes the residual metals are released into the water.



(Source: Kahu *et al.*, 2017)

Figure 2.6: Mechanisms of fluoride adsorption by chitin and chitosan

Dry mass fungal and algal were also used for defluoridation of water. Fungal dry mass consists of chitin and soluble starch, while algal biomass consists of protein, cellulose, and

lipid substances. *Aspergillus nidulance* fungal mycelia, *Pleurotus ostreatus* 1804, *Pleurotus eryngii* ATCC 90888, and *Pseudokirchneriella subcapitata*, *Chlamydomonas reinhardtii*, *Scenedesmus* algal biomass Fungal and algal dry mass have also been used for water defluoridation. However, the biosorbent removal capacities were very low. To improve their fluoride adsorption capacity, the biosorbents have also been modified. Upon treatment with Ca^{2+} solution, algal biomass of *Chlorococcum humicola* and *Anabaena fertilissima* and the biomass of *Eleocharis acicularis* showed much better fluoride removal efficiencies. Nonetheless, drawbacks such as modest efficiencies in fluoride removal, workability over a limited pH range and inefficiency in the presence of competitive anions limit the use of such biomasses for fluoride adsorption (Suvendu *et al.*, 2018).

In addition, lignocellulosic plant matter was often used for fluoride adsorption. Plant lignocellulosic matter consists of hemicellulose, cellulose, and lignin (Figure 2.7). The biosorbent has specific functional groups that may draw fluoride out of water. Lignocellulose biomaterials are considered to be of low cost relative to the alternative adsorbents available for water defluoridation (see Table 2.4). Costs for processing adsorbent, energy, regeneration, and manpower have not been included in the estimates listed in Table 2.4 and are calculated according to Roy *et al.* (2014); Biomasses, specifically, tamarind gel (Maruthamuthu & Venkatanarayana, 1987) dry duck weed mass (Shirke & Chandra, 1991), hydrilla (Sinha *et al.*, 2000), tamarind seed (Murugan & Subramanian, 2006), and *Pteris vittata* L (Zhao *et al.*, 2015) have been tested for their fluoride adsorption efficiencies. While attempts have been made to extract fluoride from water for a variety of plant matter, their removal capacities and efficiencies are not adequate to substitute the existing fluoride

removal process. As a result, few researchers had attempted to alter the lignocellulosic biomatters to boost their potential for defluoridation. Al / Fe loaded tea wastes (Cai *et al.*, 2015), Zirconium ion impregnated orange residues (Paudyal *et al.*, 2013) were prepared and used to remove fluoride from water. Some studies suggested that the removal of fluoride from the bark and leaf of *Azadirachta indica* (Jamode *et al.*, 2004) and *Tinospora cordifolia* (Pandey *et al.*, 2012) could be improved by alkali-acid treatment modifications. While (Kumar *et al.* (2008) enhanced the efficacy of fluoride removal of *Azadirachta indica* and *Acacia Arabica* by enabling them thermally. Although the efficiency of fluoride removal of lignocellulosic bio matters is enhanced after adjustment, the efficacy of removal has still not been considered sufficient to compete with the alternatives accessible. Furthermore, the efficiencies of fluoride removal in the presence of competitive anions are also considered to be impaired. Further optimization and new processes are required to improve the efficiency of removal of lignocellulosic plant issues.

While lignocellulosic biomass is widely available, low cost, and its surface contains a variety of functional groups, it exhibited lower efficiency in fluoride removal and regeneration. Such shortcomings of biomass dependent lignocellulosic processes may be minimized by chemical and/or physical modification. The capacity of any sorbent to adsorb fluoride depends on its particle size, precise surface area and functionality on its surface (Mohanty *et al.*, 2007; Bledzki *et al.*, 2010). Various methods for manipulating lignocellulosic biomass to improve their interaction with surface and waterborne anionic pollutants such as fluoride have been investigated. Biomasses are pyrolyzed at high temperatures to prepare activated charcoal, as stated earlier, to enhance the different surface area and pore characteristics of

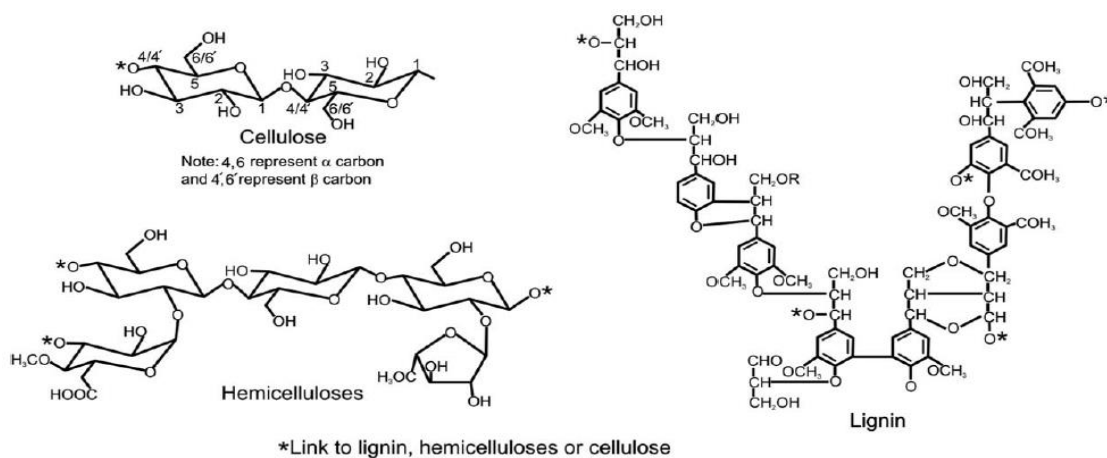
biomass and to boost the ability of adsorbents to extract pollutants. Lignocellulosic plant matter surface area and functionality can also be enhanced by mechanically and/or chemically treating them. The mechanical processes such as chopping and ball milling are also used by researchers to develop mechanical techniques (Sun & Cheng, 2002).

A number of researchers have tried alkali and/or vapor treatment to improve specific biomass surface area (McMillian *et al.*, 1994; Saha *et al.*, 2010). Sections of amorphous cellulose, hemicellulose, and lignin should be separated from the biomass surface during alkali and/or steam treatment (Bulgariu *et al.*, 2011). As a result, the amount of micro- and macropores on the surface of the biomatters increases. Further functional groups within the biomass can be reached via these pores for fluoride removal. As a result, the amount of micro- and macropores on the surface of the biomatters increases. Additionally, gamma-ray irradiation is known to be another efficient surface area modification technique. The gamma-ray splits 1, 4-glycosidic cellulose macromolecules and creating fine biomass particles with increased micro and macro pores and greater surface area (Takacs *et al.*, 2000).

Using these physical and chemical treatments could increase the surface area and pores within the lignocellulosic biomass and enhance their ability to extract fluorides. Two lignocellulosic aquatic weeds were first treated by Manna (2015) mechanically followed by alkali-steam treatment for use in fluoride adsorption studies. According to the reports after treatment the surface area of the weeds increased considerably. In addition, the efficiency of

fluoride removal of the treated weeds increased by more than 50 percent compared with their untreated counterparts.

Chemical alteration improves the nature of the surface and changes the density of lignocellulosic biomass which can be useful for enhancing the contact between the surface of the biomass and anionic pollutants. Wheat straw surface has been treated with epichlorohydrin and/or dimethylamine, which increases the density of the surface charge (Zhang *et al.*, 2011, 2012). Glutaraldehyde modified with calcium alginate also demonstrated a strong response to water-borne fluoride ions (Karnitz *et al.*, 2007). Manna *et al.*, (2015a) modified lignocellulosic jute by grafting phenolic resin juice fibers with neem oil (Figure 2.8). The grafted jute was showing improved efficiency in fluoride removal. After grafting, the jute could show improved efficiency in fluoride removal.

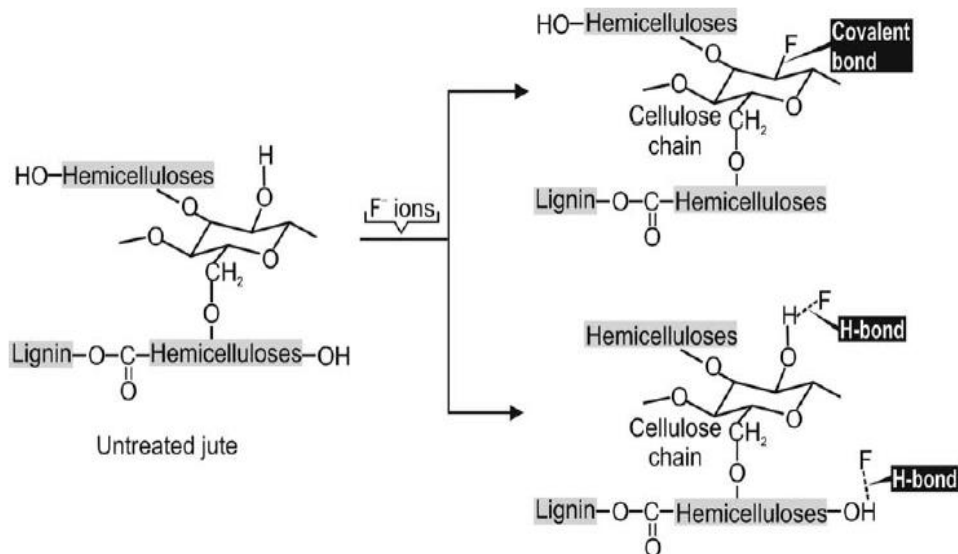


(Source: Manna *et al.*, 2015a)

Figure 2.7: Lignocellulosic plant structure
Table 2.4: Different adsorbents and their cost

Adsorbent	Removal efficiency (g/kg)	Cost (USD/kg of fluoride)
Activated alumina	1-2	15
La(III)- or Y(III)-loaded activated alumina	24	17-74
Fe(II and III) oxides	0.7-59	2
Bimetal or trimetal oxides	12-91	8
Carbon nanotubes	4-38	450
Graphene oxide	1000-2000	312200
Nanoparticle-loaded activated carbon	28	820
Clay and coal	0.2-7	<0.5
Fly ash, slag, and sludge	8-33	<1
Activated charcoal	0.3-17	2
Chitin	5	18
Chitosan	-	1800
20% La(III)-loaded chitosan	45	1850
Algal and fungal dry mass	0.5-4	0.5-6
Lignocellulosic plant matter	0.5-22	<0.3
Chemically treated lignocellulosic plant matter	0.9-4	<0.5

(Source: Roy *et al.*, 2014)



(Source: Manna *et al.*, 2015a)

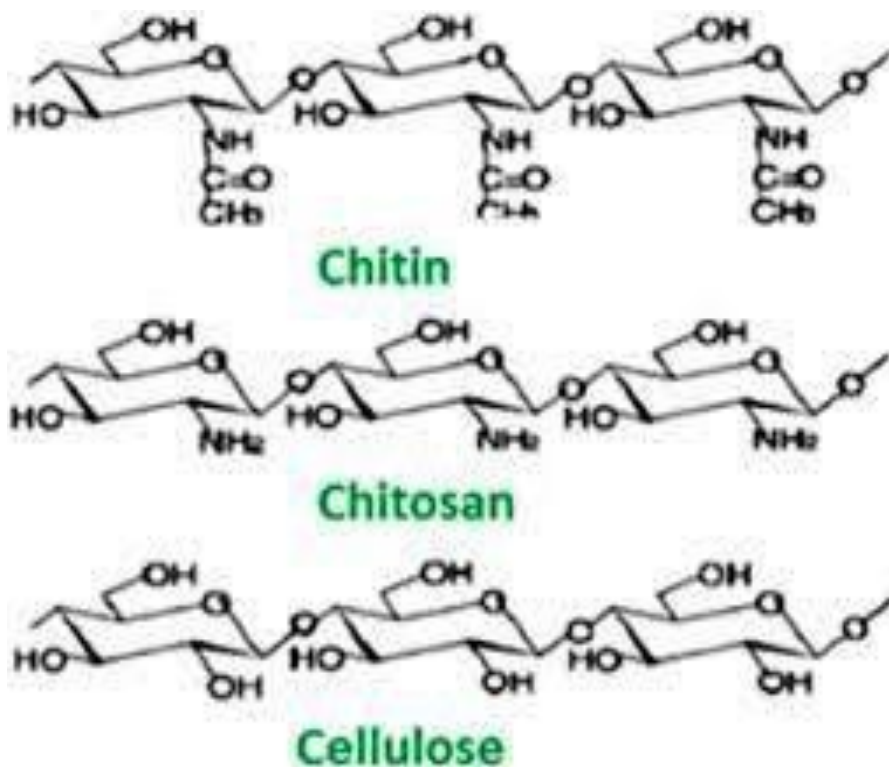
Figure 2.8: Fluoride adsorption by lignocellulosic materials treated with phenoic resin by neem oil

2.3.10 Water defluoridation by Fish scales

Chitin ($C_8H_{13}O_5N$)_n is a polysaccharide polymer hence has many merits for chemical treatment during derivative processing. Basing on its structure, it has high molecular weight, linear sequential units of N-acetyl-D-glucosamine (linked by β-1, 4 units), and similar chemically to cellulose in which the acetamide group substituted the hydroxyl group in cellulose at carbon-2. The word "chitin" originates from the Greek word "chiton" which means coat. The word "chitin" originates from the Greek word "chiton" which means coat. Chitin can be bought at low cost / price from organic sources (especially from krill, lobsters, crabs and shrimps) or from waste from certain industries in the processing of seafoods. Chitin is classified as the world's second most abundant biopolymer from a renewable organic

resource in highly potent natural polymers and can be purchased from organic sources or from waste derived from certain seafood processing industries at low cost/price (Ioannis *et al.*, 2017). Its solubility in water and other solvents is low. It has the advantage that it can be chemically and physically modified to alter its properties. This allows the spectrum of possible applications to be broadened. Chitin can be widely applied in many industries due to a huge number of valuable properties such as in cosmetics, medicine, and biotechnology and in the treatment of waste water.

Crustacean shell is made up of 30-40 percent protein, 30-50 percent calcium carbonate and calcium phosphate, and 20-30% chitin. The prime source is shellfish water, including crabs and crawfish shrimps. Chitin is formed as a linear chain of acetylglucosamine groups, whereas chitosan is recovered by removing acetyl groups ($\text{CH}_3\text{-CO}$) from chitin. The principal distinction between chitin and chitosan is the polymer's acetyl material. The presence of a free amino group on chitosan makes this chitin the most useful. Chitosan is a high molecular weight non-toxic biodegradable polymer and one of the promising sustainable polymeric materials for its large use in the pharmaceutical and biomedical industries for the enzyme immobilization. It is used as a binding, gelling, thickening, and stabilizing agent in chemical wastewater treatment and food industrial formulation (Suneeta & Pradip, 2014). The Chitin, Chitosan and Cellulose chemical structures are shown in Figure 2.9.



(Source: Suneeta & Pradip, 2014).

Fig.2.9: Composition of chitin, chitosan, and cellulose

The three basic steps necessary for Isolation of chitin from crustacean shell waste are: demineralization, deproteinization, decolorization and deacetylation. Subsequently chitin can be converted to chitosan by treatment with concentrated sodium hydroxide solution (40-50%) at 100°C or higher temperature to remove some or all acetyl group from the chitin. Quite a number of methods have been developed and proposed by many researchers over the years for preparation of chitosan from different crustacean shell wastes. But most of the

reported processes were carried out at 100° C or higher temperature with autoclaving (Suneeta & Pradip, 2014).

Fish scale is by-product of fishery. The scales are mainly formed by hydroxyapatite and collagen forming a kind of natural composite with a large specific surface area that intensifies the adsorption process. Also; fish scales in fishery waste management have been reported as adsorbents in biosorption processes due to the high binding capacities (Caroline *et al.*, 2009).

2.3.11 Water deflouridation by Keratin and its derivaties

Keratin is an essential structural protein in nature, and is present abundantly in vertebrate integument. Keratinous materials can be regarded as fibre-reinforced composites consisting of intermediate crystalline filaments embedded in an amorphous protein matrix (McKittrick *et al.*, 2012; Meyers *et al.*, 2008). They have various structures and different protein profiles and functions. They are commonly classified into two groups, such as epithelial keratins and trichocyte keratins, respectively also known as soft and hard keratins. The general role of trichocyte keratins is to serve as structural scaffolding and are present in a number of biological fibrous materials, including wool of sheep, human hair, feathers, and the nails and horns of mammals.

Keratins are commonly found in the form or association with filamentous structures, known as intermediate keratin filaments (Meyers *et al.*, 2008; Scheibel, 2005). Unlike epithelial

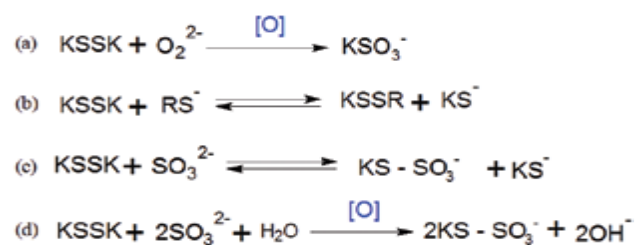
keratins with low cysteine content (including 3 mol percent), hard keratins produce a high cysteine level (4-17 percent) in particular (Aluigi *et al.*, 2012) and are characterized by a strong crosslinking of protein-proteins. Besides cysteine, keratins abound with their lateral chemical structures in amino acids such as glutamic acid, aspartic acid, threonine, leucine, proline, serine and glycine (Arun & Stewart, 2014).

Feather proteins consist of β -keratin and this keratin has a molecular mass of 10 kDa-30 kDa (Meyers *et al.*, 2008; Ghosh *et al.*, 2013). β -keratin's folding pattern is β -sheet with a diameter of 4 nm. The feather β -keratin intermediate filament has a helical structure with a pitch of 9.5 nm and four turns per unit. Interestingly, it undergoes a transformation of the undertensile load process ($\alpha - \beta$ transition) (Meyers *et al.*, 2008).

2.3.11.1 Extraction of keratins and fabrication of material

Keratins are structural proteins with high levels of cross-linking of intra and intermolecular disulfide, and as a result, it is difficult to remove keratins with preservation of the desired properties. The necessary step for the development of new materials from wool or feather is chemical deconstruction by targeted breaking of intermolecular disulfide bonds, while preserving the primary protein chain's covalent bonding. This can be accomplished by processes of reduction, oxidation, sulfitolysis or oxidant sulfitolysis (Poole *et al.*, 2009).

Cysteine residues are converted to cysteic acid when combined with strong oxidants (Figure 2.10a), an irreversible reaction. Reduction of cysteine bonds with thiols like mercaptoethanol or thioglycolic acid may produce soluble keratin through a reversible nucleophilic displacement reaction (Figure 2.10b). Sulfitolysis cleaves the disulfide bond by sulfite ion and induces the reversible reaction of the S-sulfonate anion (Figure 2.10c). Through irreversible reaction, oxidative sulfitolysis transforms the disulfide into two S-sulfonate anions (Figure 2.10d). Beyond the cleavage of disulfide bonds, the substantial non-covalent attractive forces that exist within the wool or feather must be overcome during solubilization. Which involve ionic interactions or salt bridges between acidic and basic amino acid charged residues, hydrogen bonding between polar amino acid side chains and hydrophobic interactions, or van der Waals forces between non-polar protein regions. Aqueous solutions of chaotropic reagents like urea or guanadinium hydrochloride are therefore also required to carry the bulk of the soluble proteins into solution (Arai *et al.*, 1990; Yamauchi *et al.*, 1996). Studies of ionic liquids used to solubilize keratin materials in keratin proteins by breaking intermolecular disulfide and hydrogen bonds are available (Ghosh *et al.*, 2013; Sun *et al.*, 2009). Figure 2.10 below shows reaction mechanisms of keratin extraction.



(Source: Poole *et al.*, 2009).

Figure 2.10: Keratin extraction reactions and mechanisms:

(a) Oxidation, (b) reduction, (c) sulfitolysis, and (d) oxidative sulfitolysis

Uses of extracted keratins include production of films, membranes, foams, scaffolds, hydrogels, particles and fibers or fabrics. The manufacture of fibrous membranes or mats based on functional polymers such as keratin with various polar and ion-exchangeable groups is beneficial for the active filtration of toxic substances, such as volatile organic compounds and heavy metals (Aluigi *et al.*, 2011, 2012).

Extracted keratins have poor physical and mechanical properties when wet and tend to gel quickly (Desai *et al.*, 1991). The mixing of keratin with other polymeric materials using a can solvent method provides a solution for applications requiring high mechanical performance (Dyer & Ghosh 2014; Desai *et al.*, 1991). For example, solubilized keratins can be mixed with polymers like polyamide 6, polyethylene oxide, and polyhydroxybutylateco-hydroxyvalerate to produce good mechanical properties and performance materials (Aluigi *et al.*, 2008, 2009, 2011, 2012; Chen *et al.*, 2002).

2.3.11.2 Mechanisms of pollutant removal

Extraction of pollutants from a solution or environment using keratin substances involves combining physisorption and chemisorptions. The pollutants remain in a porous network within keratinic materials during physisorption, while chemisorption takes place occurson the keratin proteins at chemical functionalities. In particular, the main functional groups provide active chemical sites for metal ions removal and organic volatiles such as formaldehyde (Arun & Stewart, 2014).

2.3.12 Water defluoridation by modified polystyrene wastes

Polystyrene (PS) is chemically very inert, is resistant to acids and bases but is easily dissolved by many chlorinated solvents and by many hydrocarbon aromatic solvents. Because of its durability and inertness, it is used in the manufacture of many commercial items. PS is soluble in many organic solvents. Foamed polystyrene finds its application in plastic packaging. Polystyrene foams are made from blowing agents which create bubbles and expand the foam. They are typically hydrocarbons such as pentane in expanded polystyrene, which can pose a flammability hazard in the manufacture or storage of newly produced material but have relatively mild environmental impact. Extruded polystyrene is typically produced from hydrofluorocarbons (HFC-134a), which have a global warming potential of around 1000–1300 times the carbon dioxide level. Discarded polystyrene is non-biodegradable, and photolysis-resistant. Animals may not understand and can even confuse polystyrene foam as an artificial substance for food. Because of their peculiar gravity, polystyrene foam flies in the wind and floats on water. This can have significant health consequences for birds or aquatic animals that drink large amounts. Restricted research on the chemical alteration and use of polystyrene waste as adsorbents are available (Gabriela *et al.*, 2004).

Addition of a functional group to a benzene ring is a characteristic segment of polystyrene (PS) facilitates the development of new polymer derivatives that have different behaviors and applications. Another such feature is the sulphonate group, and several researchers have

studied the sulphonation reaction. The addition of sulphonic groups results in an increase in hydrophilicity, proton conductivity, and the polymer is converted into ionomer. Nevertheless, swelling increases with high degrees of sulphonation, and mechanical stability is decreased. Researchers have mainly used sulphuric acid as a sulphonant but dissolved polystyrene in other solvents, such as halogenated hydrocarbon, to perform similar reactions whereas other experiments used silica sulphuric acid as a sulphonant. SPS wastes have got white sulphuric acid coffee cups with a ratio of PS: H₂SO₄ 1gr: 20 mL (molar ratio was 1:36 styrene (St): H₂SO₄) and SPS have been to reduce water hardness (Hayat *et al.*, 2016). The fact that sulphonated polystyrene has been used for reduction of water hardness, means that the adsorbent can be used for removal of pollutants from water. It is for this reason that SPS was used for water defluoridation in this study.

2.3.13 Water defluoridation by use of combined adsorbents

There are so many studies currently on of fluoride adsorption capacities by low cost adsorbents. Such studies focus on the single use of such adsorbents. There is need to study the fluoride adsorption capacities of adsorbents when combined. Research on combination of adsorbents for water defluoridation are limited. A study carried out on the potential of single and double-combined adsorbents in removing chromium from an industrial wastewater have revealed that presence of anionic resin in each double-adsorbent caused an improvement of chromium removal (Mousavi *et al.*, 2014). Adsorption of Fluoride from Aqueous Solution by a Synthetic Iron (III)–Aluminium (III) Mixed Oxide have shown that the Langmuir monolayer adsorption capacity of the adsorbent is determined to be 17.73 mg/g, which is higher than that of either of the pure oxides (Krishna *et al.*, 2007).

2.4 Analytical techniques

2.4.1 Fourier Transform Infrared Spectroscopy (FT-IR)

2.4.1.1 Introduction

IR requires the absorption of electromagnetic radiation in the spectrum infrared region that results in changes in the molecule's vibrational energy. Because typically all molecules will have vibrations in the form of stretching and bending, the absorbed energy will be used to adjust the corresponding energy levels. This is a valuable and powerful tool for the detection of organic compounds which have polar chemical bonds with strong dipoles (Skoog & Leary, 1992; Mendham *et al.*, 2009).

Infrared (IR) spectroscopy is an analytical technique commonly used by organic and inorganic chemists. It involves measurement of absorption of different IR frequencies by a sample positioned in the path of an IR beam. IR spectroscopic analysis mainly deals with determination of the chemical functional groups in the sample. Absorption of IR radiation frequencies is characteristic of different functional groups. Analysis of different samples types (gases, liquids and solids) is possible by use of various sampling accessories. Thus, IR spectroscopy is an important and popular tool for structural elucidation and compound identification (Francis & Annick, 2007).

2.4.1.2 IR Frequency Range and Spectrum Presentation

The term “infrared” generally refers to any electro-magnetic radiation falling in the region from 0.7 mm to 1000 mm. The mid- (fundamental) infrared region (IR or MIR) extends from 4000 cm^{-1} ($\lambda = 2.5\ \mu\text{m}$) to 400 cm^{-1} ($25\ \mu\text{m}$). It is surrounded by the far-IR region (FIR) from

400 cm^{-1} (25 μm) to 10 cm^{-1} (1 mm) and the very important near-IR region (NIR) from 12500 cm^{-1} (800 nm) to 4000 cm^{-1} (2.5 μm). However, the region between 2.5 mm and 25 mm (4000 to 400 cm^{-1}) is the most attractive for chemical analysis. Such spectral lines are usually narrow and distinct so that a band corresponding to the particular structural feature to be changed by a reaction can be identified and monitored. As a consequence, quantitative calibration in the mid-IR is normally straight and strong, largely resistant to the effects of spurious objects (Francis & Annick, 2007).

While the near-IR is low in different absorptions, it is an important resource for quantitative applications that is used by quality control laboratories. The technique involves minimal to no sample preparation and the sample can be quantitatively analyzed very easily, without sample consumption to destruction. The instruments for remote analysis may also be paired with UV-visible spectrometers and coupled with fiber-optic devices. By comparison, the mid-IR region offers more information about composite structures and is more widely used as a method for classifying organic compounds for which it remains a form of functional group. The far-IR involves the application of advanced optical materials and sources. In order to carry out these analyses, there is a wide range of instruments from Fourier transform spectrometers to a multiplicity of dispersive or non-dispersive type analyzers, specialized in measuring predefined compounds (e.g. gas and vapor analysis) or enabling continuous analysis on production lines. The far-IR is used for analysis of organic, inorganic, and organometallic compounds involving heavy atoms (mass number over 19). The technique provides useful information to structural studies such as conformation and lattice dynamics of samples. The Fourier transform infrared spectrometry offers numerous possibilities for

the treatment of spectra and has applications for the analysis of structured (infrared microanalysis) (Günter & Tuan, 2003).

Infrared spectroscopy is the most widely used spectroscopic method. There are a number of reasons for its tremendous popularity and distribution. The method is quick, flexible, simple to handle and offers many different sampling techniques for gases, liquids and solids. Significant aspects are the simple qualitative and quantitative measurement of the spectra (Francis & Annick 2007).

Transmittance [percentage T] versus wavenumber [cm^{-1}] is the normal format of an IR spectra. Pursuant to IUPAC recommendations, the values of the wavenumber axis decrease at its right end. The attributes of an IR spectrum (number of bands of infrared absorption, their intensities, and shapes) are directly related to a compound's molecular structure (Günter & Tuan, 2003).

2.4.1.3 Samples and sample preparation

All sample forms can be analyzed (solid, liquid, or gas). There are other sampling available tools to try. The amount of sample needed for solids is fifty to two hundred milligrams, but ten micrograms of ground with transparent matrix (such as KBr) is the minimum for qualitative determinations; if solid is soluble in suitable solvent, a minimum of one to ten micrograms is necessary. 0.5 μL is necessary for liquids if smooth, less if pure and fifty parts per billion gases needed (Frank, 1997).

Sample preparation is simple; may need to grind solid into the KBr matrix or dissolve samples in an appropriate solvent (CCl₄ and CS₂ are preferred). There are several specimen holders and cells available. Water should be separated from the sample, if possible.

In order to obtain a spectrum from a routine sample it takes approximately from 1 to 10 min depending on the type of instrument and the resolution required. Sample preparation for infrared (IR) analysis may approximately take 1 to 5 min.

2.4.1.4 Limitations, accuracy and detection limits

Generally the disadvantages of IR include: minimal elemental information given for most samples, background solvent or solid matrix must be relatively transparent in the spectral region of interest and the molecule must be active in the IR region. When exposed to IR radiation, a minimum of one vibrational motion must alter the net dipole moment of the molecule in order for absorption to be observed. In analysis of mixtures under favourable conditions, accuracy is greater than 1% while in routine analyses, it is $\pm 5\%$. The sensitivity for routine analysis is 2%; under most favorable conditions and special techniques, it is 0.01% (Frank, 1997).

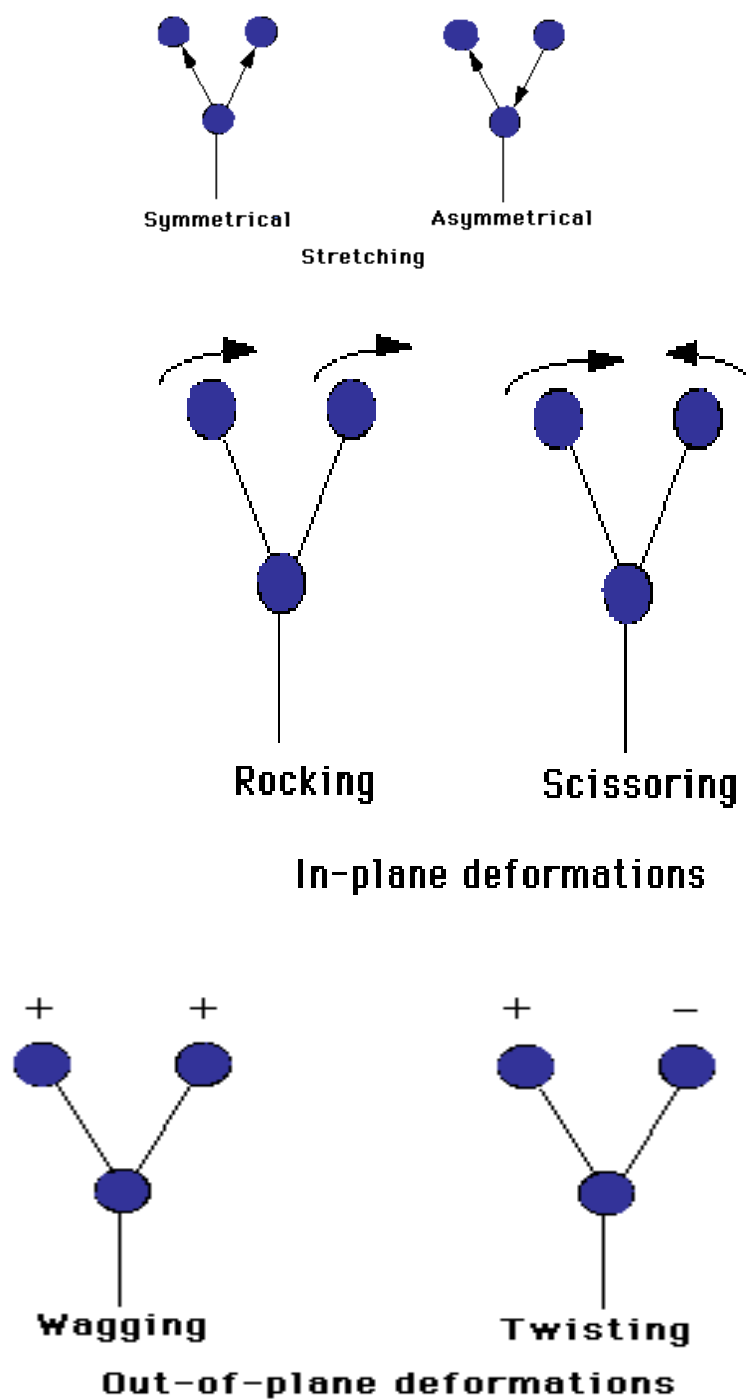
2.4.1.5 Theory of Infrared Absorption

All the atoms in molecules are in continuous vibration with respect to each other when the temperatures are above absolute zero. The molecule absorbs radiation when the frequency of a specific vibration is equal to the frequency of the IR radiation directed on the molecule. For each atom there are 3⁰ of freedom, leading to motions around one of the 3 cartesian

coordinate axes (x, y, z). A polyatomic molecule of n atoms has a complete freedom of 3n. To explain translation (the movement of the entire molecule through space), it needs 3 degrees of freedom which corresponds to the rotation of the entire molecule. For nonlinear molecules, the remaining $3n-6$ degrees of freedom are real, fundamental vibrations. Linear molecules, however, exhibit $3n - 5$ fundamental vibrational modes since only 2 degrees of freedom are enough to explain rotation. The linear and nonlinear fundamental vibrations (also known as normal vibration modes) which cause a net change in the moment of the dipole can result in an IR operation (Skoog & Leary, 1992).

The sum of the bands measured for absorption and the sum of the fundamental vibrations are incomparable. It is reduced because certain modes are not active in IR, and a single frequency can result in more than one mode of motion. In fact, the presence of the overtones also produces additional bands. The intensities of the overtone, mix, and bands of variation are smaller than those of the fundamental bands. The combination and blending of all the factors thus create a unique IR spectrum for each compound (Frank, 1997).

Mainly molecular motions stretch and bend. Fig. 2.11 displays different kinds of vibrations. Infrared radiation is absorbed and the resulting energy is translated into motions of this kind. Absorption includes the sum of discrete, quantized energy. The individual vibrational motion, however, is usually accompanied by other rotational motions.



(Source: Skoog & Leary, 1992).

Figure 2.11: Major vibrational modes for a nonlinear group, CH_2 .

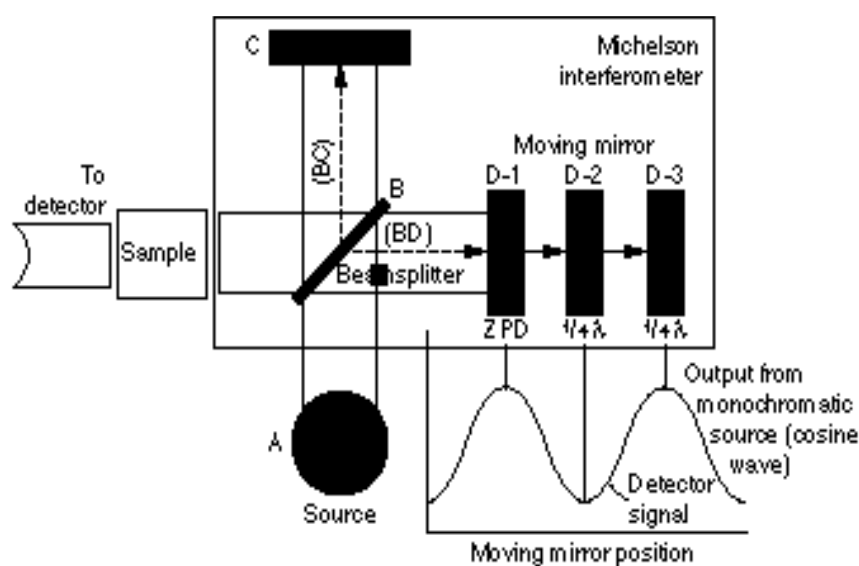
2.4.1.6 Fourier Transform Spectrometers

Thanks to their superior speed and sensitivity, FT-IR spectrometers are currently in use instead of dispersive instruments for the majority of applications. These have significantly expanded infrared spectroscopy capabilities and have been applied to many areas that are very difficult or almost impossible to study by dispersive instruments. In FT-IR spectrometers all frequencies are studied at the same time and each component frequency is presented in a sequence unlike dispersive IR spectrometers (Günter & Tuan, 2003).

FT-IR spectroscopy instruments include: radiation source, interferometer, and detector. This shows a simplified optical model of a typical FTIR spectrometer in Fig. 2.12. Radiation sources are the same for both dispersive and Fourier transform spectrometers but the source is frequently cooled by water for FT-IR for provision of improved power and stability. In addition, the approach by the FT-IR spectrometer differentiates and measures the absorption at component frequencies. The dispersive spectrometer uses a monochromator which is replaced by an interferometer for FT-IR, which divides radiant beams, generates an optical path difference between the beams and then recombines them in order to produce repetitive interference signals measured as a function of optical path difference by a detector. The interferometer serves the purpose of producing interference signals, which contain infrared spectral information generated after passing through a sample (Frank, 1997).

The interferometer commonly used by Michelson consists of: a movable mirror, a fixed mirror, and a beam splitter (Fig. 2.12). The two mirrors are each perpendicular to the other. The beam splitter is a semi-reflective tool which is often rendered by putting a thin

germanium film on a flat KBr substratum. Radiation from the source of the broadband IR is centered on the interferometer and influences the splitter of the beam. Half the IR beam is transmitted to the fixed mirror at the beam splitter and the remaining half is reflected to the mirror on the move. The two split beams from the two mirrors are recombined at the beam splitter upon reflection. The changes in the relative position of the moving mirror to the fixed mirror result in an interference pattern being formed. The resulting beam passes through the sample and eventually reaches the detector (Francis & Annick 2007),



(Source: Frank, 1997)

Figure 2.12: Simplified optical layout of a typical FTIR spectrometer

For a simplified description, the detector response for a single frequency variable from the source of the IR is given first consideration. This replicates an idealized situation, where the source is monochromatic, for example a laser source. In the optical paths, differences between the two split beams are created by changing the relative location of the moving mirror to the fixed mirror. The same length of the interferometer's two arms allows the two

split beams to travel the exact same length of path. The two beams are totally in sync with each other and thus there is optimum response from the detector. As the traveling mirror moves through space $\pi/4$ in either direction, the optical path (beam splitter – mirror – beam splitter) is altered by two $(\pi/4)$, or $\pi/2$. Mirror motion at a constant velocity allows the radiation intensity that enters the detector to differ in a sinusoidal manner to generate the interferogram output shown in Fig. 2.12. The interferogram is basically a time domain continuum and can measure changes in the detector response over time throughout the mirror scan. Unless the sample is soaked at this wavelength, the amplitude of the sinusoidal wave will be reduced by the sample total in the beam. (Frank, 1997).

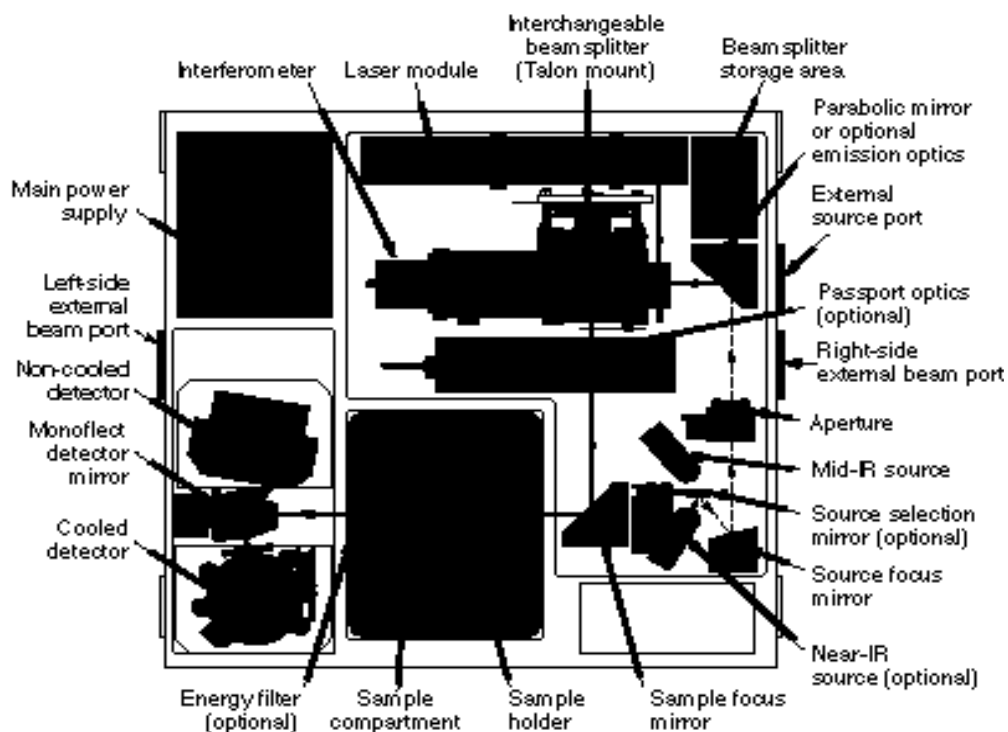
When the same process is extended three component frequencies, these results in a more complex interferogram, which is sums up the three individual modulated waves. However, the interferogram produced with a broadband IR source displays extensive interference patterns. It is a fancy summation of superimposed curved waves, each wave corresponding to a single frequency. When this IR beam is directed through the sample, the amplitudes of a set of waves are reduced by absorption if the frequency of this set of waves is the same as the characteristic frequencies of the sample.

The interferogram includes data over the entire IR area to the result that the detector is responsive. Fourier transformation is a mathematical process that transforms the interferogram into the final IR spectrum, the common frequency domain spectrum that displays intensity versus frequency. This also explains the development of the word Fourier transforming infrared spectrometry (Frank, 1997).

Throughout the mirror scan, the detector signal is measured at minute, precise intervals. The intensity is controlled by an enclosed, independent reference, a helium neon (He / Ne) laser modulated monochromatic beam centered on a different detector.

Deuterated triglycine sulphate (DTGS) and Mercury Metallic Element Compound (MCT) are the two most common detectors for an FTIR prism spectroscope area unit. The response times of multiple detectors (e.g., thermocouple and thermistor) used in dispersive IR instruments are too slow for quick scanning times of the interferometer (1 sec or less). The DTGS detector can be an electrical phenomenon detector that generates rapid responses as a result of measuring changes in temperature rather than temperature values. The MCT detector may be a gauge boson (or quantum) detector that relies on the amount of radiation and displays answers together in no time at all. While DTGS detectors work at temperature, to be efficient, MCT detectors have to be maintained at liquid nitrogen temperature (77 ° K). The MCT detector is, generally speedier and more sensitive than the DTGS detector (Francis & Annick 2007).

The design of the basic instrument is relatively straightforward. Figure 2.13 shows how a typical FTIR spectrometer is constructed. The IR radiation from a broadband source is first guided into an interferometer, where it is separated and then recombined to produce positive and destructive interference after the split beams follow separate optical paths. The resulting beam then passes through the sample compartment, entering the detector.



(Source: Francis & Annick 2007).

Figure 2.13: Schematic diagram of the Nicolet Magna-IR® 750 FTIR Spectrometer

2.4.1.7 A typical operating procedure for FTIR Spectrometer

First a context spectrum is obtained by obtaining an interferogram (raw data) followed by Fourier transform conversion processing the results. It is a mass spectrometer response curve, which takes into account the combined supply, interferometer, which detector efficiency. The background spectrum conjointly includes the contribution from any close water and dioxide gift within the setup. First, a single-beam sample spectrum is obtained which contains the sample and also the background (air or solvent) absorption bands. Finally, the ratio of the single-beam sample spectrum to the single beam background spectrum results in the sample being "double-beamed" (Skoog & Leary, 1992).

To reduce the robust background absorption from water and dioxide within the atmosphere, the optical bench is usually purged with an inert gas or with dry, carbon dioxide–scrubbed air (from a commercial purge gas generator). Spectrometer alignment, which includes optimization of the beams splitter angle, is recommended as part of a periodic maintenance or when a sample accessory is changed (Frank, 1997).

2.4.1.8 FT-IR advantages

There are distinct advantages of FTIR instruments over dispersive spectrometers: Firstly, it's rapid and highly sensitive (Fellgett advantage). A full spectrum can be obtained during one scan of the moving mirror, while all frequencies are detected simultaneously by the detector. As multiple spectra can be obtained in less than a minute without delay, sensitivity can be greatly enhanced by increasing signal to noise ratio through the coaddition of numerous repeated scans. Additionally, the optical efficiency increases (Jaquinot advantage). Energy-wasting slits don't seem to be needed within the measuring device as a result of dispersion or filtering isn't required. Alternatively, in FTIR systems typically a circular optical aperture is used. A FT-IR instrument's area of beam space is usually 75-100 times greater than a dispersive mass spectrometer's slit size. Therefore more energy from radiation is made available. With some samples or sampling methods that specifically quantify energy-limited, this constitutes a significant benefit. Thirdly, internal laser reference (Connes advantage). Use argon on optical device because the internal comparison in several FTIR systems offers automatic standardization with greater than zero precision. That reduces the need for external calibration. In addition, the mechanical design is simpler in that there is only one moving component, the moving mirror, which results in less wear and greater reliability. Apart from

those eliminating stray light, there is another advantage in emission contributions. Both the frequencies are modulated by the FTIR interferometer. No detection of unmodulated stray light and (if any) sample emissions. FT-IR is essentially a strong data centre. Modern FTIR spectrometers usually come with an efficient, computerized data system. These can perform a wide range of data processing tasks including Fourier transformation, interactive spectral subtraction, basic line correction, smoothing, integration and library search (Günter & Tuan, 2003).

2.4.1.9 General Uses and application of FT-IR

FT-IR spectrometry can be used for identification of all types of organic and many types of inorganic compounds, chromatographic effluents, determination of functional groups in organic materials, determination of the molecular composition of surfaces, quantitative determination of compounds in mixtures, analysis of samples nondestructively, determination of molecular conformation (structural isomers) and stereochemistry (geometrical isomers) and determination of molecular orientation (polymers and solutions) (Günter & Tuan, 2003).

Applications of modern FT-IR spectrometry include simple, routine identity and purity examinations (quality control) as well as quantitative analysis, process measurements, the identification of unknown compounds, and the investigation of biological materials. Identification of compounds by matching spectrum of unknown compound with reference spectrum (fingerprinting). Identification of functional groups in unknown substances and reaction components and kinetic studies of reactions. Identification of molecular orientation

in polymer films. Detection of molecular impurities or additives present in amounts of 1% and in some cases as low as 0.01%. Identification of polymers, plastics, and resins. Analysis of formulations such as insecticides and copolymers (Günter & Tuan, 2003)

2.4.3 Ion selective electrodes

An Ion selective electrode (ISE) is a transducer (sensor) which converts the activity of a specific ion dissolved in a solution into an electrical potential which can be measured by a voltmeter or pH meter. The voltage is theoretically dependent on the logarithm of the ionic activity, according to the Nernst equation. Nernst demonstrated that the potential was dependent upon the concentration of the species and varies from the standard potential. The Nernst equation:

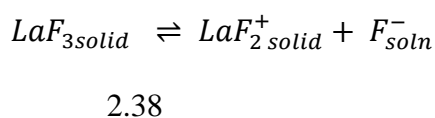
$$E = E^0 - \frac{2.3026RT}{nF} \log \frac{[Red]^b}{[Ox]^a}$$

2.37

Where E is the reduction potential at the specific concentrations, n is the number of electrons involved in the half cell reaction, R is the gas constant (8.3143 V coul deg⁻¹mol⁻¹), T is the absolute temperature and F is the Faraday constant (96,485 coul eq⁻¹) (Mendham *et al.*, 2009).

The sensing part of the electrode is usually made as an ion-specific membrane, along with a reference electrode. Ion-selective electrodes are used in biochemical and biophysical research, where measurements of ionic concentration in an aqueous solution are required, usually on a real time basis (Skoog & Leary, 1992; Mendham *et al.*, 2009).

Lanthanum fluoride, (LaF), is a nearly ideal substance for the preparation of a crystalline membrane electrode for the determination of fluoride ion. Although this compound is a natural conductor, its conductivity can be enhanced by doping with europium fluoride, EuF₂. Membranes are prepared by cutting disks from a single crystal of the doped compound. The mechanism of the development of a fluoride sensitive potential across a lanthanum fluoride membrane is quite analogous to that described for glass, pH-sensitive membranes. That is, at the two interfaces, ionization creates a charge on the membrane surface as shown by equation 2.38:



The magnitude of the charge depends on the fluoride ion concentration of the solution. Thus, the side of the membrane in contact with the lower fluoride ion concentration becomes positive with respect to the other surface. This charge produces a potential difference that is a measure of the difference in fluoride concentration of the two solutions. The potential of a cell containing a lanthanum fluoride electrode is given by an equation 2.39 analogous to Equation 2.37. That is,

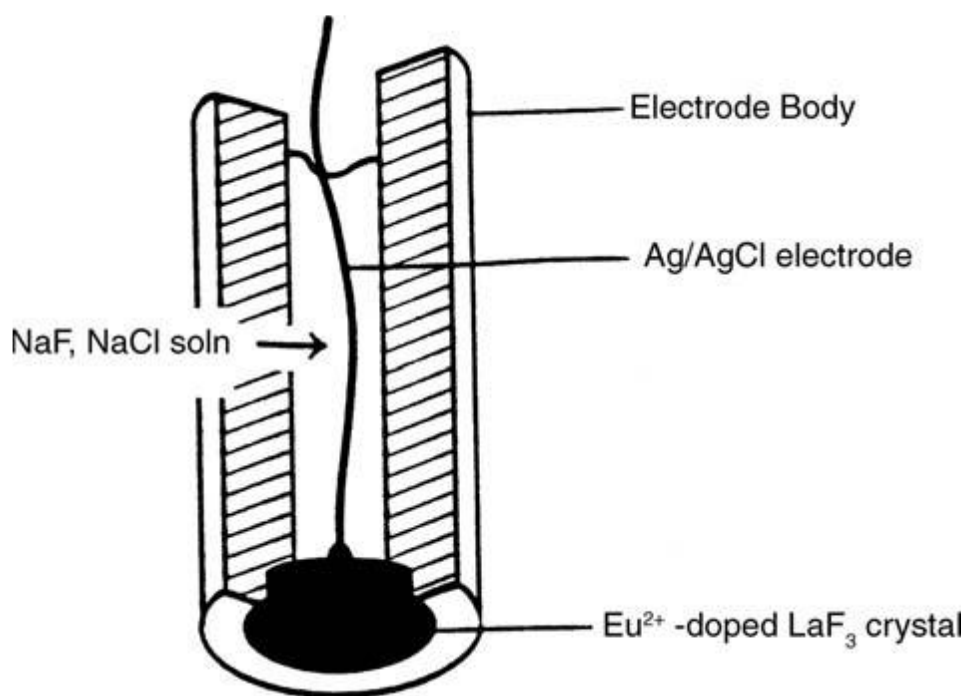
$$E_{ind} = L - 0.0592 \log a_F = L + 0.0592 p_F$$

2.39

The signs of the second terms on the right are reversed because an anion is being determined.

Commercial lanthanum fluoride electrodes come in various shapes and sizes and are available from several sources. Most are rugged and can be used at temperatures between 0

$^{\circ}\text{C}$ and 80°C . The response of the fluoride electrode is linear down to 10^{-6} M (0.02 ppm), where the solubility of lanthanum fluoride begins to contribute to the concentration of fluoride ion in the analyte solution. The only ion that interferes directly with fluoride measurements is hydroxide ion; this interference becomes serious at $\text{pH} > 8$. At $\text{pH} < 5$, hydrogen ions also interfere in total fluoride determinations. Under these conditions, undissociated hydrogen fluoride forms, and the electrode does not respond to this species. In most respects, the fluoride ion electrode approaches the ideal for selective electrodes. Figure 2.14 shows a commercial solid-state fluoride ISE.



(Source: Mendham *et al.*, 2009).

Figure 2.14: A commercial solid-state fluoride ISE.

The ion-sensitive area is a solid crystal of LaF_3 doped with EuF_2 . The filling solution contains NaF and NaCl . The electrical connection is made by an Ag/AgCl electrode.

Potentiometric techniques have been, therefore, employed in fluoride determinations and in measurement of surface pH of the adsorbents. The method is simple, versatile and rapid technique of determination.

2.4.4 Scanning electron microscopy

Scanning electron microscopes (SEM) are scientific instruments that use a beam of energetic electrons rather than light to examine objects on a very fine scale. They image the sample surface by scanning it with high energy beam of electrons in a raster scan pattern, the electrons interact with the atoms that make up the sample producing signals that contain information about the sample surface topography composition and other properties. A SEM instrument comprises of; electron sources, magnetic lenses and magnetic apertures. It comprises of a vacuum system which consists of a chamber which holds vacuum pumps valves and gauges. In addition it has a signal detector and display (Alex & Helmut, 2002).

A closely oriented, high-energy electron beam (typically 10 keV) is rastered back and forth over the sample surface. The effect of high-energy electrons ejects secondary low-energy electrons from the sample captured by a detector to create an image of the sample magnified in real time.

The technique requires conditions for vacuum. A closely centered beam of high-energy electrons (2-100 keV or greater) is rastered around the sample surface. This causes a variety of effects including the emission of low-energy secondary and Auger electrons from the

surface, the production of X-rays from inside the sample, and the primary electrons backscattering. Examination of these various emission types reveals complementary sample detail. Within the instrument, the signal from an electron or X-ray detector is sent to a monitor that is synchronized to the beam's raster frequency to create a real-time magnified sample image. The magnification is adjusted by keeping the image size constant while increasing or reducing the size of the scanned region of the sample by the electron beam. Consequently, electron microscopy does not require the use of multiple sets of optics for various magnifications, as would be the case in optical microscopy (Skoog *et al.*, 2007).

The emission of secondary electrons is very sensitive to surface topography and therefore the detection of these electrons makes it possible to obtain a topographical image of the sample that has a far greater depth of field and a far higher ultimate magnification than traditional optical microscopy techniques would have been possible.

Samples are typically conductive solids compliant to vacuum. Typically non-conductors such as biological samples are coated with a thin layer of gold to make them conductive. Biological or isolating samples under electron bombardment may also degrade (Alex & Helmut, 2002).

Based on the instrument the performance criterion includes magnifications ranging from 3x to 500,000x. Spatial resolution is maybe as strong as 20 Å. One of SEM's great strengths is

that the depth of field at low magnifications is very broad, ranging from 1 m at high magnifications to several km. It is even greater than the depth of field in traditional optical microscopy at equivalent magnifications. Therefore SEM allows obtaining realistic-looking images of highly 3D samples, such as biological structures. Depth sensitivity depends on the mode and amount of energy used for the study. SEM with low-energy secondary electrons can provide a surface sensitivity of 20 Å, while EDX reveals details about the sample's top few microns. Depth sensitivity for back-scattered electrons is highly dependent on the energy of the electron beam and the sample's elemental composition, but is usually hundreds of nanometers (Skoog *et al.*, 2007).

SEM is one of the most widely used analytical techniques across all fields of science, technology and industry. Applications include imaging of highly three dimensional biological structures, imaging and microanalysis of semiconductor structures, magnetic domain imaging for data storage applications, and imaging of fracture surfaces in component failure analysis. SEM was used for surface analysis of the adsorbents before and after adsorption of fluoride.

CHAPTER THREE

MATERIALS AND METHODS

3.1 Chemicals, equipment and Materials

3.1.1 Chemicals

Analytical Grade reagents and chemicals were used throughout the tests. The reagents were obtained from Aldrich chemical Company and supplied by Kobian Laboratory Nairobi, Kenya. A stock fluoride solution of 50.0 mg F L^{-1} was prepared by dissolving 110.5 mg of reagent grade sodium fluoride in 1.0 L of glass-distilled water and a test fluoride solution of 10 mg F L^{-1} was prepared fresh from stock fluoride solution by appropriate dilution.

3.1.2 Instruments

Samples of raw, modified and combined adsorbents were analyzed using a JEOL JMS-6400 scanning electron microscope/Bruker X FLASH 4010 SEM microanalysis detector manufactured in U.S.A, in order to observe surface morphology of the samples. The pH of the solutions was measured using a Hanna Instruments pH-211-microprocessor pH meter. The fluoride concentration using Tx EDT Model 3221 direct fluoride ISE by addition of appropriate volume of TiSAB II (Gikunju *et al.*, 1995). For ISE meter calibration, standard solutions containing 0.1, 1.0, 2.0, 2.5, 7.0, and 10.0 mg/L fluoride prepared by serial dilution of a 1000 mg/L fluoride stock solution with doubly de-ionized water (DDW) were employed. Phase separation during adsorption was done using a centrifuge (model U8V2A SER NO V 200559 and centurion 6000 series, Britain,

London). The samples were analyzed in a Bruker Tensor 27 FTIR spectrophotometer for determination of functional groups.

3.1.3 Materials

The whole group of chicken feathers were collected from a chicken slaughterhouse in Kitale town. They were packed in polythene bags and transported to the University of Eldoret chemistry laboratory three and stored. In the laboratory, they were washed several times with deionized water and sun-dried for 24 h (Rosa *et al.*, 2008). They were ground to powder in a mill, Yanchieng Jiangsu china, model S11WP and sieved using a particle size distribution analyzer, to obtain particle size of 350 μm prior to use and labelled (Bi *et al.*, 2016). The ground feathers were also chemically modified with Al^{3+} , Mg^{2+} and Ca^{2+} . This was done by adding 100 g of the ground feathers to 500 mL of 1000 ppm of each of the ions separately, transferring the solution to a mechanical shaker and shaking at 400 rpm for 12 hours for optimum adsorption. After which the filtration was done, then the chemically modified adsorbent was washed with distilled water and oven dried at 105 $^{\circ}\text{C}$.

The scales of fish as a whole were obtained from Eldoret town fish market, packed in polythene bags and transported to the University of Eldoret chemistry laboratory three where they were stored. Scales of fish were washed several times with doubly distilled water and sun-dried (Caroline *et al.*, 2009). The dried scales were ground into fine powder in a mill Yanchieng Jiangsu China, model S11WP and labelled.

The powdered scales were chemically modified by Mg^{2+} , Al^{3+} and Ca^{2+} by adding 100 g of the scales to 400 mL of each of the solutions separately and shaking at 300 rpm for 4

hrs. The product was filtered, washed with DDW and oven dried at 70 °C and labelled appropriately (Caroline *et al.*, 2009).

Polystyrene waste (PS) which is used in packaging was collected from dump sites within Eldoret town, packed in polythene bags and transported to the laboratory. It was then grated in a miller model SW1100P made from China, and then heated at 100 °C in an oven for two hours to reduce its volume. One hundred grams of polystyrene was sulfonated through addition of 0.6 L concentrated sulfuric acid (98 wt %) in a one litre flask, with 0.1 L 1, 2-dichloroethane (DCE) as the swelling agent at 80 °C for 8 hours (Yinlin *et al.*, 2014). The product was washed ten times with 100 mL doubly distilled water followed by filtration and washed with diluted solution of sodium bicarbonate to completely remove the remaining sulphuric acid and labelled (Hayat *et al.*, 2016). The sulphonated polystyrene (SPS) was further chemically modified with Al^{3+} , Mg^{2+} and Ca^{2+} . The modification was done by adding 100g of SPS to 500 mL of 1000 ppm of each of the ions separately, transferring the sample to a mechanical shaker where shaking was done at 400 rpm for 12 hours. After which the filtration was done, then the chemically modified adsorbent was washed with distilled water and oven dried at 105 °C and labelled.

Mixtures of prepared sulphonated polystyrene, feathers and powdered fish scales were combined in ratios of 1:1:1, respectively. Batch and column experiments were performed using the combined adsorbent.

3.2 Adsorbent characterization

Over the wavelength region of four hundred to four thousand wave numbers, the infrared spectra of solid untreated, chemically modified, and mixed adsorbents were obtained. Infrared spectra of adsorbents laden with fluoride ions were obtained in the adsorbents and fluoride ions to test for interactions between functional groups. Samples of raw, modified and combined adsorbents were analyzed using a JEOL JMS-6400 scanning electron microscope/Bruker X FLASH 4010. SEM microanalysis detector was done, to analyze sample surface morphology.

3.3 Batch experiments

Batch experiments were carried out to optimize fluoride ion adsorption parameters on raw, modified and combined adsorbents. The batch tests were done in 250 mL stoppered bottles by agitating a pre-weighed amount of the optimized mass of adsorbent with 50 mL of proven concentration fluoride solutions. The separation of the adsorbents was done by centrifugation. The residual fluoride concentration in the supernatant was potentiometrically measured using an ion-selective fluoride electrode.

3.3.1 Optimization of mass

To study the effect of an increase in the dose of adsorbent on removal of fluoride, experiments were conducted by adding varying doses of 0.5, 1.5, 2.5, 3, 6 and 10 g to 50 mL of a test solution containing initial fluoride concentration of 10 ppm and shaking at 400 rpm for 120 minutes at room temperature.

3.3.2 Optimization of time

The effect of increase in time on the removal of fluoride was studied by adding optimized mass of adsorbent to 50 mL of 10 ppm fluoride and shaking at 400 rpm for varying times of 1, 2, 4, 8, 15, 30, 60 and 120 minutes at room temperature.

3.3.3 Optimization of agitation rate

Using optimized mass, time and 50 mL of 10 ppm fluoride the agitation rate was optimized by varying rates of 35, 70, 200, 300, 350 and 400 rpm at room temperature.

3.3.4 Optimization of pH

The effect of pH on the adsorption of fluoride was studied using optimized mass, time, agitation rate and 50 mL of 10 ppm fluoride with varying pH values of 1, 3, 5, 7, 9, 11 and 13.

3.3.5 Optimization temperature

The temperature was optimized using optimized mass, time, agitation rate, pH and 50 mL of 10 ppm fluoride with varying temperature values of 15, 20, 30, 40, 50, 60, 70 and 80 °C.

3.3.6 The effect of fluoride concentration

The effect of fluoride concentration was studied using optimized mass, time, agitation rate, pH, and temperature and 50 mL solution of varying concentration of fluoride of 1, 2.5, 5, 10, 25, 40, 100, 200 and 500 ppm.

3.4 Equilibrium analyses

Studies of adsorption isotherm were carried out with different initial concentrations of fluoride while preserving the adsorbent dose which was the optimized mass for each adsorbent. A 50 mL of varying concentrations (1, 2.5, 5, 10, 25, 40, 100, 200 and 500 ppm) of the F^- solution was introduced into plastic bottles containing the adsorbent. These were stirred on a mechanical shaker unimax 10101 Heldoph Germany allowed to stand for 1 hr while other parameters such as temperature, pH and time were kept constant. At the end of the agitation, the mixture was centrifuged and the supernatant fluoride concentration measured using fluoride ion selective electrode. The data obtained from experiment was fitted onto Giles, Langmuir and Freundlich isotherms (Wambu, 2015).

3.5 Kinetics and thermodynamic analyses

Kinetic analyzes were carried out to estimate the sorption rates and the correct rate expressions characteristic of potential reaction mechanisms. Batch kinetic studies were performed using a mixture of 50 mL of 10 ppm of F^- solution and the optimized mass of adsorbent. Other parameters were kept constant while samples were drawn at time intervals of 1, 2, 4, 8, 15, 30, 60, and 120 minutes and analyzed. The Pseudo-first order kinetic model, the Pseudo-second order and Weber Morris intra-particle diffusion models were used.

3.6 Regeneration tests

Regeneration studies were carried out using sodium hydroxide of different concentrations on both raw and combined modified adsorbents to determine the regeneration

percentages. The used adsorbents were agitated with NaOH solutions of different concentrations.

Conversely, fluoride adsorption from natural high-fluoride water using the adsorbents was conducted in batch and column experiments using high-fluoride water from Lake Elementaita in Nakuru County, Kenya.

3.7 Data Analysis

All tests were performed in triplicate. The data were analyzed by descriptive statistics by calculating the range, mean and standard deviation on replicate results. Causative relationships were then analyzed by graphical regression of the variables and determination of correlation coefficients.

CHAPTER FOUR

RESULTS AND DISCUSSION

4.1 Chemical characterization of adsorbents

Fourier transform infrared spectroscopy is a very effective and important method utilised by many scientists to understand the mechanisms of adsorption of all pollutant forms. Changing the IR band following adsorption of contaminants makes FTIR widely employed. To understand the mechanisms of fluoride removal, FTIR spectroscopic bioadsorbent analysis could be performed before and after the fluoride adsorption (Suvendu *et al.*, 2018). The nature of interactions between reactive surface sites or functional groups in adsorbents and fluoride ions in water led to their infrared spectra and SEM showing surface morphology. The results for the FT-IR analyses are depicted in Figure 4.1.

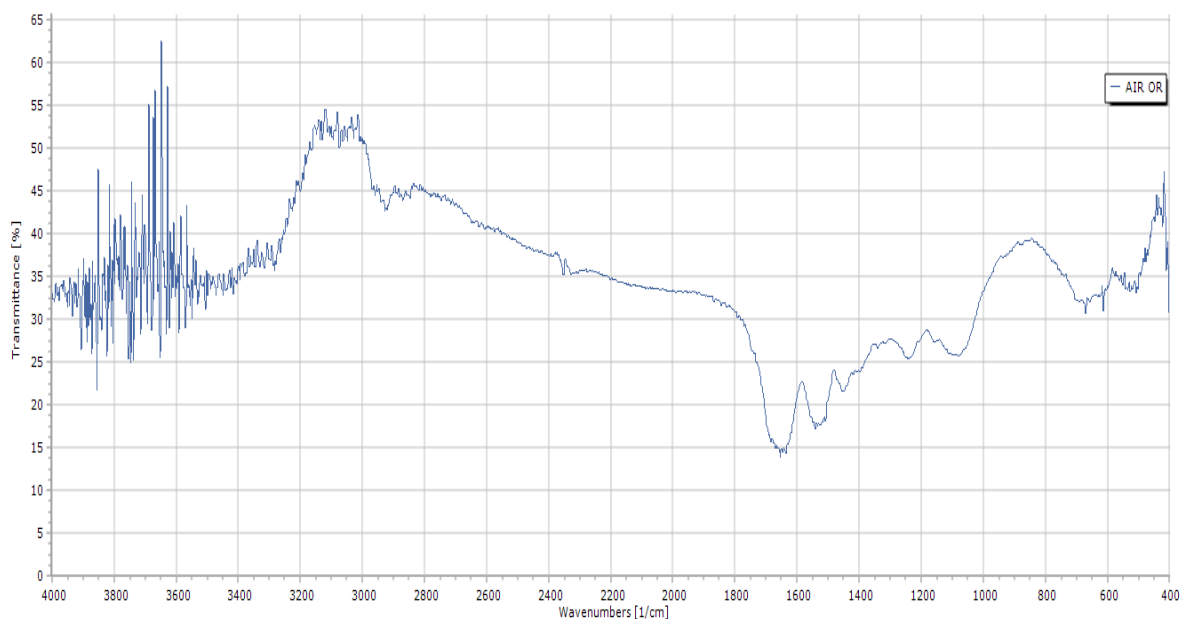


Figure 4.1(a): AIF IR spectra

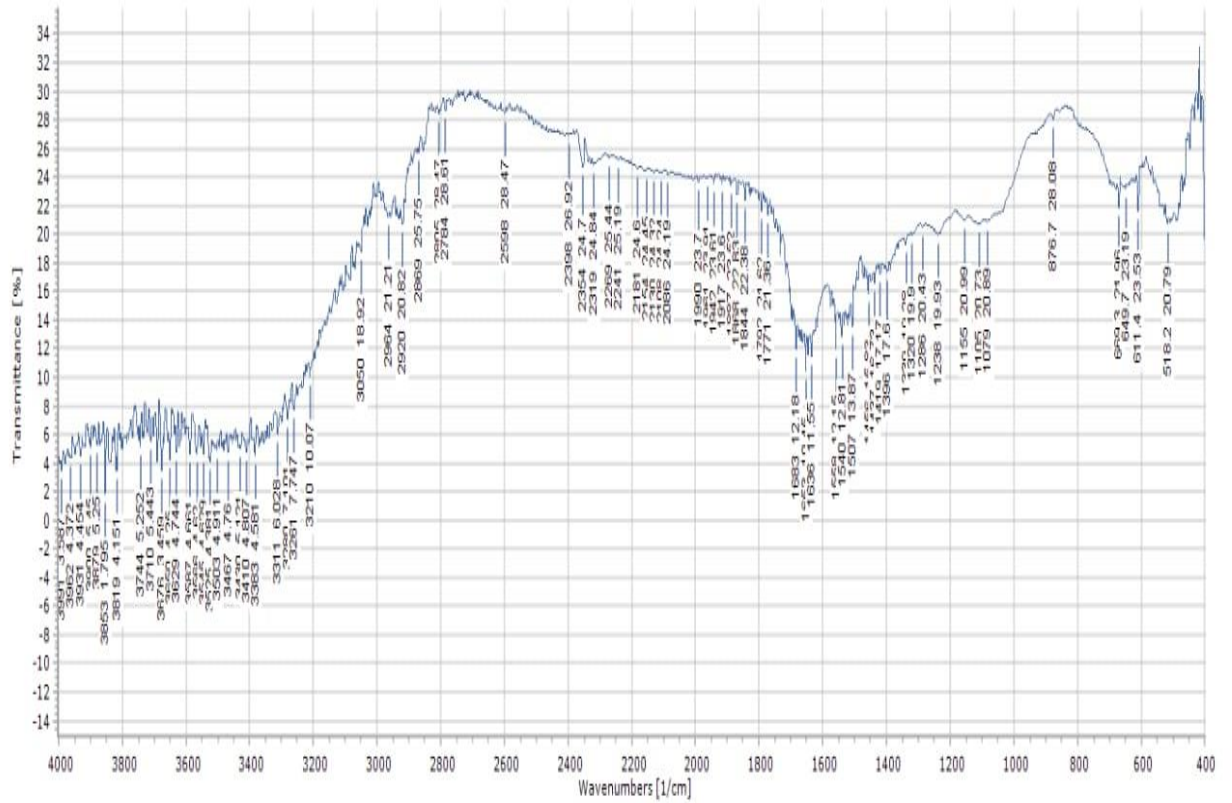


Figure 4.1 (b): AIF IR spectra after adsorption of fluoride

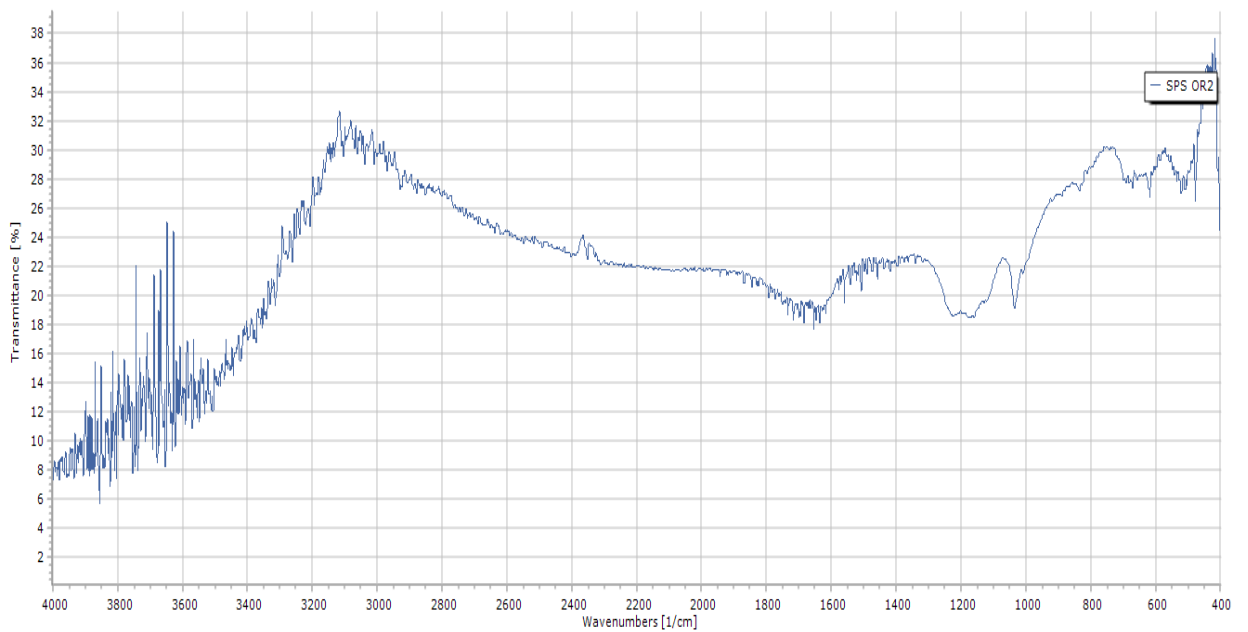


Figure 4.1 (c): SPS IR spectra

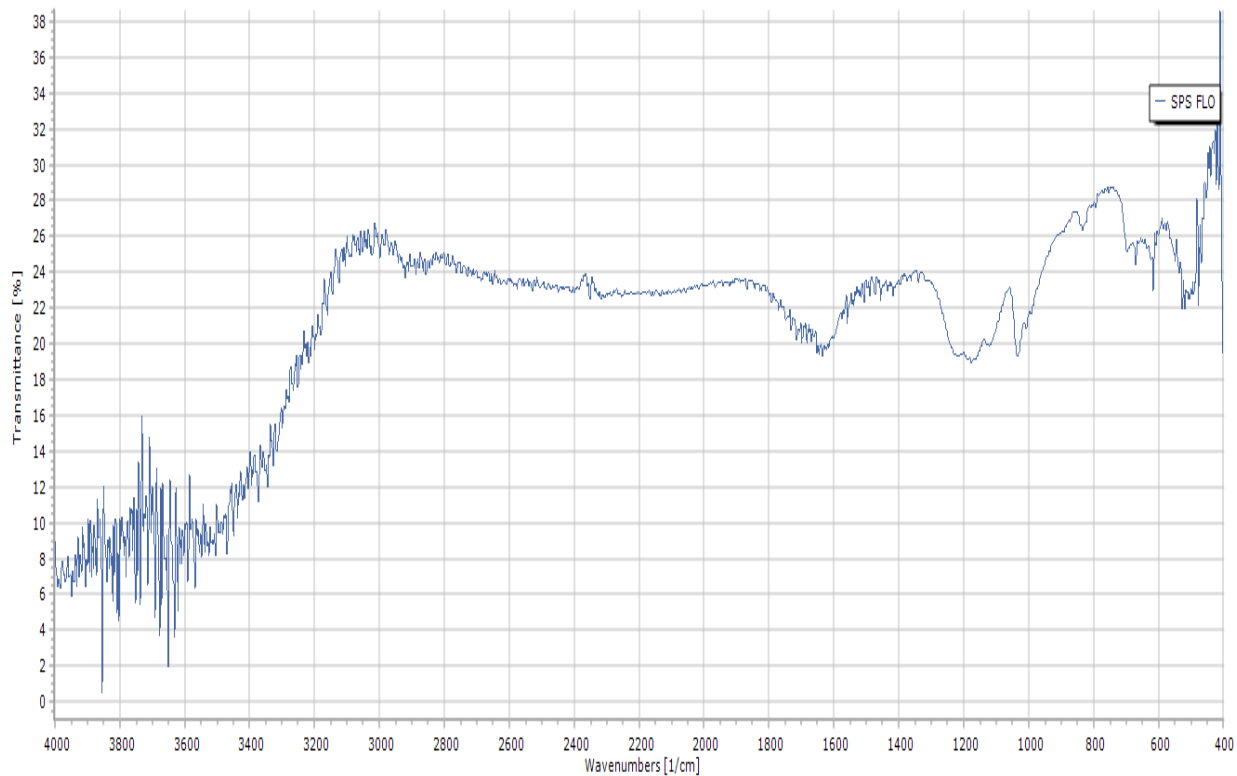


Figure 4.1 (d): SPS IR spectra after fluoride adsorption

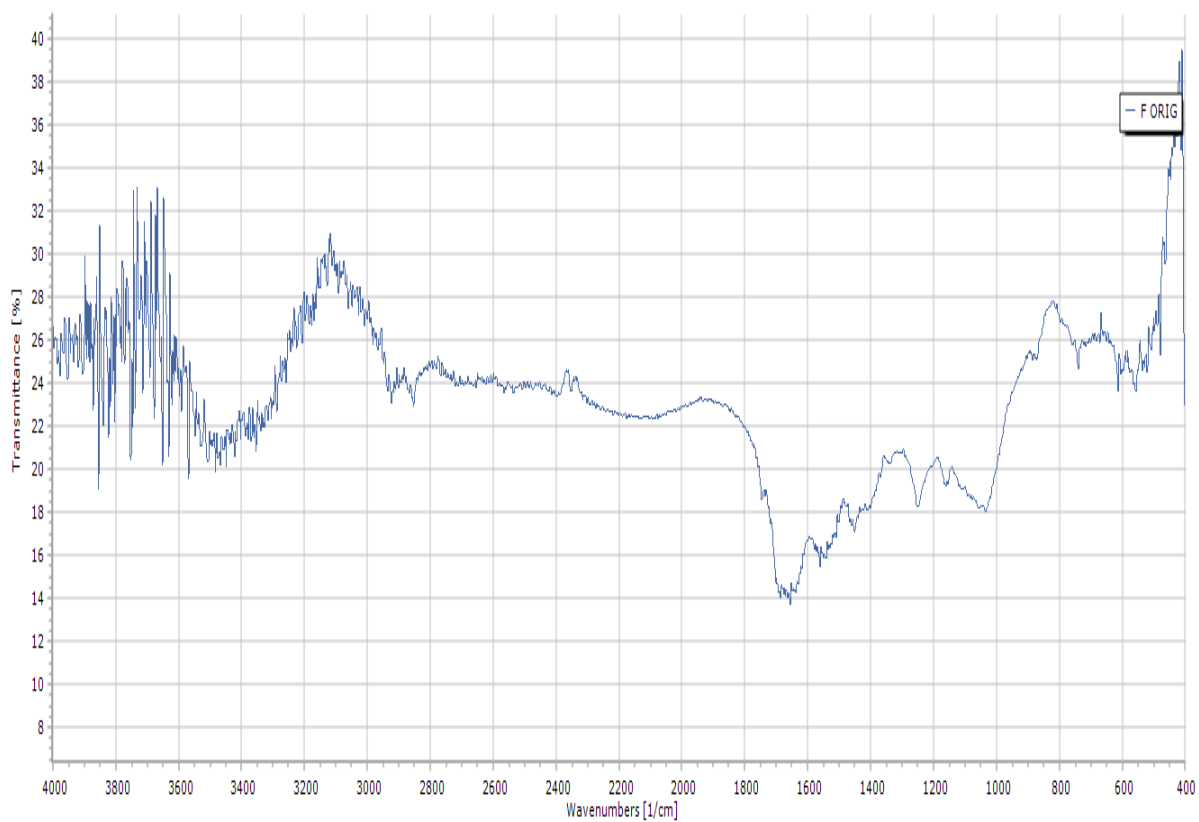


Figure 4.1 (e): Fish scales powder IR spectra

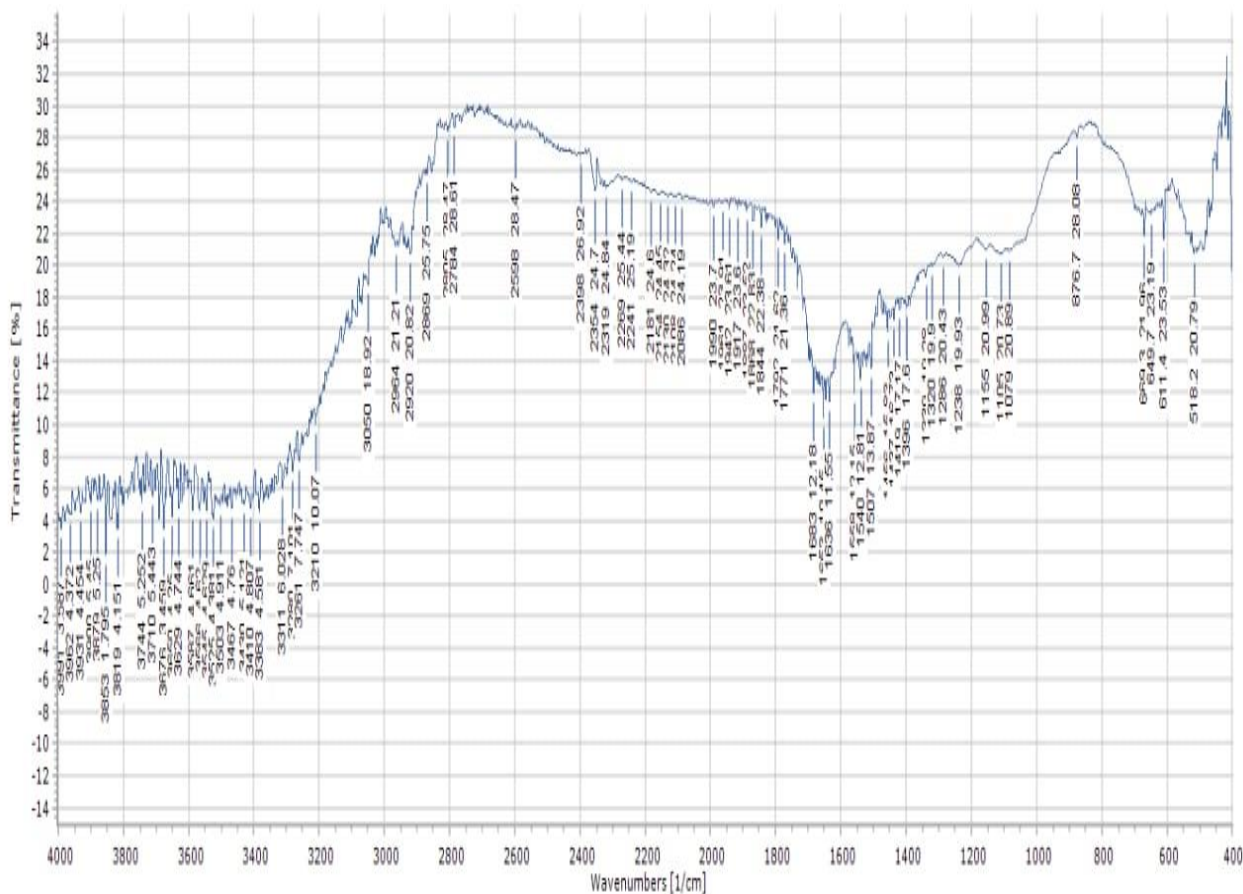


Figure 4.1 (f): Fish scales powder IR spectra after Fluoride adsorption.

From Figures 4.1 (a) and (b), the observed changes in peaks and intensities indicated that interactions leading to the adsorption actually occurred between the AIF and fluoride ions. The peaks in Figure 4.1 (a) generally shifted slightly to lower absorption values in Figure 4.1 (b). Intensity changes giving the peaks were noticeably much high implying the interactions and hence adsorption taking place.

According to Figures 4.1 (c) and (d), after fluoride adsorption, there was a reduction in the intensity of $-SO_3H$ bands at 3885 and 520 cm^{-1} in fluoride treated SPS which may be due to fluoride adsorption/exchange.

From Figure 4.1 (e) the hydroxyl group OH showed sharp peaks at around 3,850, 3750, 3650, 3350 cm^{-1} and a weak peak at 625 cm^{-1} , which corresponded to the stretching mode of hydroxyl group. A broad peak at 1250 cm^{-1} showed a single band for the phosphate group, and the peak at 1,091 cm^{-1} also corresponded to the phosphate group. The bending vibration of PO_4^{3-} was observed in bands located at 500-625 cm^{-1} , and a phosphate band appeared in the region of 400 cm^{-1} . After fluoride adsorption as depicted by Figure 4.1 (f) there was a shift in the observed peaks and more peaks appeared between 1400 to 1000 cm^{-1} , this shows the possibility of C-F bonds stretching mode. These results are in agreement with observations made by other researchers (Alhussein *et al.*, 2019).

Many studies on fluoride adsorption by different adsorbents have shown that surface sites and potential functional groups are involved and actively participate in the adsorption, especially the hydroxyl group (Xu *et al.*, 2017; Mohaptra *et al.*, 2011). However, Mondal *et al.* (2015) has found that fluoride interacts with the OH and NH groups on the coconut fiber surface impregnated with aluminum. Nonetheless, fluoride adsorption on Fe-impregnated chitosan is documented due to the fluoride-chloride ion exchange (Zhang *et al.*, 2015). Other studies using FTIR have revealed the formation of inner-spherically bonded complexes on $\gamma\text{-Fe}_2\text{O}_3$ nanoparticles with fluoride (Jayarathna *et al.*, 2015). Using FTIR and XPS analyzes it was found that hydroxyl and surface carbonates are involved in the co-exchange with fluoride ions on hierarchical magnesium oxide microspheres (Jin *et al.*, 2015) and on magnesium oxide nanoplates adsorbents (Jin *et al.*, 2016).

According to Egwuatu *et al.* (2014), the chicken feather IR spectrum has shown a range of absorption peaks that demonstrate the chicken feather's complex existence. One of

the keys to understanding the mechanism of the fluoride ion binding to chicken feathers is the functional groups. Table 4.1 displays the absorbance peaks and their corresponding intensities for the specified groups.

Table 4.1: IR data for chicken feathers

Wave number (cm^{-1})	Assigned functional group
3,379.1	OH, NH
2,919.4	C-C
1,541.08	C=C
1,031.35	PO_4^{3-} band
870.73	CO_3^{2-} band
561.79	Ca^{2+} band

The presence of NH, C=O and S=O groups on the surface of chicken feathers makes it an active site for adsorption.

Sulphonation of PS results in new absorption bands and the splitting of others, consistent with the presence of $-SO_3H$ group on the aromatic ring were observed. New absorption bands at 3,340, 1,250, and 1,078 cm^{-1} were assigned to the stretching of the $-OH$ in the -

SO₃H group and to the asymmetric and symmetric stretching of the O=S=O group, respectively (Hayat *et al.*, 2016).

The results for the SEM analyses are depicted in Figure 4.2.

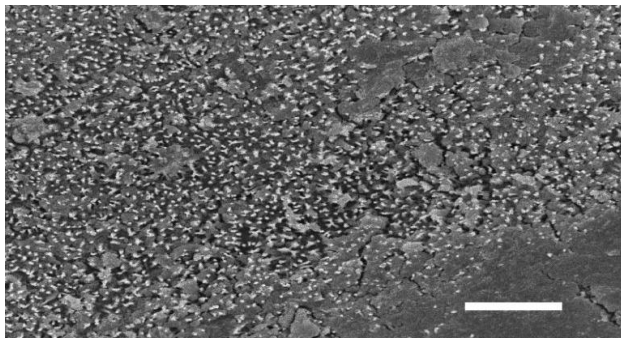


Figure 4.2 (a): AIF before adsorption

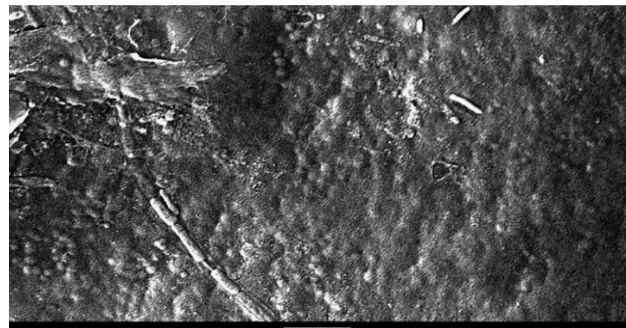


Figure 4.2 (b): AIF after adsorption

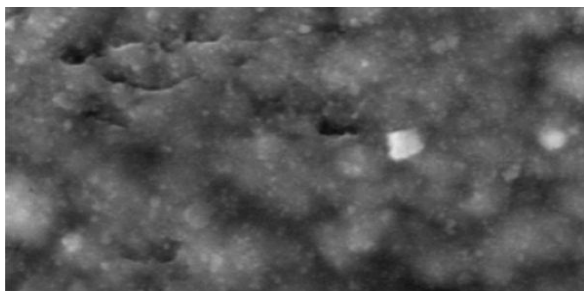


Figure 4.2 (c): SPS before adsorption

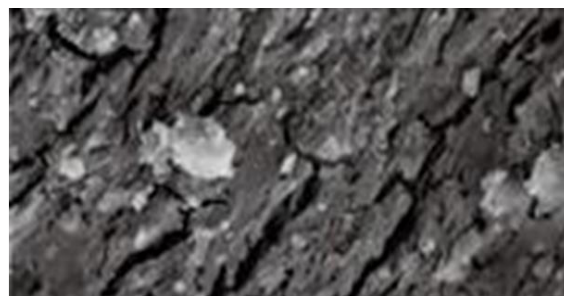


Figure 4.2 (d): SPS after adsorption

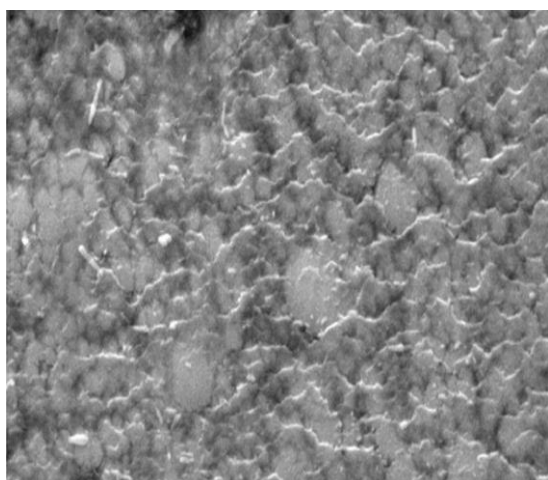


Figure 4.2 (e): Fish scales before adsorption

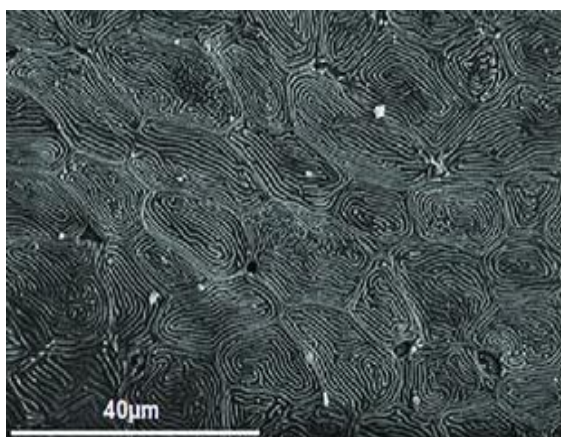


Figure 4.2 (f): Fish scales after adsorption

adsorption

(Source : Author, 2019)

From Figure 4.2 a-f the SEM images after defluoridation show morphological defects, irregular shape and in some coarse surfaces. This may be as a result of fluoride adsorption by the adsorbents. Studies carried out on characterization of physical properties and morphological structure of chicken feathers using scanning electron microscopy, indicated that a chicken feather has unique features. The barb, unlike any other natural or synthetic fibre, is a protein fibre that has low density, high flexibility, good spinning length and a hollow honeycomb structure. The rachis has low density, low rigidity, and a hollow honeycomb structure. These characteristics indicate that chicken feather barbs can be utilised to manufacture textile products either on their own or by structural interaction with other fibres. The characteristics of both the barb and the rachis, make them suitable for the manufacture of composite materials (Tesfaye *et al.*, 2017).

When Khosa *et al.* (2013) utilized chicken feathers as adsorbents for arsenic, the SEM results have shown that the untreated feathers have long shafts and barbs and a smooth surface while the surface of modified feathers shows shiny patches leading to a completely amorphous structure where the shafts and barbs of the feathers have disappeared and the original structure of the feather could not be identified. In addition, there are some regions where the surface of the feather remains intact with some levels of modification only on the surface and the surface of the feathers have become damaged and rough. The changes on the surface morphology of the adsorbents as given in Figure 4.2 are an indication of adsorption and this is further confirmed by the FTIR spectra.

4.2 Effect of modification

Modified adsorbents have been used for the anions removal because modifications alter the physical and chemical properties of adsorbents. For example, Gong *et al.* (2012), studied different types of alumina and concluded that the acidity and basicity properties of the alumina significantly affect the fluoride adsorption and not the surface area. Surfaces of biomasses contain amine, carboxyl, hydroxyl, sulfhydryl, and phosphate functional groups which could bind pollutants and remove them. The efficacy of any adsorbent is known to depend on their affinity toward fluoride ions and the capacity and specificity of the functional groups present within the adsorbent.

4.2.1 On fish scales

Table 4.2 shows the % adsorption of different modified form of the fish scales.

Table 4.2: Effect of modification on fish scales.

Type of modification	% fluoride adsorption
Ground fish scales	99.44
Magnesium modified fish scales	98.26
Aluminium modified fish scales	96.45
Calcium modified fish scales	92.38

Relative to other modified adsorbents the ground fish scales showed the highest percentage of adsorption. Thus modification did not increase the fluoride uptake by the fish scales, but modification appeared to decrease the adsorption marginally with Ca²⁺ providing the highest drop. Researchers modified chitin and chitosan by use of metal ions or covering them with silica to enhance the efficiency of fluoride adsorption from

water. The amino group that is present within chitosan establishes a coordination bond with the metal ions and helps enhance fluoride adsorption. Nonetheless, these biosorbents have demonstrated very low efficiency of removal in alkaline pH. This may be due to breakage of coordination bonds in alkaline pH and release of metal ions. This inevitably reduces the capacity of certain biosorbents to adsorb fluoride. While the efficacy of fluoride removal of modified biosorbents is considered high, they operate within a relatively small pH difference and their removal efficiency is often low when other anions are available (Suvendu *et al.*, 2018).

4.2.2 On feathers

The effect of modification on the feathers is shown in Table 4.3.

Table 4.3: Effect of modification on feathers

Type of modification	% fluoride adsorption
Ground feathers	52.38
Magnesium modified feathers	89.02
Aluminium modified feathers	94.61
Calcium modified feathers	68.03

Chemical modification greatly improved the % adsorption by the feathers; modification by aluminium gave the best adsorption of 94.61% while magnesium modified feathers gave 89.02 %. Tang *et al.* (2009) attempted to modify activated alumina to generate hydrous manganese-coated alumina (HMOCA) using manganese oxide. This study showed that HMOCA would adsorb fluoride at a pH of 5.2 ± 0.05 (adsorption capacity

q_e 7.09 mg / g). Bansiwal *et al.* (2010) synthesized copper oxide-coated aluminum (COCA) by impregnating mesoporous aluminum in a solution of copper sulfate accompanied by calcination in soil. COCA's adsorption potential is 7.220 mg / g which has been found to be three times greater than unmodified alumina.

4.2.3 On sulphonated polystyrene

The effect of modification on the sulphonated polystyrene is shown in Table 4.4.

Table 4.4: Effect of modification on sulphonated polystyrene

Type of modification	% adsorption
sulphonated polystyrene (SPS)	97.58
Magnesium modified SPS	90.05
Aluminium modified SPS	96.89
Calcium modified SPS	90.79

The results indicate that modification did not improve the adsorption of the sulphonated polystyrene, since SPS had higher percentage adsorption compared with the modified forms. Recently, it has been noted that, due to their low cost and availability, fluoride adsorption can also be achieved by chemically modified activated carbon based on biomass. Those chemically modified activated carbons, for example, are zirconium-impregnated coconut shells, aluminum hydroxide-coated rice husks and tamarind carbon shells (Kumar *et al.*, 2019). Researchers have been using metal ions and/or oxides in the recent past to alter the activated carbon. AC modified with Al^{3+} , Zr ions, Ca ions, and

manganese oxide coated demonstrated greater efficiency in fluoride removal than the unmodified ACs. In comparison, these forms of activated charcoal modifications are pollutants; use a lot of energy and modified ACs are only workable over a small pH. In addition, the metal ions used for modification could leach into the treated water and could cause health risks if ingested (Suwendu *et al.*, 2018).

4.2.4 Combined adsorbent

The feathers, sulphonated polystyrene and fish scales were combined in the ratio 1:1:1 and the fluoride adsorption percentage for the combined adsorbent was 94.95 %. Informed by the results from Table 4.2, 4.3 and 4.4, ground fish scales, sulphonated polystyrene, aluminium modified feathers and combined adsorbent were studied further on their potential of being utilized for water defluoridation. This combined adsorption value is however, lower than values for ground fish scales and SPS but higher than that of ground feathers. Therefore combined adsorbents didn't improve adsorption properties since functional groups were not modified.

4.3 Optimization of adsorption parameters

4.3.1 Effect of change in mass of adsorbent

The amount of contact surface between an adsorbent and adsorbate solution plays an important role in adsorption process. Its surface determines the amount of the reactive adsorbent surface available to the adsorbing electrolyte particles in the solution. In most cases, the amount of available sorptive surface and the amount of fluoride adsorbed increase in proportion to mass of adsorbent. The effect of change in mass of aluminium modified feathers, sulphonated polystyrene, powdered fish scales and combined adsorbents on their fluoride uptake from water was, therefore, studied under conditions

of constant adsorbate volume, adsorbate concentration (1000 mg/L), temperature (293 K), pH value (7.0) and time of contact (120 min). The results are presented in Figure 4.3.

From Figure 4.3 (a) the fluoride adsorption by Al feathers increased from just about 48.5% to 88.9% when the mass of the Al feathers was increased from 0.1 g to 0.8 g. The percentage of fluoride uptake by Al feathers then further increased to about 94.6% when the adsorbent mass was further increased to 1.6 g, thereafter increase in mass didn't result into a higher fluoride adsorption percentage. Such improvement in F⁻ removal efficiency with increased adsorbent dosage may be ascribed to improved adsorptive surface quality in solution. Further increase in the doses did not lead to major changes in defluoridation. It is because the active sites converge at higher adsorbent concentrations, thus lowering the total surface area (Piyush *et al.*, 2012) and also due to non-adsorbability of fluoride ion as a result of sorbent-sorbate interaction (Puthenvedu *et al.*, 2012).

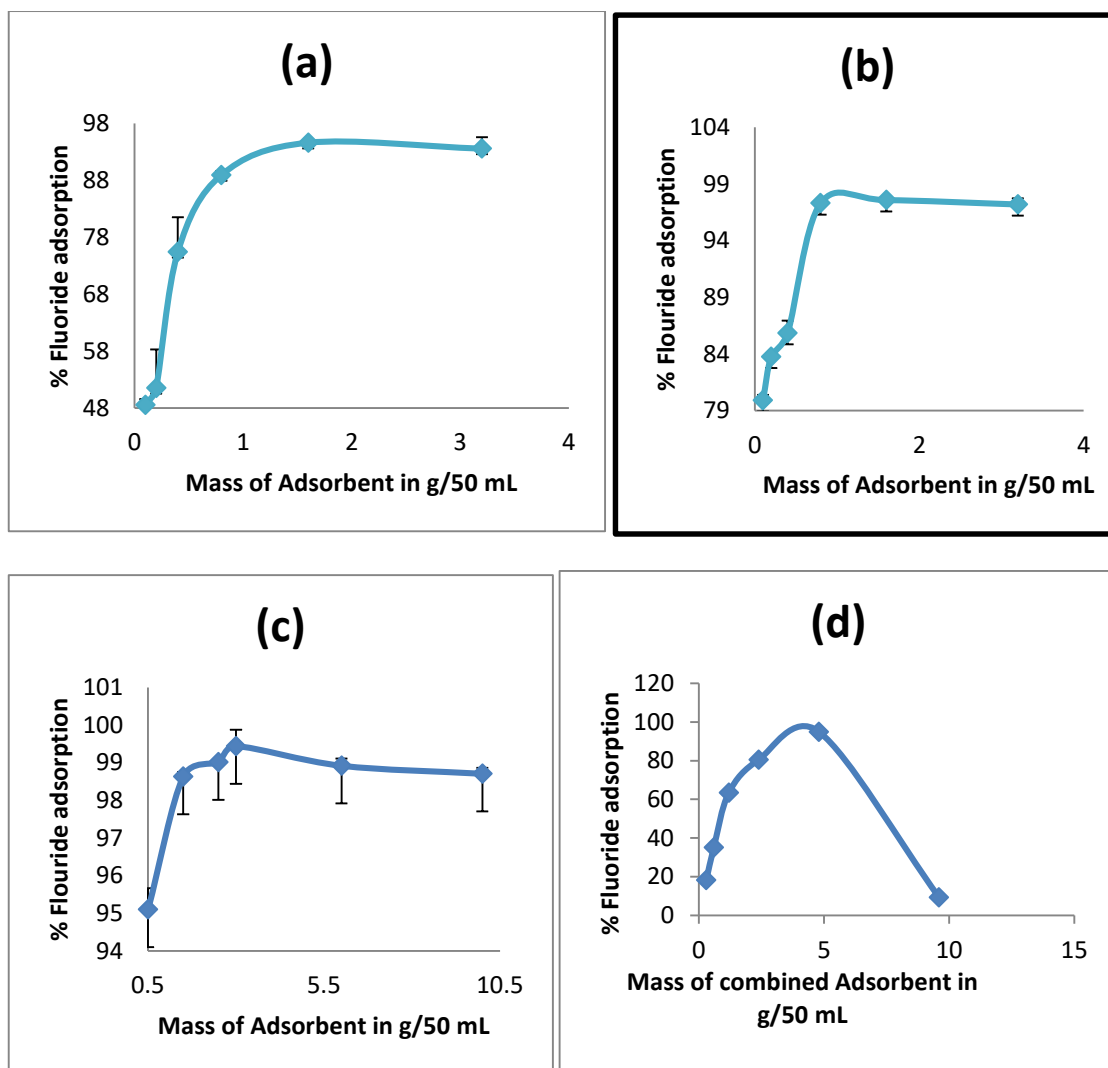


Figure 4.3: Effect of change in adsorbent dosage on fluoride adsorption onto different adsorbents.

(a) Aluminium modified feathers, (b) sulphonated polystyrene and (c) fish scales (d) combined adsorbent. [Experimental conditions: 1000 mg/L fluoride concentration, 120-min contact time, and pH value of 7.0 at 293 K]

The highest fluoride adsorption percentage by Al feathers was observed at a mass of 1.6 g of adsorbent. Adsorbent doses of 1.6 g/mL were, therefore, adopted in all subsequent fluoride uptake tests using feathers.

Figure 4.3 (b) shows, on the other hand, fluoride uptake by sulphonated polystyrene (SPS) increased with increasing mass of adsorbent. Fluoride removal from solution could be achieved at 1.6 g/mL doses. The adsorbent ratio of 1.6 g/mL which was maintained in all the subsequent tests was adequate for over 95% fluoride adsorption from water under the conditions of these tests. This shows that sulphonated polystyrene can be used as a low-cost adsorbent for water defluoridation.

The effect of increase in mass on fluoride adsorption by powdered fish scales is illustrated by Figure 4.3 (c). The percentage adsorption of fluoride onto the powdered fish scales increased from 95% with a mass of 0.5 g/mL to 99% with a mass of 3 g/mL. Such a trend is mostly attributed to an increase in the sorptive surface area and the availability of more active adsorption sites. This Figure also shows a slight decrease of percent removal with increase of adsorbent dose. This behaviour could be due to the formation of aggregates between the powdered scale particles and overlapping of active sites at high adsorbent doses, reducing the effective active site area (Hugo *et al.*, 2013). The adsorption of fluoride by combined adsorbent Figure 4.3 (d) also increased steadily with increase in mass from 18% to 94.9 % with mass ranging between 0.3 to 4.8 g/mL, thereafter it decreased sharply to about 9% when the mass was 9.6 g/mL, this could be due to adsorbate-adsorbent interactions. Therefore 4.8 g was used as optimum mass for combined adsorbent.

4.3.2 Effect of change in adsorption contact time

Adsorption of fluoride ion by adsorbent also depends on the interactions of functional groups between the solution and the surface of adsorbent. Adsorptions can be assumed to be complete when equilibrium is achieved between the solute of solution and the

adsorbent. However, specific time is needed to maintain the equilibrium interactions to ensure that the adsorption process is complete (Kavita *et al.*, 2016). The effect of change in contact time unto the adsorption of fluoride by Al feathers, sulphonated polystyrene, powdered fish scales and combined adsorbent is shown in Figure 4.4.

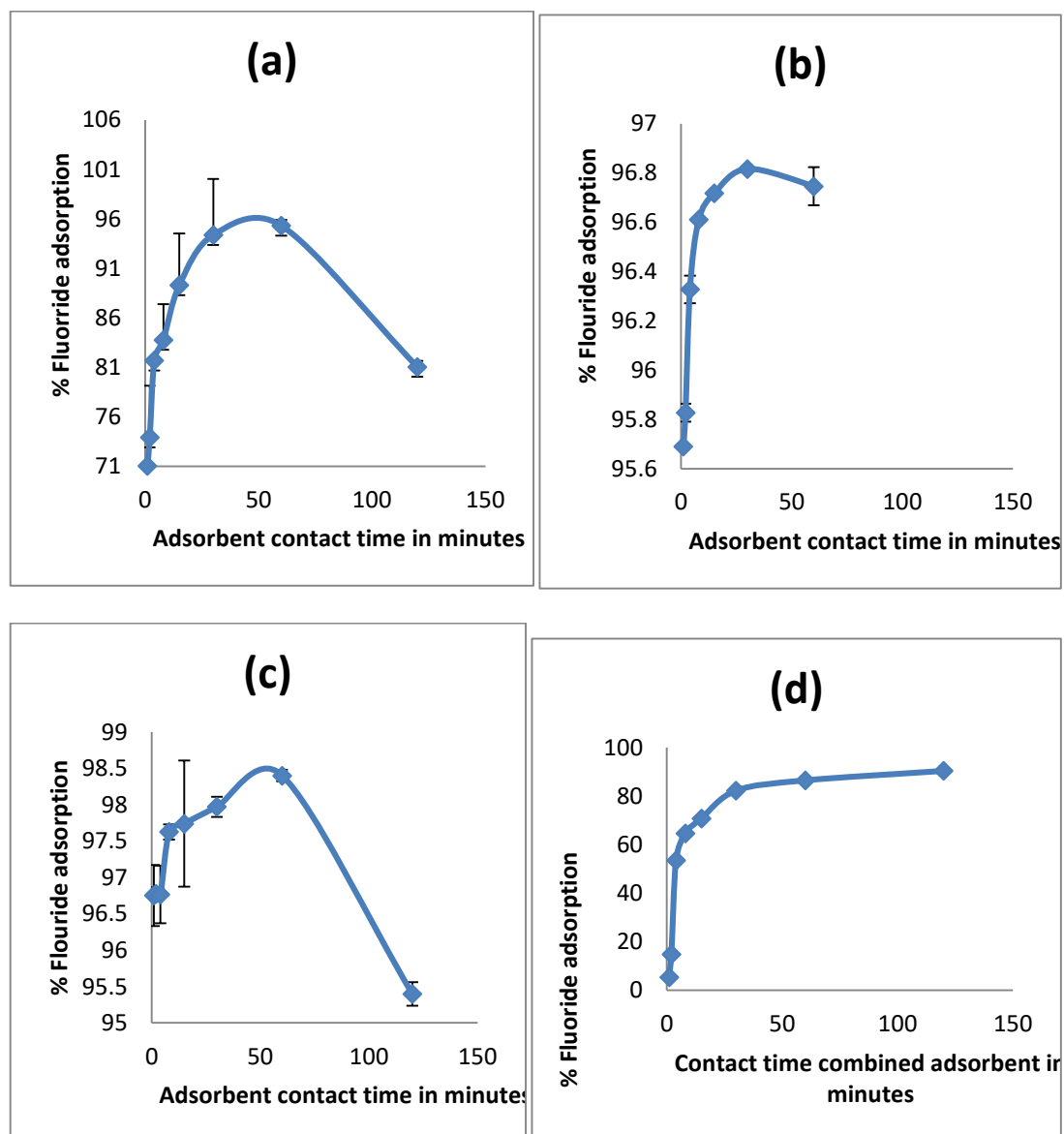


Figure 4.4: Effect of contact time on fluoride adsorption onto different adsorbents.

(a)Al feathers, (b) sulphonated polystyrene, (c) powdered fish scales and (d) combined adsorbent and [Experimental conditions: Fluoride concentration, = 1000 mg/L; pH 7.0, Temperature, T= 293 K; and mass of adsorbent 1.6 g/mL for Al feathers, 1.5 g/mL SPS, 3 g/mL for fish scales and 4.8 g/mL for combined adsorbent batch dosage].

The effect of contact time on fluoride adsorption onto Al feathers is shown by Figure 4.4 (a). The percentage adsorption of fluoride onto the feathers increased from 71% when time was 1 minute to the highest % of 95 after 60 minutes, beyond this time adsorption percentage decreased sharply. Similarly, the equilibrium time for the sulphonated polystyrene, fish scales and combined adsorbent from Figures 4.4 (b), (c) and (d) was 30 minutes, 60 minutes and 120 minutes, respectively. The percentage adsorption showed a similar trend for the feathers and fish scales, where it rose steadily and then dropped sharply after equilibrium time. On the other hand % adsorption by the SPS and combined adsorbents remained constant after the equilibrium time. This observation may be as a result of adsorption sites having been exhausted. For each of the adsorbent the optimum contact time was adopted for the subsequent batch experiments. A significant factor in the fluoride removal is the contact time between adsorbing material and aqueous solution. Studies have shown that at the start of the remediation process, the rate of removal of contaminants from water using biomaterials was higher (Waheed *et al.*, 2009). It is because reaction sites are depleted as activity progresses resulting in lower pollutant absorption rate (Waheed *et al.*, 2009; Mbugua *et al.*, 2014).

4.3.3 The effect of change of agitation rate on adsorption

The effect of the agitation rate increases to some degree, after which the adsorption rate remains constant (Puthenveedu *et al.*, 2012). How the agitation rate affected the adsorption of fluoride onto the adsorbents is shown in Figure 4.5.

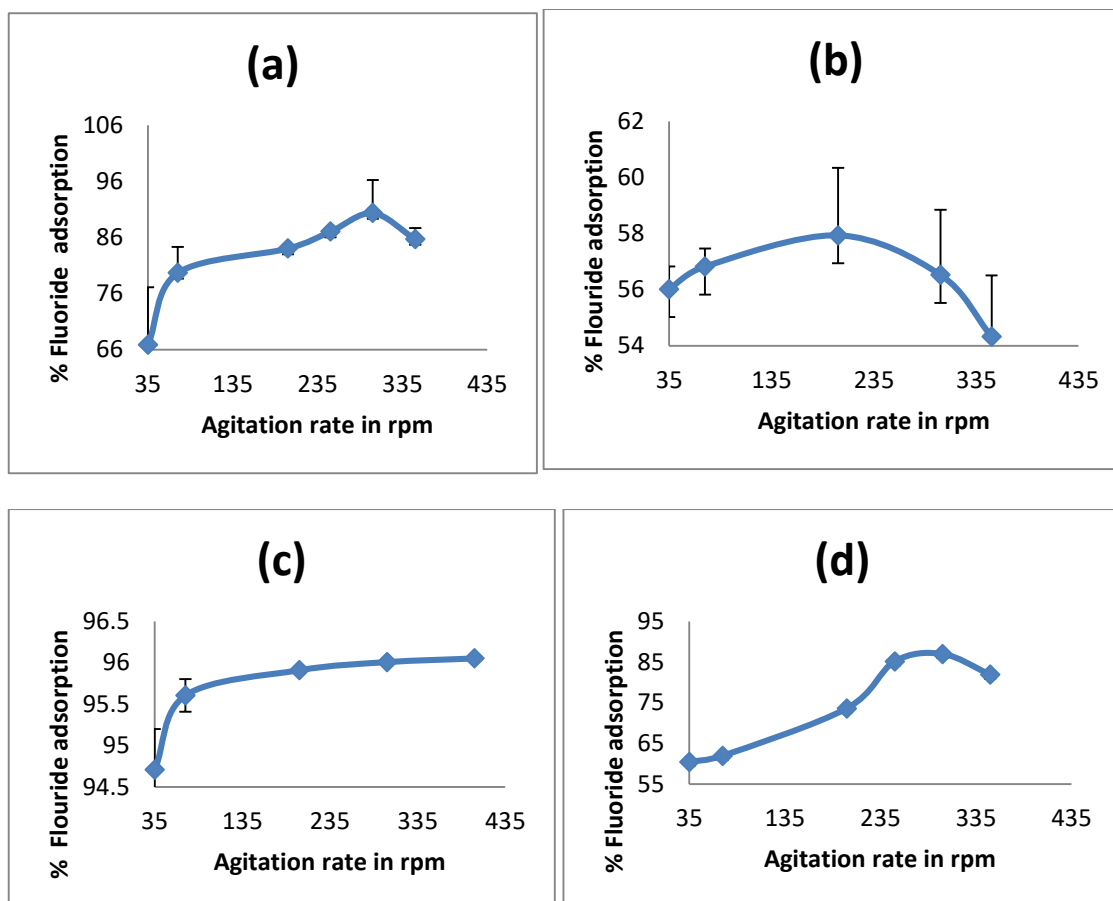


Figure 4.5: Effect of agitation rate on fluoride adsorption onto different adsorbents.

(a) Al feathers, (b) sulphonated polystyrene, (c) powdered fish scales, (d) combined adsorbent and [Experimental conditions: Fluoride concentration, $C_0 = 1000$ mg/L; Temperature, pH 7.0, $T = 293$ K; 1.6 g/mL for Al feathers, 1.5 g/mL SPS, 3 g/mL for fish scales and 4.8 g/mL adsorbent batch dosage, time of 60 minutes for Al feathers and fish scales, 30 minutes for SPS and 120 minutes for combined adsorbent]

From Figure 4.5 (a), the percentage adsorption increased steadily from 66-90% with agitation rate of 35-300 rpm, thereafter a decrease in the adsorption percentage is observed as the agitation rate increase. The percentage adsorption for SPS, Figure 4.5 (b) ranged between 55-57% with agitation rate between 35-200 rpm, beyond agitation rate of 200 rpm the percentage adsorption decreased sharply to about 54%. According to Figure 4.5

(c), the effect of agitation rate on adsorption had values of 95-96% with agitation rate between 35-435 rpm, initially percentage adsorption increased steadily then remained constant. For the combined adsorbents, Figure 4.5 (d) when agitation rate was 35 rpm the percentage adsorption was 60, thereafter increase in agitation rate resulted in steady increase in adsorption up to 87% and then decreased. In all the four adsorbents when there was increase in agitation rate, the % adsorption increased up to an optimum percentage and thereafter decreased except for SPS where the % adsorption remained constant.

The optimum agitation rate for Al feathers was 300 rpm with % adsorption of 90, 400 rpm for fish scales with % adsorption of 96%, 300rpm for SPS with a % adsorption of 58% and 300 rpm for combined adsorbent with adsorption of 87%. Reduced adsorption may be due to increased turbulence and therefore reduced thickness of the boundary layer around the adsorbent particles as a result of increasing the degree of mixing. This is in line with the knowledge in the literature (Puthenveedu *et al.*, 2012). Reduction of the thickness of the boundary layer around the adsorbent particles as a result of stirring or agitation increases adsorption efficacy (Hanafiah *et al.* 2009). Hence the concentrations of fluoride ions near the adsorbent surface may be increased with increasing stirring intensity. Also, increased agitation results to enhanced mass transfer of fluoride ions from bulk solution to the adsorbent surface reducing the adsorption equilibrium time.

4.3.4 Effect of change in fluoride solution pH

The effect of pH on fluoride adsorption by different adsorbents was studied at pH values of 1-13. The adsorbate pH was adjusted by addition of small amounts of 1 M NaOH or 1 M HCl using 50- μ L pipettes. The percentage of fluoride adsorption was plotted as a

function of initial solution pH and the results presented in Figure 4.6. From Figure 4.6 (a), fluoride adsorption onto Al feathers increased from 82% to 90% when the solution pH was increased from 1 to 5 and then dropped beyond pH 7. This shows that the highest fluoride uptake by feathers occurred at pH 5.

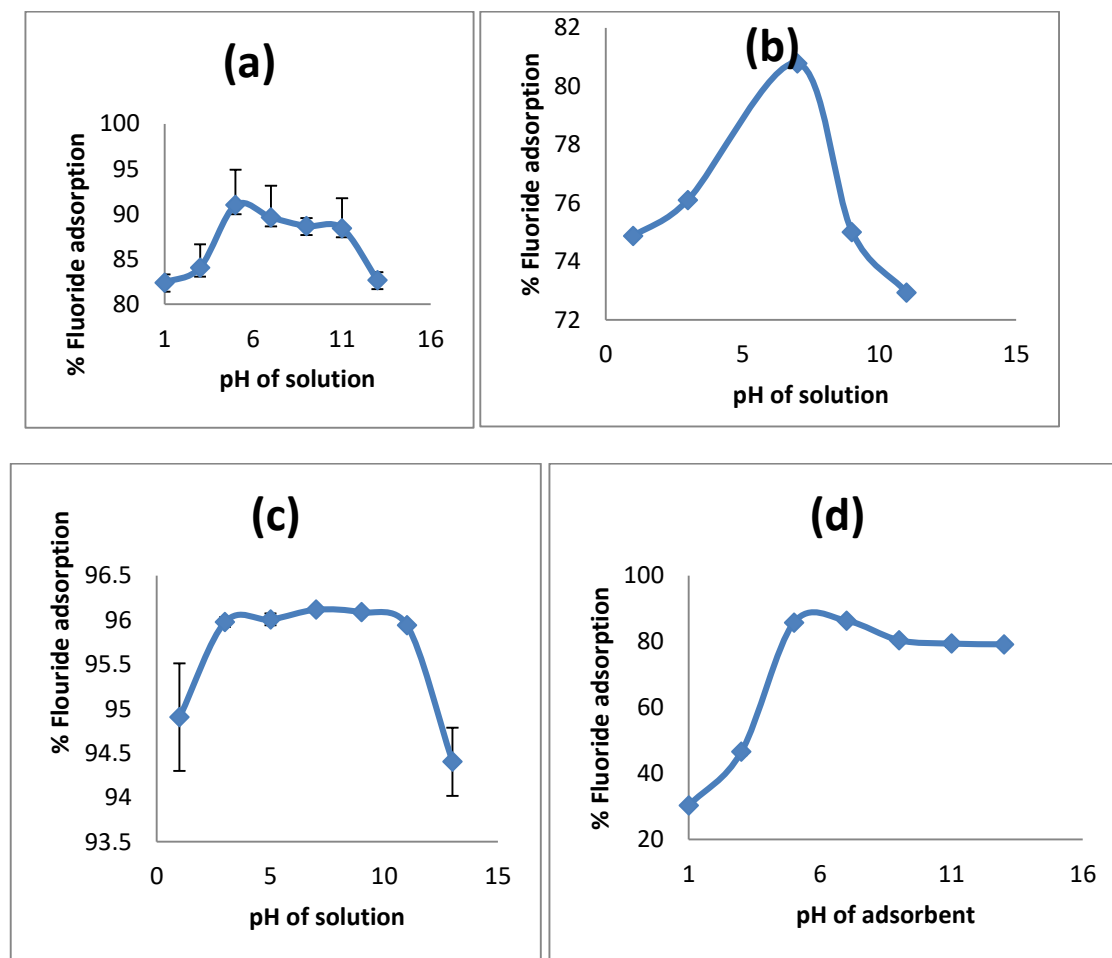


Figure 4.6: The Effect of change in solution pH on fluoride adsorption onto different adsorbents.

(a) feathers, (b) sulphonated polystyrene, (c) powdered fish scales, (d) combined adsorbent and [Experimental conditions: Fluoride concentration, $C_0 = 1000$ mg/L; Temperature, $T = 293$ K; 1.6 g/mL for Al feathers, 1.5 g/mL SPS, 3 g/mL for fish scales and 4.8 g/mL combined adsorbent batch dosage, time of 60 minutes for Al feathers and fish scales, 30 minutes for SPS and 120 minutes for combined adsorbent, agitation rate

of 300 rpm for Al feathers, 400 rpm for fish scales, 350 rpm for SPS and 300 rpm for combined adsorbent].

From Figure 4.6 (b), percentage adsorption of fluoride by SPS increased steadily from 74% to 87% with a pH range of 1-7, there after the adsorption percentage decreased sharply when the pH was between 9-11. Fluoride adsorption by fish scales at different pH values according to Figure 4.6 (c) showed that the adsorption percentage increased from 94% to 96%, which, however, remained constant between pH 4-11 but dropped beyond pH values of 10. In Figure 4.6 (d) the percentage adsorption rose steadily from 30-86% with pH values between 1-7, but with increased pH the percentage adsorption dropped to a constant value of 80%. The optimum pH of solution for combined adsorbent was 6 and the adsorption of fluoride was found to be pH dependent.

It has been found that fluoride removal efficiency of adsorbent increases with increased pH values (Keerthi, 2015). Because the protonated surface is responsible for adsorption of anions, the highest adsorption of fluoride in many adsorbents occurs at acidic pH (Goswani & Purkait, 2012) and decreases at higher pH values. For adsorbents such as activated alumina, pH regulation of the fluoride adsorption at zero loads (pH_{zpc}). Due to the positively charged alumina complexes on fluoride removal by acidic alumina, adsorption showed an growing pattern at a given selected pH. After pH_{zpc}, fluoride adsorption decreased because the concentration of protonated surface sites decreased with increased pH (Kamble *et al.*, 2010) which causes strong competition of hydroxide ions. Furthermore, fluoride adsorption into different adsorbents has been reported to vary significantly at high and low pH values (Yasinta *et al.*, 2018).

4.3.5 Effect of change in solution temperature

Temperature plays a double role in the fluoride sorption process. Temperature can impact physical binding processes of fluoride to a sorbent. However, temperature also can have a direct impact on the physical properties of a sorbent, if thermally treated prior to exposure, so that sorption capacities can be significantly altered. Most sorption studies are conducted at room temperature in laboratory settings. As temperature increased, sorption was shown to be less favoured most likely due to increased deprotonation or hydroxylation of the surface causing more negatively charged sorbent surfaces. This is an important observation to note when attempting to apply defluoridation methods on site in hot climates, for sorption capacities attained under room temperature conditions may be higher than in the field as a result of increased temperatures (Kavita *et al.*, 2016). The effect of change in solution temperature on fluoride adsorption onto Al feathers, SPS, fish scales and combined adsorbent was carried out at different temperatures between 288 K - 353 K and the results are shown in Figure 4.7.

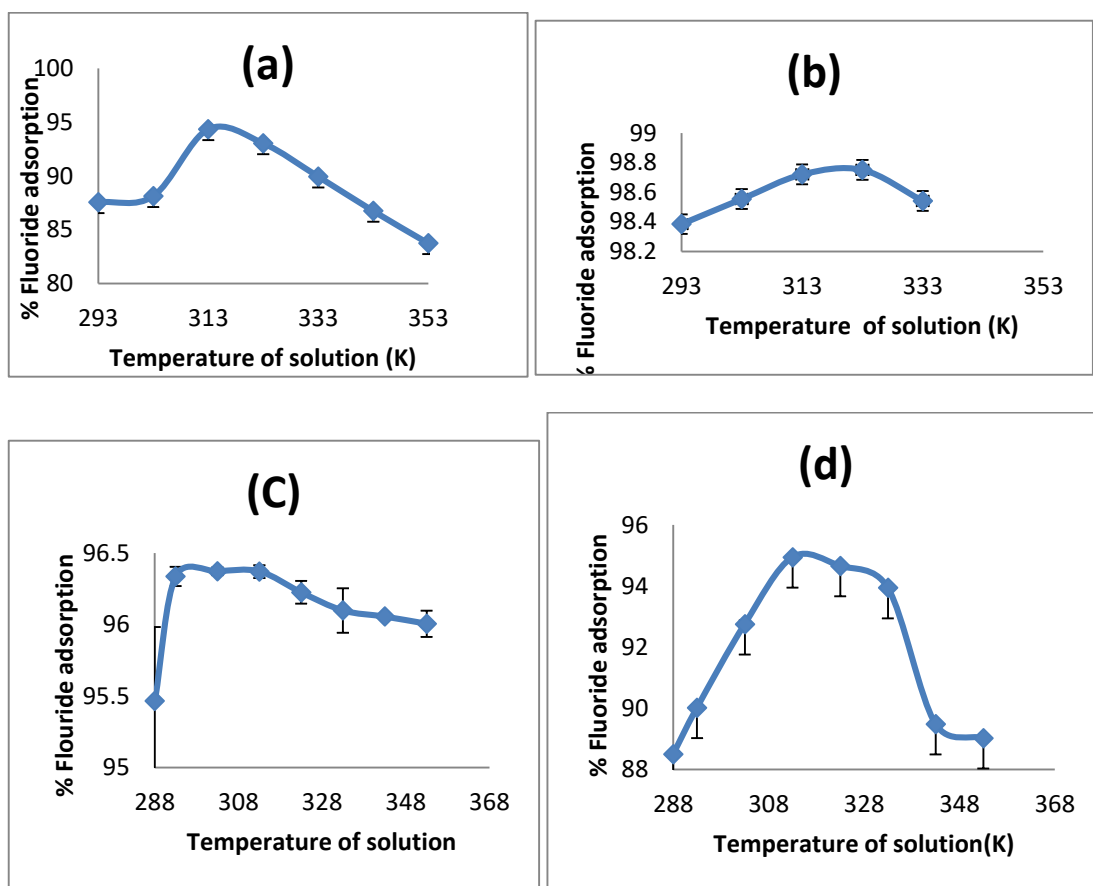


Figure 4.7: The Effect of change of temperature on fluoride adsorption onto different adsorbents.

(a) Al feathers, (b) sulphonated polystyrene, (c) powdered fish scales, (d) combined adsorbent and [Experimental conditions: Fluoride concentration, $C_0 = 1000$ mg/L; 1.6 g/mL for Al feathers, 1.5 g/mL SPS, 3 g/mL for fish scales and 4.8 g/mL combined adsorbent batch dosage, time of 60 minutes for Al feathers and fish scales, 30 minutes for SPS and 120 minutes for combined adsorbent, agitation rate of 300 rpm for Al feathers, 400 rpm for fish scales, 350 rpm for SPS and 300 rpm for combined adsorbent, pH of 5 for Al feathers, pH 7 for SPS and scales and pH 6 for combined adsorbent].

From Figure 4.7 (a) the adsorption of fluoride onto Al feathers increased steadily from 87-94% between a temperature range of 293-313 K, and then decreased thereafter between temperature of 313-353 K. The adsorption of fluoride onto SPS at different temperatures from Figure 4.8 (b), illustrates that the optimum temperature was 323 K with 98.75% adsorption, in addition the adsorption percentage across the different temperatures did not have a wide range since mostly the adsorption was 98%. For the fish scales the effect of thermal change from Figure 4.7 (c) revealed that the adsorption was between 95-96% across the different temperatures, the optimum temperature was however, 303 K with adsorption of 96.37%. Similarly, for the combined adsorbent Figure 4.7 (d), adsorption increased from 88-94% with temperature of 288-313 K, a decrease in adsorption followed thereafter with increase in temperature. The current results, therefore, showed that fluoride adsorption onto feathers, SPS fish scales and combined adsorbent was typically an endothermic process as also postulated elsewhere in literature (Sujana *et al.*, 2009).

4.3.6 Effect of adsorbate concentration

The effect of change in fluoride concentration on its removal from water using the adsorbents was studied under conditions of 1.6 g/mL for Al feathers, 6 g/mL SPS, 3 g/mL for fish scales and 4.8 g/mL combined adsorbent batch dosage, time of 60 minutes for Al feathers and fish scales, 30 minutes for SPS and 120 minutes for combined adsorbent, agitation rate of 300 rpm for Al feathers, 400 rpm for fish scales, 350 rpm for SPS and 300 rpm for combined adsorbent, pH of 5 for Al feathers, pH 7 for SPS and scales and pH 13 for combined adsorbent and constant temperature (313 K Al for feathers, 303 K fish scales, 323 K for SPS and 313 K for combined adsorbent and the results presented in Figure 4.8.

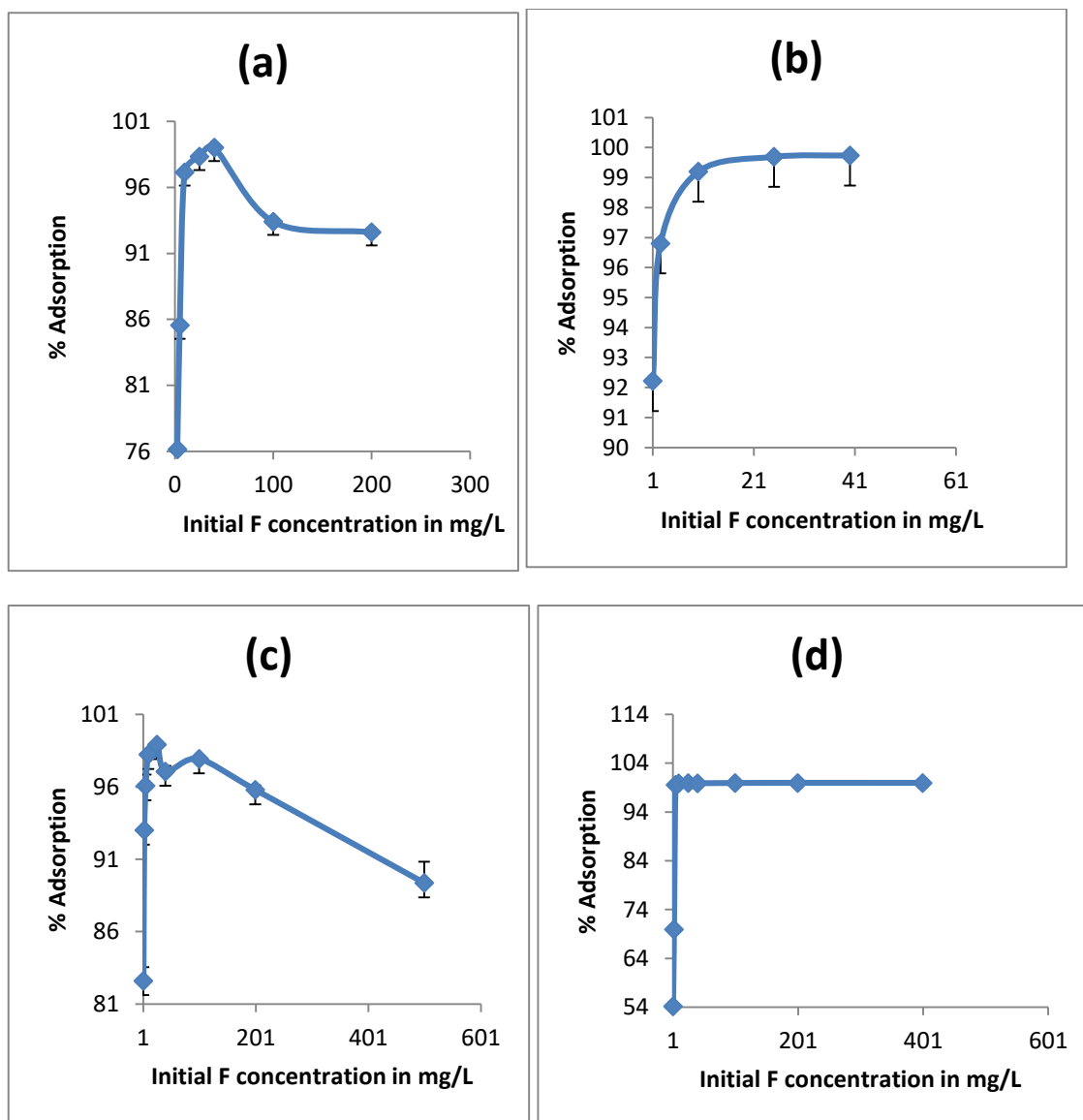


Figure 4.8: Effect of change in initial adsorbate concentration on fluoride adsorption onto different adsorbents.

(a) Al feathers, (b) SPS (c) fish scales and (d) combined adsorbent.

The results from Figure 4.8 (a) indicate that the percentage removal for feathers increased between 2.5-40 mg/L initial fluoride concentration where the adsorption percentage ranged from 76-99 %, there after the adsorption decreased. According to Figure 4.8(b) SPS adsorption increased with an increase in the initial concentration of fluoride then remained constant (99.7 %) after 10 mg / L fluoride solution concentration. This is due

to the lack of the active sites accessible on the adsorbent surface. The effect of initial fluoride concentration on adsorption of fluoride by fish scales, Figure 4.8 (c) shows a similar trend as the feathers where the adsorption increased to 98% with 25 mg/L initial fluoride concentration and then reduced steadily. For the combined adsorbent, Figure 4.8 (d) shows that adsorption increased sharply from 54-99% with initial fluoride concentration between 1-5 mg/L, but remained almost constant at around 100% with increase in fluoride concentration from within a range of 5-400 mg/L. Active sites for adsorption are fixed and as the concentration increased more of these sites were occupied resulting in the observed increase in fluoride uptake. But, it got to a point where nearly all the active sites are filled up at high concentration which accounts for the formation of plateau at high concentrations. According to Palanisamy *et al.* (2012) the capacity of the adsorbent gets sharply exhausted with increase in the initial concentration of fluoride in aqueous phase. Adsorption sites for a fixed amount of an adsorbent are limited and become saturated at high concentration (Bhaumik *et al.*, 2011).

Fluoride removal efficiency decreased with increasing initial fluoride concentration for a constant adsorbent dose and contact time. The decrease in removal efficiency at higher initial fluoride concentrations is due to the saturation of the active sites of the adsorbent. The total capacity of the adsorbents increased when the initial fluoride concentration increased. This can be attributed to the utilization of the less accessible or energetically less active sites because of increase in diffusivity and activity of fluoride ion upon increasing initial fluoride concentration. The interiors of the porous adsorbents contain more sites than exteriors. However, the sites present on the interior surface of a pore may not be as easily available as the sites on the exterior surface because of the resistance to the pore diffusion (Kefyalew *et al.*, 2012).

4.4 Equilibrium Analysis

Adsorption isotherms are useful in describing how the adsorbate particles interact with adsorbent sites at equilibrium and they are relevant in optimization of adsorption protocol. The Langmuir and Freundlich isotherms are perhaps the most satisfactory models for describing the removal of adsorbates from aqueous systems (Wambu, 2015). The Giles, Langmuir and the Freundlich isotherms were applied in this study. The “isotherm”, a curve describing the retention of a substance on a solid at various concentrations, is a major tool to describe and predict the mobility of this substance in the environment. These retention/ release phenomena are sometimes strongly kinetically controlled, so that time-dependence of the sorption isotherm must be specified.

4.4.1 The Giles isotherm

The Giles isotherms for the data obtained in this study are shown in Figure 4.9.

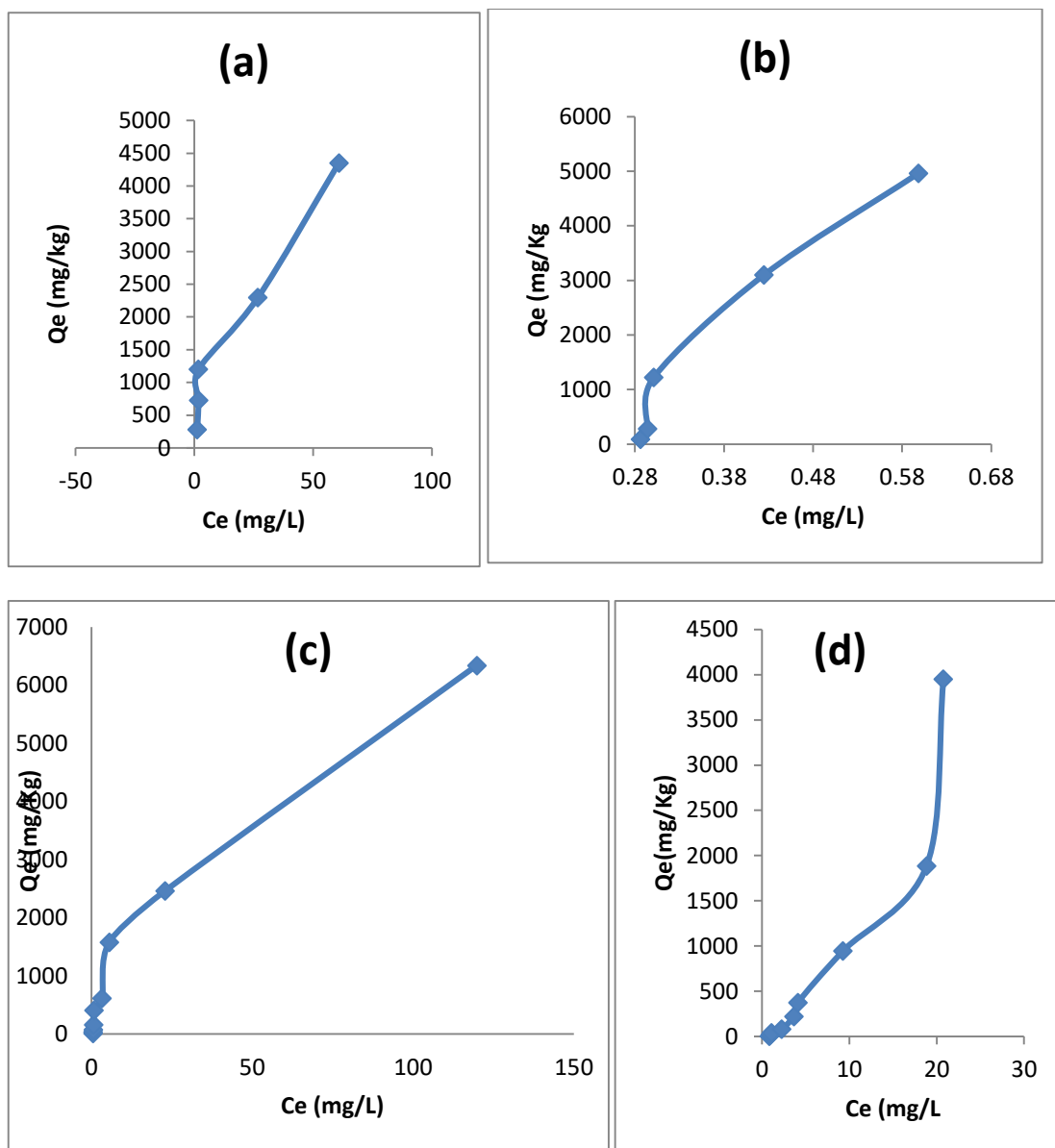


Figure 4.9:The Giles isotherms for (a) Al feathers, (b) SPS, (c) fish scales and (d) combined adsorbent.

According to Figure 4.9 Al feathers, SPS and fish scales show a similarity with the C isotherm classification by Giles. The feature common to these systems is a substrate which is microporous and a solute which on general chemical considerations is expected to have higher affinity for the substrate than has the solvent. A linear isotherm is therefore consistent with conditions in which the number of sites (not necessarily of equal energy)

remains constant throughout the whole range of solute concentrations up to saturation of the substrate.

This means that the surface available for adsorption expands proportionally with y , the amount of solute adsorbed (Hinz, 2001). On the other hand combined adsorbents curve shows a resemblance with the S Giles classification of isotherms. The tangent of the angle, relative to the y -axis, of any portion of these curves represents the increment of concentration of solute (or vapour) in the external phase, necessary to maintain a constant increment of concentration, at equilibrium, in the substrate. The complement of this angle, that is, the slope of the isotherm at any point, may thus be regarded as a measure of the ease with which bombarding solute molecules can find vacant sites in the surface. The slope at first increases with concentration, because in cooperative adsorption, sites capable of retaining a solute molecule increase, this means that the fluoride adsorption at equilibrium for the AIF, SPS and fish scales was as a result of at least two opposite mechanisms hence cooperate adsorption.

4.4.2 Langmuir isotherm

Langmuir equation is based on the assumption of a monolayer of adsorbate molecules.

It is of the form,
$$Q_e = \frac{x}{m} = \frac{(aV_m C_e)}{(1+aC_e)}$$

4.1

where,

a = adsorption bond energy;

V_m = maximum adsorption density (corresponding to monolayer formation on the adsorbent).

C_e = equilibrium concentration

Q_e = equilibrium adsorption capacity

Linear form of the equation is,

$$\frac{C_e}{x} = \frac{1}{aV_m} + \left(\frac{1}{V_m}\right) C_e$$

4.2

A plot of $\frac{C_e}{x}$ against C_e , yields a straight line. The Langmuir constants a and V_m were calculated from intercept and slope, respectively. The respective linear plots of Langmuir isotherms for fluoride adsorption onto the adsorbents were constructed from the relevant equilibrium data and presented in Figure 4.10. The resulting equilibrium constants were then computed and presented in Table 4.5.

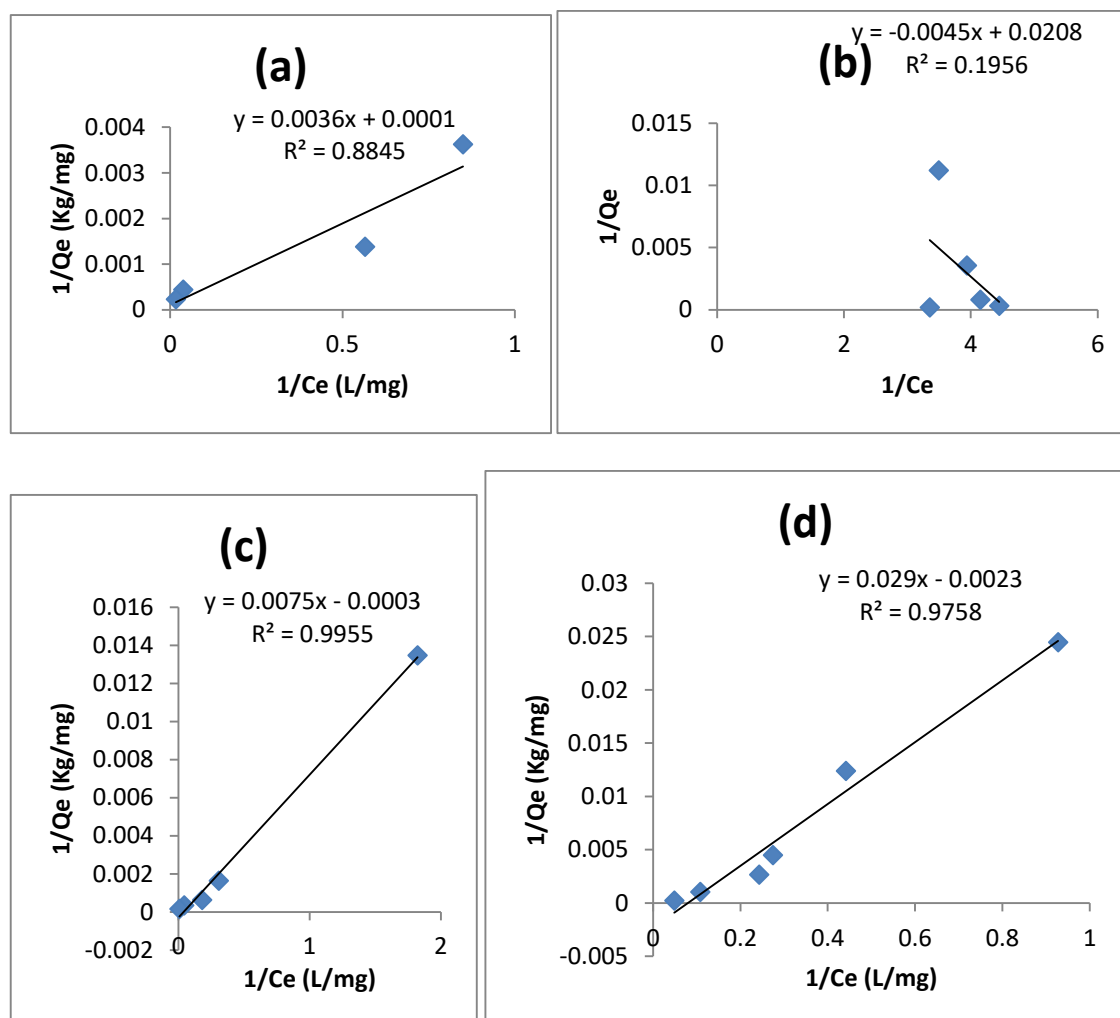


Figure 4.10: Langmuir isotherm plots for the adsorption of fluoride onto different adsorbents. Al feathers, (a) SPS (b); Fish scales(c) and combined adsorbents (d).

Table 4.5: Langmuir isotherm constants for the adsorption of fluoride onto the adsorbents

Adsorbent	pH	Temperature(K)	q_m (mg/g)	b	R^2
Al feathers	5	313	285.7143	0.00000035	0.8845
SPS	7	303	22.22222	0.000936	0.1965
Fish scales	7	323	133.1327	0.00000229	0.995503
Combined adsorbent	13	313	34.48276	0.0000667	0.9758

From Figure 4.10, it was observed that the equilibrium data were very well represented by the Langmuir isotherm model for fish scales, combined adsorbents and Al feathers with correlation coefficients values of 0.9955, 0.9758, and 0.8845, respectively. The SPS, Figure 4.10 (b) had a correlation coefficient of 0.1956 meaning the system didn't fit the Langmuir isotherm. The best fit of equilibrium data in the Langmuir isotherm expression predicted the monolayer coverage of fluoride ions onto the adsorbents (Uddin *et al.*, 2007). Therefore, the results suggest that a monolayer of fluoride ions is adsorbed on homogeneous adsorption sites on the surface of the adsorbents (Mourabet *et al.*, 2017). From Table 4.5 it was also observed that the maximum sorption capacity of Al feathers, SPS, fish scales, and combined adsorbents were found to be 285.71, 22.22, 133.13, and 34.48 mg/g, respectively. This study demonstrated that Al feathers had relatively high adsorption capacity compared to other adsorbents used in the study. The

values of the Langmuir constants, q_m and b , indicated efficient fluoride binding onto the adsorbents. However, fish scales gave strongest binding followed by combined adsorbents while SPS was least. This results are consistent with other results by other reasearchers (Mourabet *et al.*, 2017).

4.4.3 Freundlich isotherm

Freundlich 's nonlinear form of equation is:

$$\frac{x}{m} = KC_e^{\frac{1}{n}}$$

4.3

where,

$\frac{x}{m}$ = Quantity adsorbed per unit adsorbent weight (mg / g) or capacity for adsorption

C_e = Concentration of the solution in equilibrium in mg / L.

V = volume of the solution in mL.

K = Unit constant depending on temperature and is known as adsorption coefficient Freundlich. This reflects the capability to adsorb.

n = Freundlich constant, which for preferred adsorption should be between 1 and 10.

Values of "n" larger than unity indicate that adsorption at low concentration is relatively more effective.

This equation is conveniently used in the linear form by taking the log on both sides as,

$$\log \frac{x}{m} = \log K + \left(\frac{1}{n}\right) \log C_e$$

4.4

A $\log(x / m)$ plot against $\log C_e$, yield a straight line. The constants K and n , respectively, are calculated from the intercept and the slope.

The respective linear plots of Freundlich isotherms for fluoride adsorption onto the adsorbents were constructed from the relevant equilibrium data and presented in Figure 4.11. The resulting equilibrium constants were then computed and presented in Table 4.6.

Table 4.6: Freundlich isotherm constants for the adsorption of fluoride onto the adsorbents

Adsorbent	pH	Temperature(K)	K_f	n	R^2
Al feathers	5	313	347.5123	1.651528	0.939
SPS	7	303	22.22222	0.000936	0.0421
Fish scales	7	323	133.1327	0.00000229	0.969666
Combined adsorbent	13	313	34.48276	0.0000667	0.9931

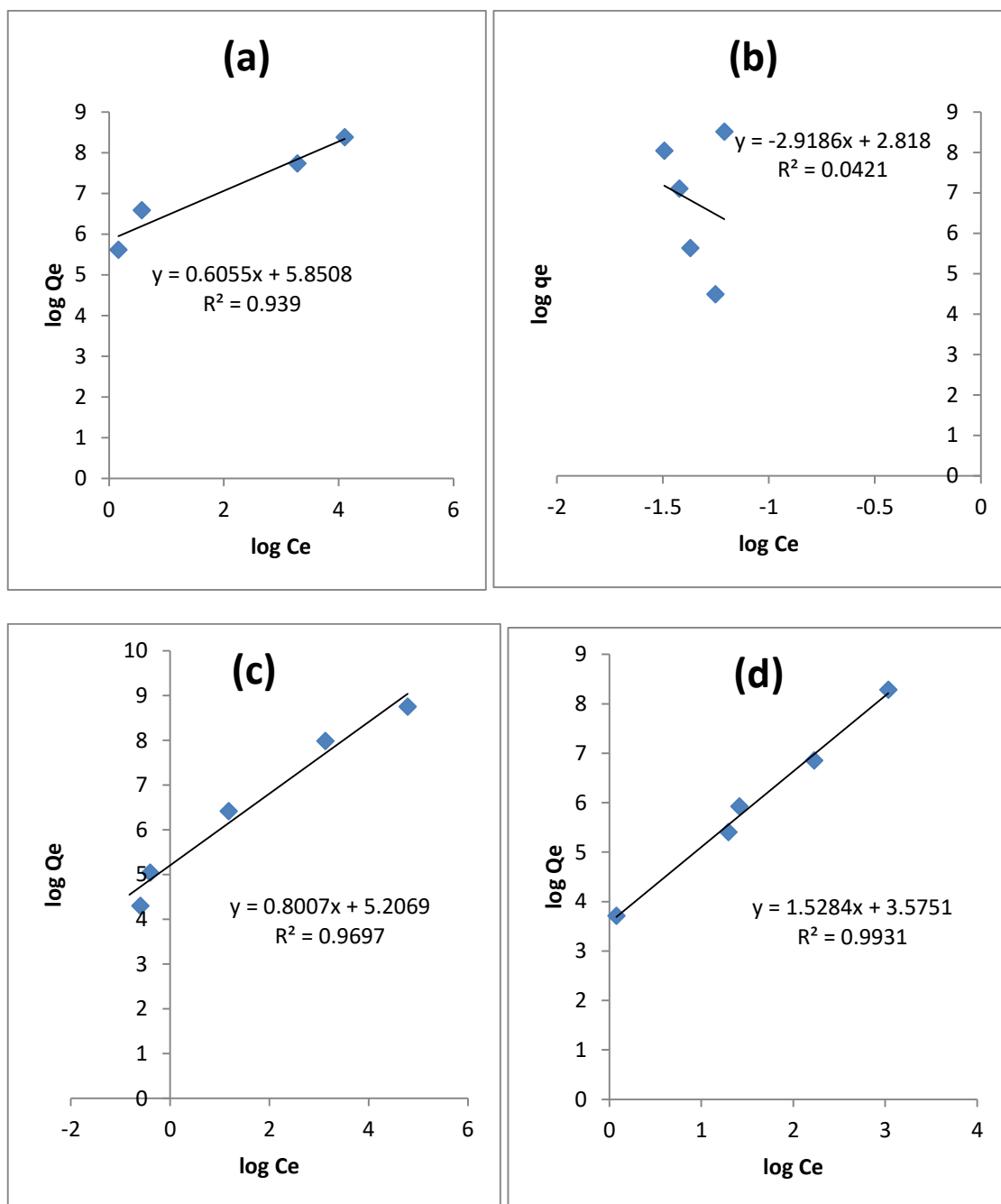


Figure 4.11: Freundlich isotherms for fluoride adsorption onto the adsorbents.

(a) Al feathers, (b) SPS, (c) fish scales, and (d) combined adsorbents.

From Table 4.6, the constant n , adsorption intensity values for SPS, fish scales and combined adsorbents were less than one implying favourable adsorption while that of Al feathers was 1.65 to suggest that adsorption at low concentrations was relatively more

effective. The k_f values followed the order of AIF>fish scales>combined adsorbents>SPS and compared to other results the value of k_f were high indicating rate of adsorbate removal was high (Fairouz *et al.*, 2015). The combined adsorbents, fish scales and Al feather had high correlation R^2 values greater than 0.9 hence the adsorbents well fitted the Freundlich model except SPS which had an R^2 value of 0.0421 meaning the system could not be well described by this model.

4.5 Adsorption kinetics

Fluoride adsorption onto surfaces requires the movement of adsorbent fluoride particles from the bulk adsorbent solution to the adsorbent surface. The adsorbate particles then interact with reactive sites in the adsorbent surface or penetrate into the inner adsorbent sites in the crystalline lattice of soil adsorbents (Wambu, 2015). The pseudo-first order kinetic model equation 2.22, pseudo-second order kinetic model equation 2.27 and the Weber and Morris intra particle diffusion model equation 2.28 were applied onto the adsorbents. This was done to test the influence of external diffusion on fluoride adsorption onto the adsorbents, to investigate the nature of interactions between fluoride particles and the adsorbent sites and to assess existence of intraparticle diffusion of fluoride into inner pores of the adsorbents.

4.5.1 Pseudo First order kinetic model

Lagergren's pseudo-first order rate law was applied onto Al feathers, SPS, fish scales and combined adsorbent. The linear plots for the law was constructed and the derived kinetics constants presented in Figure 4.12 and in Table 4.7.

Table 4.7: Kinetics constants for Pseudo-first order fluoride adsorption onto the adsorbents.

Adsorbent	$K_{1\text{ ads}}(\text{min}^{-1})$	$q_e(\text{mg/kg})$	R^2
Al feathers	2.412	32099.63	0.9972
SPS	0.499751	2.893343	0.9882
Fish scales	0.478103	1.001842	0.9974
Combined	0.23007	123026.9	0.9525

adsorbents

[T (K): 303; Co (mg/L): 1000; pH: 7; M (g/100 mL): 293-40].

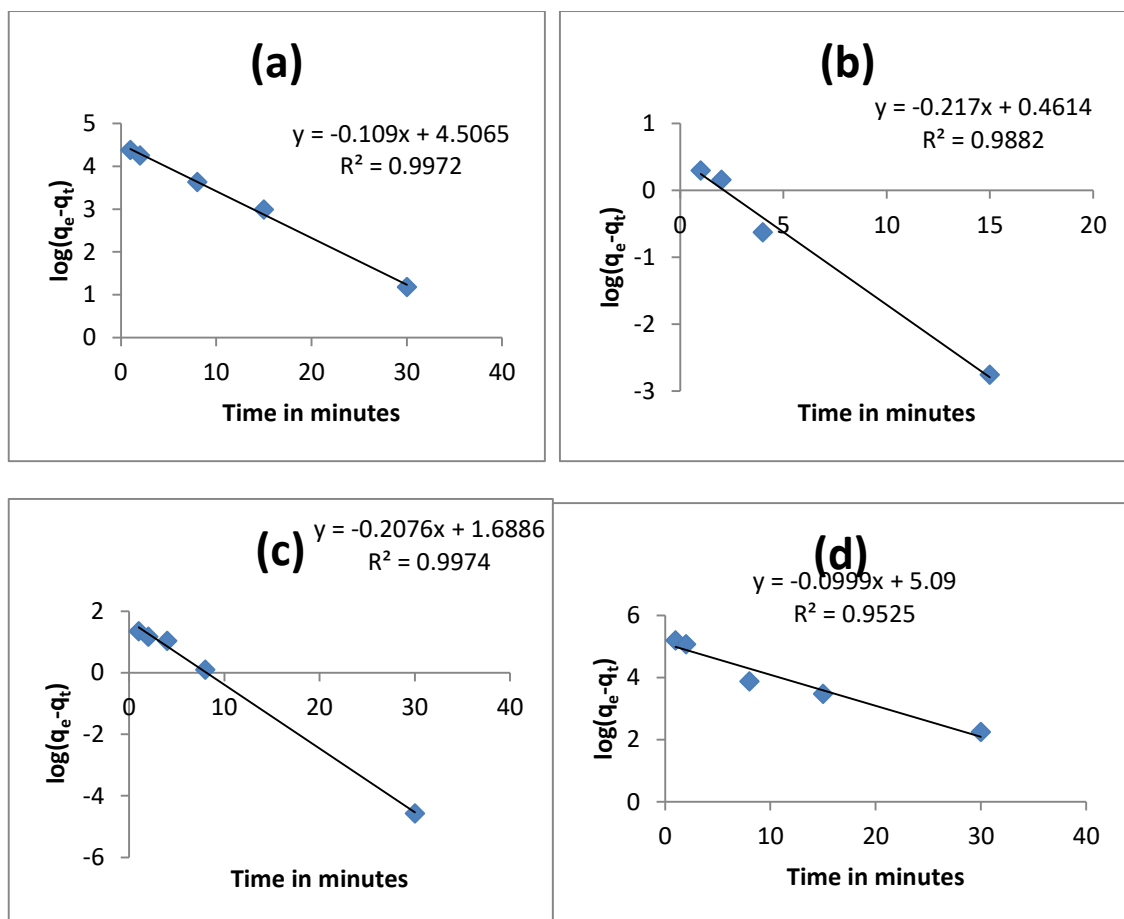


Figure 4.12: Time profile for fluoride adsorption onto adsorbents showing Lagergren pseudo-first order plot.

(a) Al feathers, (b) SPS, (c) Fish scales and (d) combined adsorbent. [Experimental conditions: T (K): 303; Co(mg/L): 1000; pH7; M (g/100 mL): 50].

From Figure 4.12, the R^2 were in the order of fish scales > Al feathers > SPS > combined adsorbents. Therefore the fish scales were best described by this model with R^2 value of 0.9974, closely followed by Al feathers with R^2 value of 0.9972. The Lagergren's rate equation is one of the most widely used rate equations to describe the adsorption of adsorbate from the liquid phase. The plots were found to be linear with good correlation coefficients (>0.9) indicating the applicability of pseudo first-order model in this study. The pseudo first-order rate constant (K_1) and $q_e(\text{cal.})$ values were determined for each adsorbent from the slope and the intercept of corresponding plot. Basing on these results

the applicability of this model is feasible on the fish scales and AI feathers. The results of this study are consistent with other studies (Zazouli *et al.*, 2014).

4.5.2 Pseudo Second order kinetic model

The plots of t/q_t versus t for the four adsorbents are shown in Fig. 4.13. The values of $q_e(\text{cal.})$ and K_2 were determined for each adsorbent from the slope and intercept of the corresponding plot and are compiled in Table 4.8

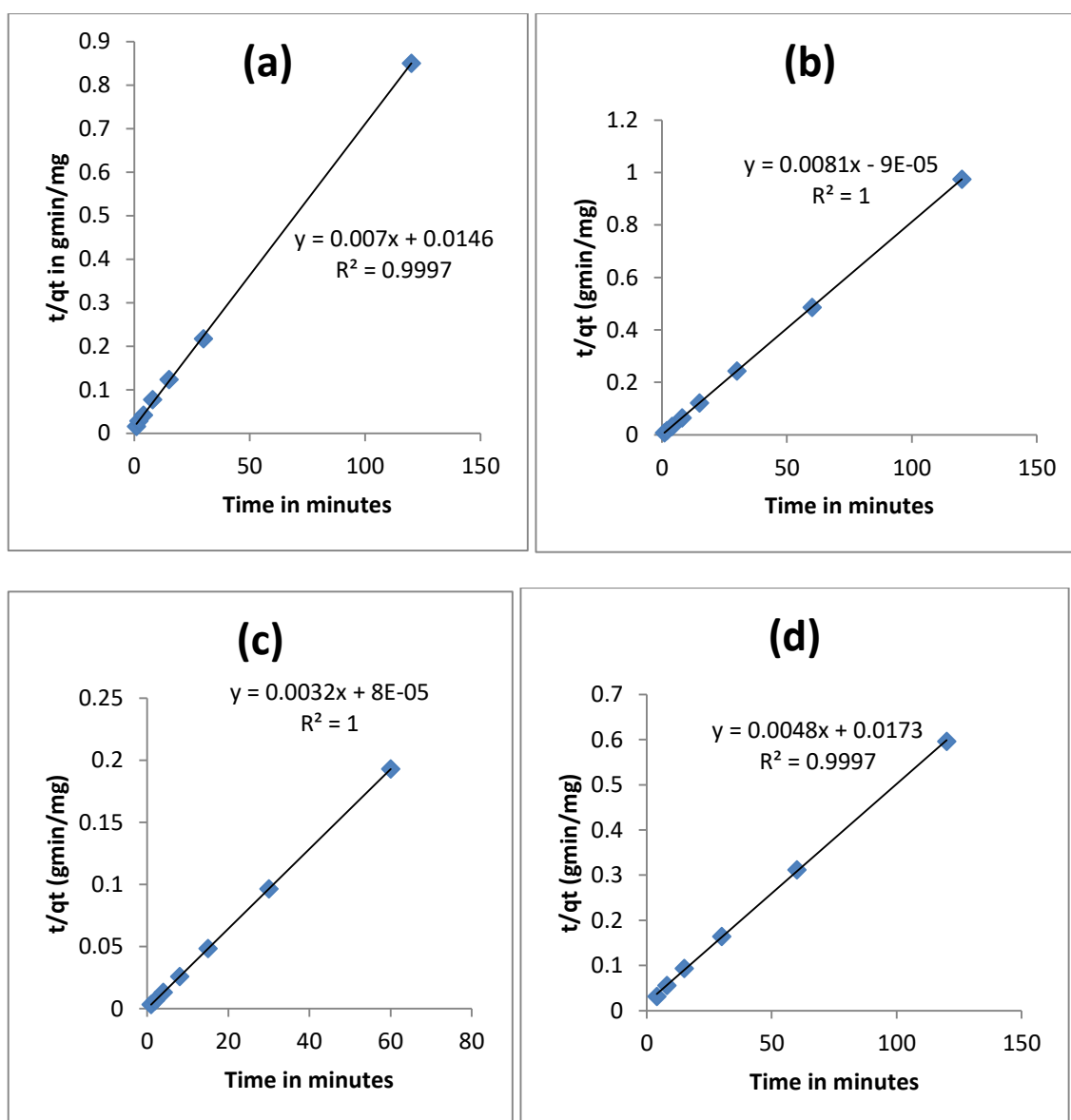


Figure 4.13: Time profile for fluoride adsorption onto adsorbents showing pseudo-second order plot.

(a) Al feathers, (b) SPS, (c) Fish scales and (d) combined adsorbent. [Experimental conditions: T (K): 303; C_o (mg/L): 1000; pH7; M (g/100 mL):50].

Table 4.8: Kinetics constants for Pseudo-second order fluoride adsorption onto the adsorbents.

Adsorbent	$h_0=k_{2,ads} q_e^2$ (mg/g/min)	$k_{2,ads}$ (g/mg/min)	q_e (mg/g)	R^2
Al feathers	68.49315	0.47945	142.8571	0.9997
SPS	11111.11	89.971	123.4568	1
Fish scales	12500	40	312.5	1
Combined	57.8035	0.27746	208.333	0.997

[T (K): 303; C_o (mg/L): 1000; pH: 7; M (g/100 mL): 293-40].

The correlation coefficient (R^2) values for pseudo second-order adsorption model had high values, that is, above 0.999 for all adsorbents. Comparatively in each case, the R^2 value were higher than those of the corresponding pseudo first-order model. This indicates that the adsorption kinetics of fluoride onto Al feathers, SPS, fish scales and the combined adsorbent could be better described by pseudo second order model. A similar phenomenon has been observed by others for the adsorption of fluoride on various adsorbents (Tej & Majumder, 2016). This showed that the rate of fluoride adsorption onto the adsorbents was controlled more strongly by surface reactions between the adsorbent sites and adsorbate fluoride particles than by external transfer processes. The results concur with what is reported in literature (Waghmare & Arfin, 2015).

4.5.3 Weber and Morris Intra-particle Diffusion Model

The rate of sorption is frequently used to analyze the nature of the “rate-controlling step,” and the use of the intra-particle diffusion model has been greatly explored in this regard which is represented by the following Weber and Morris equation 2.28. Weber and Morris plots of q_t versus $t^{0.5}$ are shown in Fig. 4.14 for, (a) Al feathers, (b) SPS, (c) fish scales and (d) combined adsorbent, Table 4.9 shows the kinetic constants.

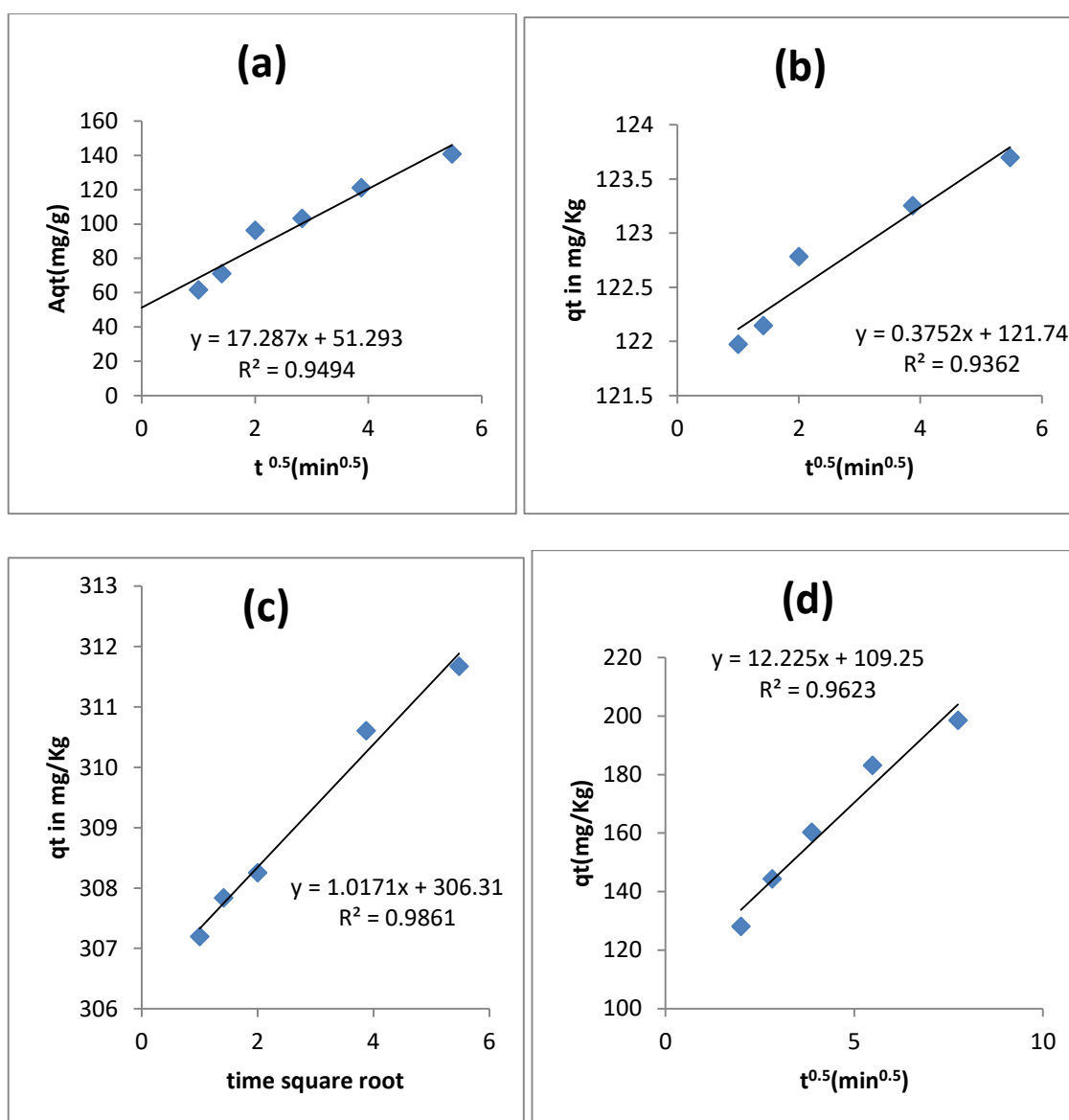


Figure 4.14: Time profile for fluoride adsorption onto adsorbents showing Weber-Morris intraparticle diffusion plot.

(a) Al feathers, (b) SPS, (c) Fish scales and (d) combined adsorbent. [Experimental conditions: T (K): 303; C₀(mg/L): 1000; pH7; M (g/100 mL):50].

Table 4.9: Kinetics constants for Weber and Morris Intra-particle Diffusion Model fluoride adsorption onto the adsorbents.

Adsorbent	k _p (mg/Kg/min ²)	C	R ²
Al feathers	17.287	51.293	0.9494
SPS	0.3752	121.74	0.9362
Fish scales	1.0171	306.31	0.9861
Combined	12.225	109.25	0.9623

[T (K): 303; C₀ (mg/L): 1000; pH: 7; M (g/100 mL): 293-40].

According to this model, the plot of uptake, q_t , versus the square root of time ($t^{0.5}$) should be linear if intraparticle diffusion is involved in the adsorption process and if these lines pass through the origin then intra-particle diffusion is the rate-controlling step (Yakout & Elsherif, 2010). When the plots do not pass through the origin, this is indicative of some degree of boundary layer control and this further shows that the intra-particle diffusion is not the only rate-limiting step, but also other kinetic models may control the rate of adsorption, all of which may be operating simultaneously.

In this study all the R² values were greater than 0.9, implying applicability of this model to the adsorption data. Intra-particle diffusion kinetics, therefore, controlled fluoride adsorption onto the adsorbents. The plots did not pass through the origin therefore there was some level of boundary layer control hence the intra-particle diffusion is not the only

rate-limiting step. The linear plots show that nearly 50% of fluoride was rapidly taken up by adsorbents. This is attributed to the immediate utilization of the most readily available adsorbing sites on the adsorbent surfaces. The fluoride adsorption by adsorbents may be governed by the initial intra-particle transport of fluoride controlled by surface diffusion process (Yakout & Elsherif, 2010).

4.6 Adsorption Thermodynamics

In any adsorption process, both energy and entropy considerations must be taken into account in order to determine what process will occur spontaneously. Values of thermodynamic parameters are the actual indicators for practical application of a process (Yakout & Elsherif, 2010). The Gibb's free energy change, ΔG^0 , is the fundamental criterion for assessment of the spontaneity of a chemical process. A more negative value of ΔG^0 indicates a more feasible process (Wambu, 2015). The ΔG for fluoride uptake by adsorbents was examined based on the Langmuir thermodynamic equilibrium constant, b according to the equation:

$$\Delta G^0 = RT \ln(b) \quad 4.4$$

The enthalpy change (ΔH^0) and entropy change (ΔS^0) were then determined based on equation:

$$\Delta G^0 = \Delta H^0 + T\Delta S^0 \quad 4.5$$

The corresponding van't Hoff's plots as well as the values of ΔG^0 , ΔH^0 and ΔS^0 , which were computed from the respective plots, are presented in Figure 4.15 and in Table 4.10.

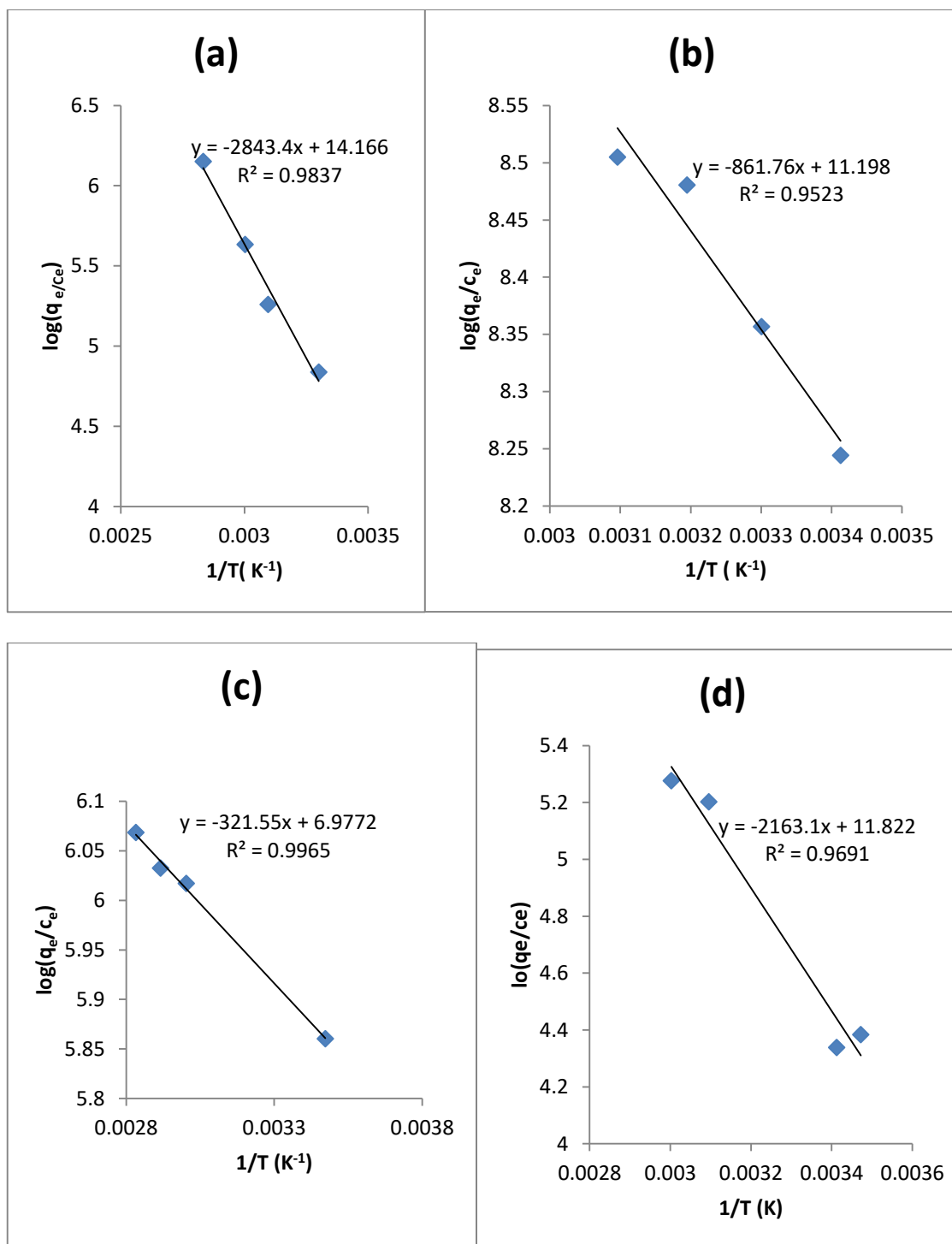


Figure 4.15: Regressions of van't Hoff's plot for fluoride adsorption onto different adsorbents. (a) Al feathers, (b) SPS, (c) Fish scales and (d) combined adsorbent

Table 4.10: Thermodynamic parameters for the uptake of fluoride by the adsorbents.

Thermodynamic quantity	Temperature (K)	Al feathers	SPS	Fish scales	Combined adsorbent
ΔH° (kJ/mol)	-	+23640.03	+7163.34	+2673.37	+17938.32
ΔS° (kJ/mol/K)	-	+117.776	+93.100	+58.008	+98.288
ΔG° kJ/mol)	288	-35594.03	-	-31096.39	-23023.2
			16698.52		
	293	-36211.98	-	-31636.26	-23422.9
			16988.42		
	303	-37447.88	-	-32715.99	-32715.99
			17568.23		
	313	-38683.79	-	-33795.73	-25021.74
			18148.04		
	323	-39919.69	-	-34875.46	-25821.15
			18727.85		

The values of ΔG° decreased with increasing temperature of fluoride adsorption onto the adsorbents. The positive values of ΔS° with the corresponding negative value of ΔG° confirmed feasibility of fluoride adsorption onto the adsorbents. It also showed that spontaneity of fluoride adsorption onto the adsorbents increased with increasing temperature of reaction. The values of the adsorption enthalpy, ΔH for fluoride adsorption onto the adsorbents were positive, as expected for a spontaneous endothermic process.

The results are in agreement with what is reported in literature (Waghmare & Arfin, 2015). The positive values of ΔH indicate the presence of an energy barrier in the adsorption and endothermic process (Yakout & Elshirif, 2010). The positive values of entropy change (ΔS) reflect good affinity of fluoride ions towards the sorbent and the increasing randomness at the solid-solution interface during the adsorption process.

4.7 Fluoride removal from natural high-fluoride water

4.7.1 Batch tests

To verify the applicability of the Al feathers, SPS, fish scales and combined adsorbent in practical defluoridation of water, batch adsorption experiments were then conducted on water samples from a high-fluoride natural source from Lake Elementaita, Nakuru County, Kenya and the results presented in Figure 4.16.

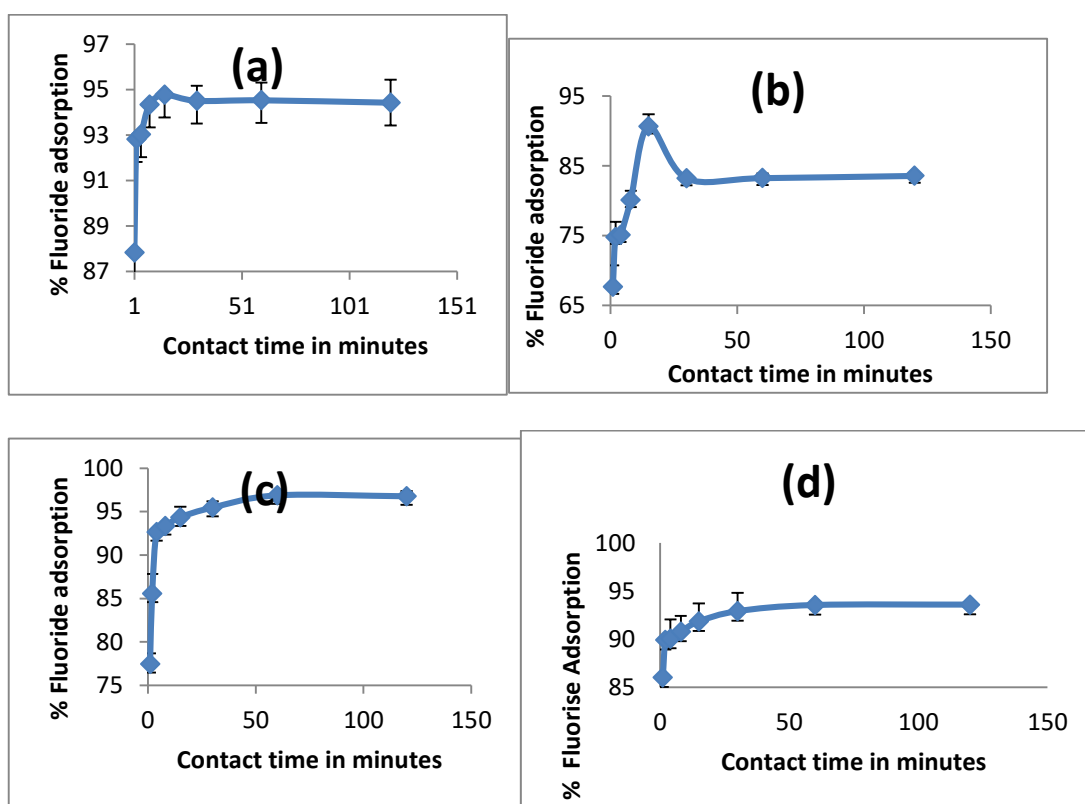


Figure 4.16: Fluoride removals from natural high-fluoride water using (a) Al feathers, (b) SPS, (c) Fish scales and (d) combined adsorbent.

[Experimental conditions: Fluoride concentration = 50 mg/L, pH = 7 T = 299 K, adsorbent dosage = 0.1 g/mL].

As depicted in Figures 4.16 (a) and (b), after an initial rapid increase in fluoride adsorption to 95% and 90% for Al feathers and SPS, respectively the percentage fluoride adsorption from water using the adsorbent declined to 94% and 83% for the adsorbents. The build-up adsorption took place in 15 min for both Al feathers and SPS. It showed that after initial fluoride adsorption, adsorbed fluoride was desorbed from the adsorbent surface back into the water. It can be assumed that the water contained components for example other anions that were able to solubilise sorbed fluoride particles from the adsorbent surfaces and kept it in solution. In addition this was due to decrease in the availability of the binding sites as the concentration increased. A similar trend was observed in the analysis of environmental water samples from Lake Baringo (Topperwien *et al.*, 2007). However, the percentage removal was slightly lower as compared to that of model solutions. This can be attributed to the environmental factors such as presence of other ions which may compete with the uptake of fluoride ions in the environmental water.

Figure 4.16 (c) and (d) show that adsorption increased up to a given percentage then remained constant. These matrices displayed very high % and were as follows: 96% and 93% for fish scales and combined adsorbent respectively, within 60 minutes.

The removal of fluoride from water using Al feathers, fish scales and combined adsorbent depicted a stepwise process indicating heterogeneity in the adsorptive surface of the adsorbents. The adsorption process, in this case, was not accompanied by concordant resolubilization of solute fluoride from the adsorbent surface (Wambu, 2015). It

demonstrated the probability of convenient use of these adsorbents in water defluoridation. Column adsorption tests using natural high-fluoride water were, therefore, conducted for the combined adsorbent and the results discussed in the subsequent sections.

4.7.2 Column water defluoridation using combined adsorbent

The performance of the combined adsorbents in water defluoridation was studied in up-flow adsorption experiments mounted in Pyrex columns using natural water containing 400 mg/L fluoride and the breakthrough curve shown in Figure 4.17, from which the values of C_0 (initial adsorbate concentration), increased with increase in effluent volume. At a flow rate of 10 mL/min, more than 87% fluoride removal was achieved in the initial stages. The effluent fluoride concentration then remained constant at 348.8 mg/L after about 75 mL of effluent volume. Initially sorbent was regarded to be exhausted easily, breakthrough point was at 145 mg/L selected arbitrarily at lower value of break point concentration for the effluent concentration and exhaustion point concentration was 348.8 mg/L closely imminent influent concentration of adsorbate. From Figure 4.17, 25 mL and 65 mL were the volume of effluent corresponding to break point concentration and exhaustion point concentration, respectively. These results agree with what has been reported in literature by other researchers (Patel, 2019).

The fluoride adsorption data based on the column experiments were analyzed using the Thomas model (equation 2.7) and the results presented in Figure 4.18. The Thomas rate constant (K_{Th}), and adsorption capacity (q_{Th}), were then computed from the slope and intercept of linear plots of $\log \left[\frac{C_0}{C_v} - 1 \right]$ versus V . The Thomas model fitted the adsorption data with $R^2 = 0.9538$ a bed height (m) of 4.8 g and effluent flow rate θ of 9.9 mL/min.

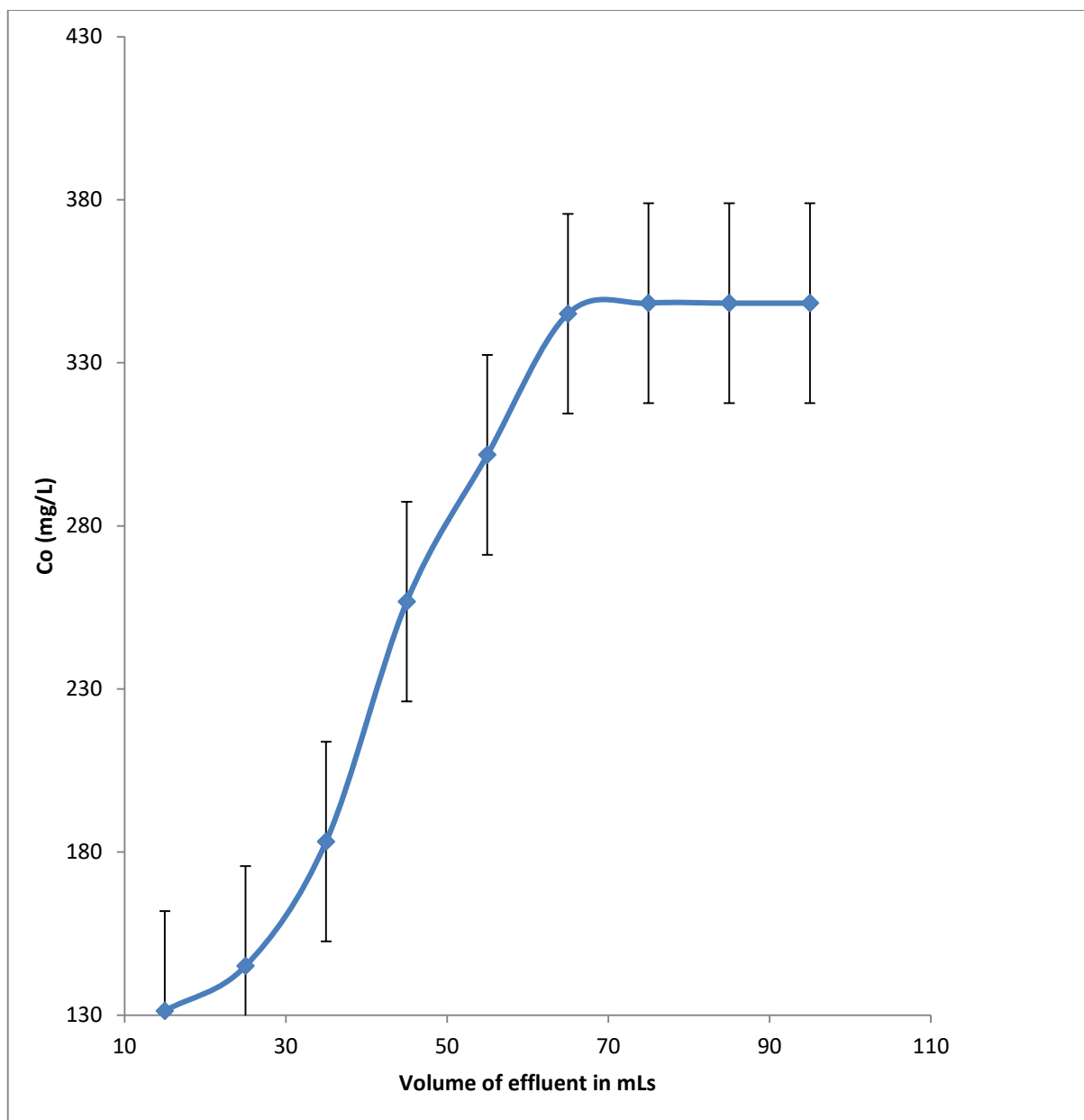


Figure 4.17: Breakthrough curves at a dose of 4.8 g of combined adsorbent and at 75 mg/L effluent fluoride concentrations at a flow rate of 9.9 mL/min.

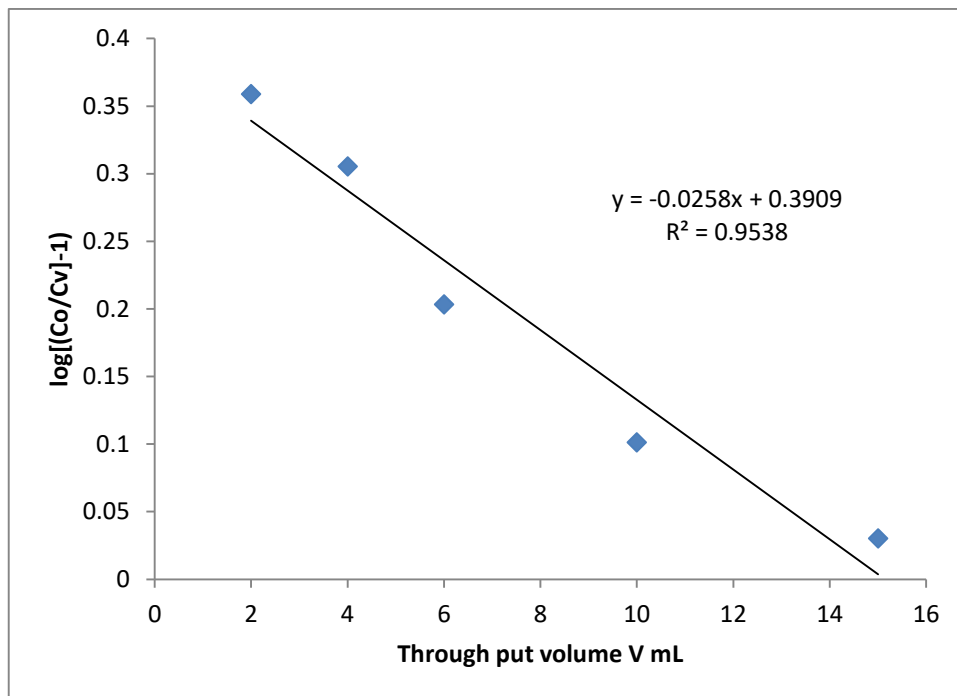


Figure 4.18: Thomas plots for fluoride removal from water using combined adsorbents [Experimental conditions: $C_o = 5$ mg/L, $T = 298$ K, $m = 4.8$ g, $Q = 9.9$ mL/min].

The Thomas rate constant, K_{Th} (0.07818 L/mg.min) and maximum adsorption capacity, q_{Th} (0.68064083), values showed efficient fluoride removal from water using these materials. The values of q_{Th} predicted by the Thomas model were consistent with the Langmuir adsorption capacity predicted in section 4.4.2. This showed that column fluoride sorption onto the combined adsorbents could be described by this model. Findings such as reported in the current work have also been reported in literature (Patel, 2019).

4.8 Regeneration tests

The regeneration of adsorbents is an important function for commercial application of their ability. The structures and surface properties of adsorbents depend largely on solution pH and can affect the system's absorption / desorption characteristics through changing electrostatic or ionic interactions (Ghosh & Collie, 2014). Regeneration experiments were performed using aqueous solution with different concentrations of sodium hydroxide of 0.0125 M, 0.5 M, 1 M, 1.5 M and 2 M. The exhausted combined adsorbent recovered at different concentrations for 12 h in NaOH solution was then washed with deionized distilled water followed by drying at 50°C in the oven. Figure 4.19 shows the adsorption results when the adsorbent was regenerated using different concentrations of NaOH.

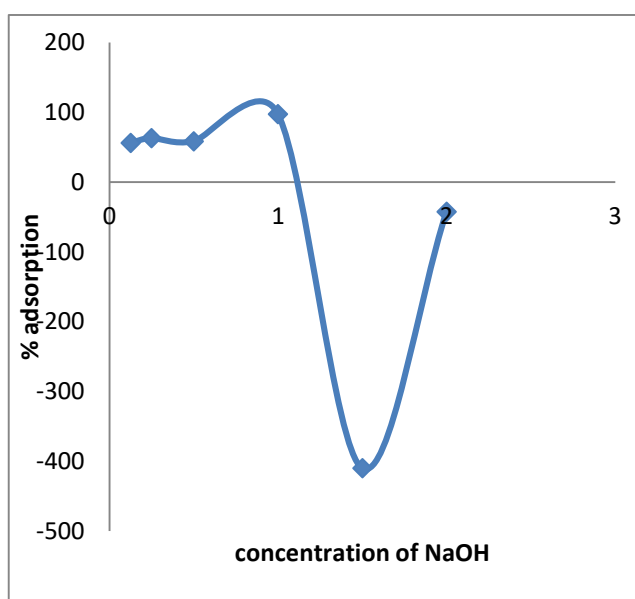


Figure 4.19 Regeneration tests for combined adsorbent with different concentrations of sodium hydroxide.

From Figure 4.19 adsorption percentages by the adsorbent regenerated using different concentrations of NaOH ranged between 42-56%. The adsorbent regenerated using 1

M NaOH gave an adsorption percentage of 97.50. Therefore from the results the combined adsorbent can be regenerated using 1 M NaOH. Other researchers have also done desorption experiments using NaOH and other desorption reagents. Activated alumina has been regenerated by flushing it with a solution containing 4% sodium hydroxide, which displaces fluoride from alumina surface (Waghmare & Arfin, 2015). Karthikeyan *et al.* (1997) studied the behaviour of activated alumina by batch calibration method in which regeneration studies were performed by 2% hydrochloric acid, 2% sodium hydroxide or 1% sulfuric acid. Ghorai & Pant (2004) investigated the removal of fluoride using activated alumina (Grade OA – 25) in batch and continuous operation and regeneration procedure resulted in 85% efficiency.

Kamble *et al.* (2010) examined adsorption of fluoride by alumina of alcoxide origin. The adsorbent solution was regenerated with sulphuric acid. Chitosan beads were used in experiments on fluoride removal using lanthanum. Studies of desorption have shown that 1 M ammonium chloride solution tends to be a successful regeneration medium showing regeneration of 81.22%. In addition to chitosan-based mesoporous Ti – Al binary metal oxide assisted beads for water defluoridation, alum appears to be a promising regeneration media with regeneration of 80%. In addition to adsorption of fluoride from aqueous solution using low cost bentonite / chitosan beads, sodium hydroxide could be used to recycle the fluoride filled adsorbent. Exhausted bentonite / chitosan beads were recovered at 0.5 M NaOH for 12 h and washed with deionized distilled water, then dried in the oven at 50 °C (Waghmare & Arfin 2015).

CHAPTER FIVE

CONCLUSIONS AND RECOMMENDATIONS

5.1 Conclusions

The various adsorbents were successfully synthesized and this was confirmed by FTIR analysis which indicated the presence of the anchored functional groups. From the SEM analysis the images showed morphological defects, irregular shape and coarse surfaces.

Chemical modification by Al^{3+} on the chicken feathers improved fluoride adsorption capacity up to 95 %. However the chemical modification on the fish scales and SPS did not improve their fluoride adsorption capacity which were quite high when compared to those of other low-cost adsorbents that have been reported in literature especially in the most recent past.

According to the batch simulation tests, AIF showed the highest maximum fluoride adsorption capacities of 285 mg/g, while fish scales had 133 mg/g, SPS 22 mg/g and combine adsorbent 34 mg/g.

The fluoride adsorption capacities of the adsorbents were, however, strongly controlled by solution parameters including the pH, temperature, adsorbent mass, contact time and

agitation time. Optimum fluoride adsorption by the adsorbents would best be conducted in low acidic pH of 1-6 at temperatures between 303 K -323 K.

The fluoride adsorption equilibrium data for the adsorbents were fitted by the Giles, the Langmuir and the Freundlich isotherms. The Al feathers, the SPS and fish scales showed a similarity with the C isotherm classification by Giles, on the other hand the combined adsorbents curve shows a resemblance with the S Giles classification of isotherms. Basing on the Langmuir and Freundlich isotherms, fluoride adsorption onto the adsorbents was therefore based on mixed reactions. However the SPS did not fit on both the Langmuir and Freundlich isotherms giving R^2 of 0.1965 and 0.0421 respectively.

The fluoride adsorption data for the adsorbents were correlated to pseudo-first order, pseudo second order and Weber-Moris intraparticle diffusion kinetic models. However, the correlation coefficient (R^2) values for pseudo second-order adsorption model had high values, that is, 0.999 for all adsorbents meaning the data was better described by this model. Surface reactions between the fluoride particles and reactive sites in the adsorbents were therefore chemical and rate controlling. The fluoride adsorption onto the adsorbents described by Weber-Moris intraparticle diffusion model, had all the R^2 values greater than 0.9 therefore intraparticle diffusion kinetics controlled fluoride adsorption onto the adsorbents and boundary layer control.

For column experiments, The Thomas model fitted the adsorption data with $R^2 = 0.9538$ a bed height (m) of 4.8 g and effluent flow rate θ of 9.9 mL/min.

5.2 Recommendations

Recommendations from this work

- 5.2.1 There is need for industrial scale-up using powdered fish scale, chicken feathers and sulphonated polystyrene for water defluoridation to harness this abundant and cheap resources for high-fluoride water treatment so as to reduce human exposure to excessive fluoride through water and lessen its concomitant toxic effects to the communities in the affected areas in the country.
- 5.2.2 Further studies on the chemical modification of the low cost adsorbents for use as efficient fluoride adsorbents should be carried out.
- 5.2.3 Studies on chemical modification of combined adsorbents to enhance fluoride adsorption capacity to be carried out.

REFERENCES

- Alex, W. and Helmut, G. (2002). *Handbook of analytical techniques*. Wiley-VCH, New York. pp 1061-1125. ISBN 3527301658.
- Alhussein, A.M., Ismail, Z., Che, N.A.J., Mustafa, M., Alsailawi, H.A., Abbas, A. and Fouad, W.M. (2019). Preparation of fish scales hydroxyapatite (FsHAp) for potential use as fillers in polymer. *J. Chem. Chem. Eng*, **13**:97-104
- Aluigi, A., Vineis, C., Varesano, A. and Mazzuchetti, G. (2008). Structure and properties of keratin/PEO blend nanofibres. *Eur. Polym. J*, **44**: 2465-2475.
- Aluigi, A., Vineis, C., Tonin, C., Tonetti, C., Varesano, A. and Mazzuchetti, G. (2009). Wool keratin-based nanofibres for active filtration of air and water. *J. Biobased Mat. Bioenergy*, **3**: 311-319.
- Aluigi, A., Tonetti, C., Vineis, C., Tonin, C. and Mazzuchetti, G. (2011). Adsorption of copper (II) ions by keratin/PA6 blend nanofibres. *Euro. Pol. J*, **47** :(9), 1756-1764.
- Aluigi, A., Tonetti, C., Vineis, C., Varesano, A., Tonin, C. and Casasola, R. (2012). Study on the adsorption of chromium (VI) by hydrolyzed keratin/polyamide 6 blend nanofibres. *J. Nanosci. Nanotechnol* **12**: 7250-7259.
- Adeogun, A.I., Kareem, S.O. Durosanya, J.B. and Balogun, E.S. (2012). Kinetics and Equilibrium Parameters of the Biosorption and Bioaccumulation of Lead ions from Aqueous Solutions by *Trichoderma Longibrachiatum*. *Journal of Microbiology, Biotechnonlogy and Food Science*, **1**(5):1221-1234.
- Andersson, L.I., Müller, R., Vlatakis, G., Mosbach, K. (1995). Mimics of the binding sites of opioid receptors obtained by molecular imprinting of enkephalin and morphine. *Proc. Natl. Acad. Sci. USA*, **92**: 4788–4792.
- Arai, K., Kameda, T. and Ichikawa, R. (1990). Mechanical properties of regenerated keratin fibres under processing conditions. *In the Proceedings of the 8th International Wool Textile Research Conference, Christchurch, New Zealand, 1990*; Crawshaw, G. H., Ed. Wool Research Organisation of New Zealand (Inc): Christchurch, New Zealand, pp. 449.
- Arun, G. and Stewart, R. C. (2014). Keratinous Materials as Novel Absorbent Systems for Toxic Pollutants. *Defence Science Journal* **64** (3): 209-221.
- Bansiwal, A., Pillewan, P., Biniwale, R.B. and Rayalu, S.S. (2010). Copper oxide incorporated mesoporous alumina for defluoridation of drinking water. *Microporous Mesoporous Mater*, **129**:54–61. <https://doi.org/10.1016/j.micro meso.2009.08.032>

- Badmus, M. Audu, T. and Anyata, B. (2007). Removal of Lead Ion from Industrial Wastewaters by Activated Carbon Prepared from Periwinkle Shells (*Typanotonus fuscatus*). *Turkish J. Eng. Env. Sci.*, **31**: 251-263.
- Bernini, M.C., Gandara, F., Iglesias, M., Snejko, N., Gutierrez-Puebla, E., Brusau, E.V., Narda, G.E. and Monge, M.A. (2009). Reversible breaking and forming of metal–ligand coordination bonds: Temperature-triggered singlecrystal to single-crystal transformation in a metal–organic framework. *Chemistry: A European Journal*, **15**: 4896–4905.
- Bhaumik, R., Mondal, N., Das, B., Roy, P., Pal, K., Das, C., Banerjee, A. and Datta, J. (2011). Eggshell powder as an adsorbent for removal of fluoride from aqueous solution: equilibrium, kinetic and thermodynamic studies. *E-Journal of Chemistry*, **9**: 1457-1480.
- Bi, C., Long, Y., Xia, L. and Jessica, L.W. (2016). Poultry keratin based decolorants for dyeing wastewater treatment. *Journal of Bioresource and Bioproducts* **1**: 30-35.
- Bledzki, A.K., Mamun, A.A., & Volk, J. (2010). Physical, chemical and surface properties of wheat husk, rye husk and soft wood and their polypropylene composites, Composites Part A: *Applied Science and Manufacturing*, **41**: 480–488.
- Bulgariu, L., Bulgariu, D, and Macoveanu, M. (2011). Adsorptive performances of alkaline treated peat for heavy metal removal. *Separation Science and Technology*, **46**: 1023–1033.
- Bunin, G., François, G. and Bonvin, D. (2013). A real-time optimization framework for the iterative controller tuning problem. *Processes*, **1**: 203–237.
- Cai, H., Chen, G., Peng, C., Zhang, Z., Dong, Y., Shang, G., Zhu, X., Gao, H. and Wan, X. (2015). Removal of fluoride from drinking water using tea waste loaded with Al/ Fe oxides: A novel, safe and efficient biosorbent, *Applied Surface Science*, **328**: 34–44.
- Caroline, H. C., Bruno, Z. S., Amanda, P.G. Y. and Mitiko Y. (2009). Adsorption isotherm of uranyl ions by fish scales of corvina. *International Nuclear Atlantic Conference - INACISBN: 978-85-99141-03-8*.
- Chen, G.X., Hao, G.J., Guo, T.Y., Song, M.D. and Zhang, B.H. (2002). Structure and mechanical properties of poly (3-hydroxybutyrate-co-3-hydroxyvalerate) (PHBV)/clay nanocomposites. *J. Mater. Sci. Letters*, **21**:1587-1589.
- Crittenden, J., Trussell, R.H., Howe, K. and Tchobanoglous, G. (2005). “*Water Treatment: Principles and De-sign*,” John Wiley and Sons, New York.
- Cunningham, R.E. and Williams, R.J.J., (1980). *Diffusion in Gases and Porous Media*. 1st ed. Boston: Springer.

- Dabhade, M.A., Saidutta, M.B. and Murthy, D.V.R. (2009). Adsorption of Phenol on Granular Activated Carbon from Nutrient Medium: Equilibrium and kinetic Study. *Int. J. Environ. Res.*, **3** (4): 557-568.
- Desai, N.P. and Hubbell, J. A. (1991). Solution technique to incorporate polyethylene oxide and other water-soluble polymers into surfaces of polymeric biomaterials. *Biomaterials*, **12**(2): 144-153.
- Donato, D., Napoli, I. and Catapano, G. (2014). Model-based optimization of scaffold geometry and operating conditions of radial flow packed-bed bioreactors for therapeutic applications. *Processes* **2**: 34–57.
- Donohue, M. D. and Aranovich, G. L., 1998. Classification of Gibbs Adsorption Isotherms. *Advances in Colloid and Interface Science*, pp. 137-152.
- Dyer, J.M. and Ghosh, A. (2014). Keratin nanomaterials: Development and applications. *In Handbook of functional nanomaterials, edited by Aliofkhazraei, Nova Publishers: New York, 4.*
- Doyle, W.M., McIntosh, B.C. and Clarke, W.L. (1980). Refractively scanned interferometers for Fourier transform infrared spectrophotometry, *Appl. Spectrosc.*, **34** :599.
- Edmunds, W.M. and Smedley, P.L. (1996). Groundwater geochemistry and health: an overview. In Appleton, Fuge and McCall [Eds] *Environmental Geochemistry and Health. Geological Society Special Publication*, **113**:91–105.
- Egwuatu, C. I., Umedum, N. I., Anarado, C.J.O. and Eboatu, A.N. (2014). Chicken feathers as a sequestrant for lead ions in aqueous solution, *International Journal of modern Analytical and Separation Science*, **3** (1): 51-66.
- Fairooz, N. E., Jwad, Z. A. and Zahra, Mohammed A.A. (2015). Adsorption Isotherms and Thermodynamic Data for Removal Pesticides from Aqueous Solution on Pomegranate Peel Surface. *American Journal of Applied Chemistry*, **3**(4):147-152.
- Francis, R. and Annick, R. (2007). *Chemical analysis: modern instrumentation methods and techniques*. Joney Wiley & sons limited, England, second edition. Pp 207-208.
- Frank, A.S. (1997). *Handbook of instrumental techniques for analytical chemistry*. A Simon and Schuster company, New Jersey. Pp 252-260.

- Gabriela, B., Arlete, Q., Ana, M., Paulo, F. and Jose, F. (2004). Enhancement of the thermooxidative degradability of polystyrene by chemical modification. *Polymer Degradation and Stability*, **86**: 493-497.
- Gaciri, S. J. and Davies, T. C. (1993). The occurrence and geochemistry of fluoride in some natural waters of Kenya. *Journal of Hydrology*, **143** (3-4): 395-412.
- George, Z., Kyzas, J.F., and Kostas, A.M. (2014). New Biosorbent Materials: Selectivity and Bioengineering Insights. *Processes*, **2**: 419-440.
- Ghorai, S., and Pant, K.K. (2004). Investigations on the column performance of fluoride adsorption by activated alumina in a fixed-bed. *Chemical Engineering Journal*, **98** (1-2): 165-173.<http://dx.doi.org/10.1016/j.cej.2003.07.003>.
- Ghosh, A., Clerens, S., Deb, C. S. and Dyer, J. (2013). Thermal effects of ionic liquid dissolution on the structures and properties of regenerated wool keratin. *Polym.Degrad*, **64** (3):209-221.
- Ghosh, A. and Collie, R.S. (2014). Keratinous Materials as Novel Absorbent Systems for Toxic Pollutants. *Defence Science Journal*, **64** (3): 209-221.
- Gikunju, J .K., Mbaria, J .M., Murcithi, W., Kyule, M. N., McDermott, J. J. and Maitho, T. E. (1995).Water fluoride in the Molo division of Nakuru district, Kenya. *Research Report 28* **1** (1): 17-20.
- Giles, C. H. and David S. (1974). A General Treatment and Classification of the Solute Adsorption Isotherm. Theoretical. Department of Mathematics, University of Strathdyde, Glasgow G1, Scotland, **47**:3.
- Gong, W.X., Qu, J.H., Liu, R.P. and Lan, H.C. (2012). Adsorption of fluoride onto different types of aluminas. *Chemical Engineering Journal*, **189-190**: 126-133.
- Goswami, A. and Purkait, M.K. (2012). The defluoridation of water by acidic alumina. *Chemical Engineering Research and Design*, **90** (12): 2316-2324.
- Griffiths, P.R. (1975). *Chemical Infrared Fourier Transform Spectroscopy*, Wiley, New York, NY, pp. 3.
- Günter, G. and Tuan, V. (2003). *Handbook of Spectroscopy*. WILEY-VCH Verlag GmbH & Co. KGaA, Weinheim ISBN 3-527-29782-0 pp 41.44.
- Guo, B., Hong, L. and Jiang, H.X. (2003). "Macroporouspoly(calciumacrylate-divinylbenzene) bead-selective orthophosphate sorbent," *Ind. Eng. Chem. Res* **42**: 5559-5565.

- Hanafiah, M., Zakaria, H. and Wan N.W.S. (2009). Preparation, characterization, and adsorption behavior of Cu (II) ions on to alkali-treated weed (*Imperata cylindrica*) leaf powder. *Water Air Soil Pollut*, **201**(1–4):43–53.
- Hayat, T. M., Hassan, A. K. and Zaki, A. (2016). Sulphonation of expanded polystyrene waste with commercial sulphuric acid for potential use in removal of heavy metals from contaminated waters. *Kategorizirani radovi Polimeri*, **36** (1-2):11-14.
- Hinz, C. (2001). Description of sorption data with isotherm equations. *Geoderma*, **99** (2001): 225–243.
- Hem, J.D. (1989). Study and Interpretation of the Chemical Characteristics of Natural Water. *Water Supply Paper 2254*, 3rd edition, US Geological Survey, Washington, D.C., pp 263.
- Ho, Y., Ng, J. and McKay, G. (2000). Kinetics of pollutant sorption by biosorbents: review. *Sep. Purif. Method*, **29**: 189-232.
- Hugo, A. S., Raúl, C. and Ruth, A. (2013). Fluoride Removal from Aqueous Solutions by Mechanically Modified Guava Seeds. *International Journal of Sciences: Basic and Applied Research (IJSBAR)* **11** (1):159-172.
- Ioannis, A, Amit, B., Dimitrios., N.B. and George Z. K. (2017). Chitin Adsorbents for Toxic Metals: A Review. *International Journal of Molecular Sciences*, **18**:114.
- Jamode, A.V., Sapkal, V.S., and Jamode, V.S. (2004). Defluoridation of water using inexpensive adsorbent, *Journal of Indian Institute of Science*, **84**: 163–171.
- Jayarathna, L., Bandara, A., Ng, W.J. and Weerasooriya, R. (2015). Fluoride adsorption on γ -Fe₂O₃ nanoparticles, *Journal of Environmental Health Science and Engineering*, **13**:54.
- Jin, Z., Jia, Y. and Luo, T. (2015). Efficient removal of fluoride by hierarchical MgO microspheres: Performance and mechanism study. *Applied Surface Science*, **357**: 1080–1088.
- Jin, Z., Jia, Y. and Zhang, K.S. (2016). Effective removal of fluoride by porous MgO nanoplates and its adsorption mechanism. *Journal of Alloys and Compounds*, vol. **675**: 292–300.
- Kahama, R.W., Kariuki, D.N., KNHN and LW. (1997). Fluorosis in children and sources of fluoride around Lake Elementaita Region of Kenya. *Fluoride*, **30** (1):19-25.
- Kahu, S., Shekhawat, A., Saravanan, D. and Jugade, R. (2017). Stannic chloride impregnated chitosan for defluoridation of water, *International Journal of Biological Macromolecules*, **104**: 1528–1538.

- Kamble, S.P., Jagtap, S., Labhsetwar, N.K., Thakare, D., Godfrey, S., Devotta, S., and Rayalu, S.S. (2007). Defluoridation of drinking water using chitin, chitosan and lanthanummodified chitosan. *Chemical Engineering Journal*, **129**: 173–180.
- Kamble, S.P., Deshpande, G. and Barve, P.P. (2010). Adsorption of fluoride from aqueous solution by alumina of alkoxide nature: Batch and continuous operation. *Desalination*, **264** (1-2): 15–23.
- Karnitz, O., Gurgel, L.V., de Melo, J.C., Botaro, V.R., Melo, T.M., de Freitas, Gil, R.P., and Gil, L.F. (2007). Adsorption of heavy metal ion from aqueous single metal solution by chemically modified sugarcane bagasse. *Bioresource Technology*, **98**: 1291–1297.
- Karthikeyan, G., Apparao, B. V., and Meenakshi, S (1997). Defluoridation property of activated alumina. 2nd International Workshop on Fluorosis Prevention and Defluoridation of Water, Nazreth, Ethiopia, pp. 78-82.
- Kavita, P., Sarita, S., Ashok, S. and Sanjay, V. (2016). Defluoridation of contaminated water by using low cost adsorbents: A review. *International Journal of Advanced Science and Research* **1** (6): 28-32.
- Keerthi, B. G. (2015). Adsorption on fluoride removal by using batch techniques. *Proceeding of NCRIET-2015 & Indian J.Sci.Res.* **12**(1): 209-213.
- Kefyalew, G., Feleke, Z., Bernd, H. and Negussie, M. (2012). Fluoride removal by adsorption on thermally treated lateritic soils. *Chemical Society of Ethiopia* **26**(3): 361-372.
- Khosa, A.M., Wu, J. and Ullah, A. (2013). Chemical modification, characterization, and application of chicken feathers as novel biosorbents. *Royal society of chemistry*, **3**: 20800-20810.
- Krishna, B., Sanat, K.M. and Uday, C.G. (2007). Adsorption of Fluoride from Aqueous Solution by a Synthetic Iron (III) –Aluminum (III) Mixed Oxide. *Ind. Eng. Chem. Res.*, **46**: 16, 5346–5356.
- Kumar, S. and Gopal, K. (2000). A Review on Fluorosis and its Preventive Strategies. *Indian J. Environmental Protection*, **20** (6):430-6.
- Kumar, S., Gupta, A., and Yadav, J.P. (2008). Removal fluoride by thermally activated carbon prepared from neem (*Azadirachta indica*) and (*Acacia Arabica*) leaves. *Journal of Environmental Biology*, **29**: 227–232.
- Kumar, P.S.K., Suganya, S., Srinivas, S., Priyadarshini, S., Karthika, M., Karshima, S.R., Swetha, V., Naushad, M. and Lichtfouse, E. (2019). Treatment of fluoride contaminated water. A review. *Environmental Chemistry Letters*, **17**:1707-1726.

- Lagergren, S. (1989). About the theory of so-called adsorption of soluble substances. *Kung Seventeen Hand*, **24**: 1-39.
- Larsen, M.J. and Pearce, E.I.F. (2002). Defluoridation of Drinking Water by Boiling with Brushite and Calcite. *Caries Research*, **36**:341-346.
- Loukidou, M.X., Karapantsios, T.D., Zouboulis, A.I. and Matis, K.A. (2004). Diffusion kinetic study of cadmium (II) biosorption by *Aeromonas caviae*. *J. Chem. Technol. Biotechnol.*, **79**: 711–719.
- Mahamadi, C. (2011). Water hyacinth as a biosorbent: A review. *African Journal of Environmental Science and Technology* **5**(13): 1137-1145.
- Malkoc, E. and Nuhoglu, Y. (2006). Removal of Ni (II) ions from aqueous solutions using waste of tea factory: adsorption on a fixed-bed column. *J. Hazard. Mater.*, **135**: 328-336.
- Manna, S. (2015). Fluoride and 2,4-dichlorophenoxyacetic acid removal from water using modified jute. PhD Dissertation, Indian Institute of Technology Kharagpur, WB, India.
- Manna, S., Saha, P., Roy, D., Sen, R., and Adhikari, B. (2015a). Defluoridation potential of jute fibers grafted with fatty acyl chain. *Applied Surface Science*, **356**: 30–38.
- Manji, F., Baelum, V., Fejerskov, O. and Gemert, W. (1986). Enamel changes in two low-fluoride areas in Kenya. *Clinical science*, **20**:371–380.
- Mariappan, P. and Vasudevan, T. (2011). Domestic defluoridation techniques and sector approach for fluorosis mitigation. Pages 1-11. Available from: URL: www.twadboard.gov.in.
- Maruthamuthu, M., and Venkatanarayana, R. (1987). Binding of fluoride with tamarind gel. *Fluoride*, **20**: 109–112.
- Mbugua, G., Mbuvi, H. and Muthengia, J. (2014). Rice husk ash derived zeolite blended with water hyacinth ash for enhanced adsorption of cadmium ions. *Current World Environment*, **9**: 280-286.
- McKittrick, J., Chen, P.Y., Bodde, S.G., Yang, W., Novitskaya, E.E. and Meyers, M.A. (2012). The structure, functions, and mechanical properties of keratin. *JOM* **64** (4): 449-468.
- McMillan, J.D., Himmel, M.E., Baker, J.O., & Overend, R.P. (1994). Enzymatic conversion of biomass for fuels production Washington, DC: American Chemical Society. pp. 292–324.

- Mendham, J.; Denny, R.C.; Barnes, J.D.; Thomas, M. and Sivasankar, B. (2009). Vogel's text book of quantitative chemical analysis. 6th edition, Prentice Hall India, India. Pg 465-470, 562-563, 675-679.
- Meyers, M.A.; Chen, P.Y.; Lin, A. Y.M. and Seki, Y. (2008). Biological materials: Structure and mechanical properties. *Progress Mat. Sci*, **53** (1): 1-206.
- Mohanty, K., Jha, M., Meikap, B.C., and Biswas, M.N. (2007). Removal of chromium (VI) from dilute aqueous solution by activated carbon developed from Terminalia asjuna nuts activated with zinc chloride. *Chemical Engineering Journal*, **60**: 3049–3059.
- Mondal, N.K., Bhaumik, R. and Datta, J.K. (2015). Removal of fluoride by aluminum impregnated coconut fiber from synthetic fluoride solution and natural water. *Alexandria Engineering Journal*, **54** (4): 1273–1284.
- Mohapatra, M., Rout, K. and Singh, P. (2011). Fluoride adsorption studies on mixed-phase nano iron oxides prepared by surfactant mediation-precipitation technique. *Journal of Hazardous Materials*, **186** (2-3): 1751–1757.
- Moturi, W. K., Mwakio, P. T. and Davies, T.C. (2002). The Contribution of Drinking Water towards Dental Fluorosis: A case study of Njoro Division, Nakuru District, Kenya. *Environmental Geochemistry and Health* **24** (2): 123–130.
- Mourabet, M., El Rhilassi, A., El Boujaady, H., Bennani-Ziatni, M. and Taitai, A. (2017). Use of response surface methodology for optimization of fluoride adsorption in an aqueous solution by Brushite. *Arabian Journal of Chemistry*, **10**: S3292–S3302.
- Mousavi, S.F., Rostamian, R. and Aghakhani, A. (2014). Potential of single and double-combined adsorbents in removing chromium from an industrial wastewater.
- Mwaniki, D.L., Courtney, J.M. and Gaylor, J.D. (1994). Endemic fluorosis: An analysis of needs and possibilities based on case studies in Kenya. *Social Science and Medicine*, **39** (6): 807-813.
- Murugan, M. and Subramanian, E. (2006). Studies on defluoridation of water by tamarind seed, an unconventional biosorbent. *J Water Health*, **4**:453-461.
- Nair, K.R., Manji, F. and Gitonga, J.N. (1984). The occurrence and distribution of fluoride in groundwaters of Kenya. In: *Challenges in African Hydrology and Water Resources*, Proceedings of the Harare Symposium, IAHS Publ. **144**: 75–86.

- Nath S.K., and Dutta, R.K. (2010). Fluoride Removal from Water Using Crushed Limestone. *Indian Journal of Chemical Technology* **17**:120-125.
- Nilanjan, D.; Vimala, R. and Karthika, P. (2007). Biosorption of Heavy metals-An overview. *Indian journal of biotechnology*, **7**:159-169.
- Ochieng, M. A. (2013). Determination of the extent to which the bucket flouride filters supplied by the catholic diocese of Nakuru are able to remove excessive flouride from drinking water in Nakuru town, Kenya. *International Journal of Advanced Research* **1** (10): 392-399.
- Ole, F., Jan, E.E. and Brian, A. B. (1996). *Fluoride in Dentistry*. 2nd ed; Munksgaard: John Wiley and Sons, Limited; pp.167.
- Opeolu, B.O., Bangbose, O., Arowolo, T.A., and Adetunji, M.T. (2010). Utilization of biomaterials as adsorbents for heavy metals' removal from aqueous metrics. *Scientific Research and Essays*, **5**(14): 1780-1787.
- Palanisamy, P., Agalya, A. and Sivakumar, P. (2012). Polymer composite—A potential biomaterial for removal of active dye. *E-Journal of Chemistry*, **9**: 1823-1834.
- Pandey, P.K., Pandey, M., & Sharma, R. (2012). Defluoridation of water by a biomass: *Tinospora cordifolia*. *Journal of Environmental Protection*, **3**: 610–616.
- Patel, H. (2019). Fixed-bed column adsorption study: a comprehensive review. *Applied Water Science*, **9**:45.
- Paudyal, H., Pangen, B., Inoue, K., Kawakita, H., Ohte, K., Ghimire, K.N., Harada, H., and Alam, S. (2013). Adsorptive removal of trace concentration of fluoride ion from water by using dried orange juice residue. *Chemical Engineering Journal*, **223**: 844–2853.
- Perry, R. H. and Green, D. W. (2008). *Perry's Chemical Engineers' Handbook*. 8th Edition. New York: McGraw-Hill.
- Piddennavar, R. and Krishnappa, P. (2013). Review on Defluoridation Techniques of Water. *The International Journal of Engineering and Science*, **2** (3):86-94.
- Piyush, K. P., Madhurima, P. and Rekha, S. (2012). Defluoridation of Water by a Biomass: *Tinosporacordifolia*. *Journal of Environmental Protection*, **3**: 610-616.
- Poole, A. J., Church, J.S. and Huson, M. G. (2009). Environmentally sustainable fibers from regenerated protein. *Biomacromolecules*, **10** (1): 1-8.
- Puthenveedu, S., Pillai, H., Chonattu, J. and Tharayil, M. (2012). Defluoridation of water using biosorbents. *Natural science*, **4** (4): 245-251.
- Quiñones, I.; Cavazzini, A.; Guiochon, G. (2000). Adsorption equilibria and overloaded band profiles of basic drugs in a reversed-phase system. *J. Chromatogr. A*, **877**: 1–11.

- Radke, C. J. & Prausnitz, J. M. (1972). Adsorption of Organic Solutes from Dilute Aqueous Solution on Activated Carbon. *Industrial Engineering Chemistry Fundamentals*, **11**(4): 445-451.
- Rampey, A.M., Umplebyli, R.J., Rushton, G.T., Iseman, J.C., Shah, R.N.; Shimizu, K.D. (2004). Characterization of the imprint effect and the influence of imprinting conditions on affinity, capacity, and heterogeneity in molecularly imprinted polymers using the freundlich isotherm-affinity distribution analysis. *Anal. Chem.*, **76**: 1123 1133.
- Romanos, J., Beckner, M., Rash, T., Firlej, L., Kuchta, B., Yu, P., Suppes, G., Wexler, C., and Pfeifer, P. (2012). Nanospace engineering of KOH activated carbon. *Nanotechnology*, **23**: 015401.
- Rosa, G., Reynel-Avila, H. E., Bonilla-Petriciolet, A., Cano-Rodríguez, I., Velasco-Santos, C. and Martínez-Hernández, A. L. (2008). Recycling Poultry Feathers for Pb Removal from Wastewater: Kinetic and Equilibrium Studies. *World Academy of Science, Engineering and Technology*, 47.
- Rouessac, F. and Rouessac, A. (2005). *Chemical Analysis. Modern Instrumentation Methods and Techniques*. Second Edition, University of Le Mans, France, John Wiley & Sons Ltd, pp 207-208.
- Roy, D., Manna, S., Sen, R., Adhikari, B., Saha, P. (2014). Methods for decreasing aqueous halide and organohalid levels using plant biomass, US patent 20140374357.
- Ruthven, D. M. (1984). *Principles of Adsorption and Adsorption Processes*. New York: John Wiley & Sons.
- Saha, P., Manna, S., Chowdhury, S.R., Sen, R., Roy, D., & Adhikari, B. (2010). Enhancement of tensile strength of lignocellulosic jute fibers by alkali-steam treatment. *Bioresource Technology*, **101**: 3182–3186.
- Sajonz, P., Kele, M., Zhong, G., Sellergren, B. and Guiochon, G. (1998). Study of the thermodynamics and mass transfer kinetics of two enantiomers on a polymeric imprinted stationary phase. *J. Chromatogr. A*, **810**: 1–17.
- Sanghratna, S. W. and Tanvir, A. (2015). Defluoridation by adsorption with chitin, chitosan alginate, polymers, cellulose, resins, algae and fungi - A Review. *International Research Journal of Engineering and Technology*, **2** (6): 1179.
- Salman, H. A., Ibrahim, M. I., Tarek, M. M. and Abbas, H. S. (2014). Biosorption of Heavy Metals: A Review. *Journal of Chemical Science and Technology*, **3** (4): 74-102.
- Scheibel, T. (2005). Protein fibers as performance proteins: new technologies and applications. *Current Opinion Biotech*, **16**(4): 427-433.

- Seyfried, M.S., Sparks, D.L., Bar-Tal, A. and Feigenbaum, S. (1989). Kinetics of calcium-magnesium exchange on soil using a stirred-flow reaction chamber. *Soil Sci. Soc. Am.*, **1** (53): 406.
- Shirke, P.A., and Chandra, P. (1991). Fluoride uptake by duckweed *Spirodela polyrrhiza*, *Fluoride*. **24**: 109–112.
- Sinha, S., Saxena, R., and Singh, S. (2000). Fluoride removal from water by *Hydrilla verticillata* (L.f.) royal and its toxic effects. *Applied Microbiology and Biotechnology*, **56**: 89–92.
- Skoog, A. and Leary, J.J. (1992). Principle of instrumental analysis. 4th edition, Harcourt college publishers. New York, pp 252- 253, 211, 494.
- Skoog, D.A., Holler, F.J. and Crouch, S.R. (2007) *Principles of instrumental analysis*. Sixth edition, pp 613-620.
- Sposito, G. (1998). On points of zero charge. *Environmental science and technology*, **32**(19): 2815-2820.
- Sun, Y., and Cheng, J. (2002). Hydrolysis of lignocellulosic materials for ethanol production: A review. *Bioresource Technology*, **83**: 1–11.
- Sujana, M.G., Pradhan, H.K. and Anand, S. (2009). Studies on sorption of some geomaterials for fluoride removal from aqueous solutions. *Hazard. Mater*, **161**: 120-5.
- Suneeta, K. and Pradip K. R. (2014). Extraction and Characterization of Chitin and Chitosan from (Labeo rohita) Fish Scales 3rd International Conference on Materials processing and Characterisation (ICMPC 2014). *Procedia Materials Science*, **6** (2014): 482 – 489.
- Sun, P., Liu, Z.T. and Liu, Z.W. (2009). Particles from bird feather: A novel application of an ionic liquid and waste resource. *J. Hazard. Mater*, **170**(2–3): 786-790.
- Suwendu, M., Debasis R., Basudam A., Sabu T. and Papita D. (2018). Biomass for Water Defluoridation and Current Understanding on Biosorption Mechanisms: A Review. *Wiley Online Library* (wileyonlinelibrary.com). DOI **10**:1002/ep.12855.
- Takacs, E., Wojnarovits, L., Fold-vary, C.S., Borsa, J., and Saja, I. (2000). Radiation activation of cotton cellulose prior to alkali treatment, *Research on Chemical Intermediates*, **27**: 1837–1840.
- Tang, Y., Guan, X. and Su, T. (2009). Fluoride adsorption onto activated alumina: modeling the effects of pH and some competing ions. *Colloids Surf A Physicochem Eng Asp*, **337**:33–38. <https://doi.org/10.1016/j.watres.2015.08.012>.

- Tej, P. S. and Majumder, C.B. (2016). Comparing fluoride removal kinetics of adsorption process from aqueous solution by biosorbents. Department of Chemical Engineering, IIT Roorkee, Roorkee **247**:667, Uttarakhand, India.
- Tesfaye, T., Sithole, B., Ramjugernath, D. and Chunilall, V. (2017). Valorisation of chicken feathers: Characterisation of physical properties and morphological structure. *Journal of Cleaner Production*, **149**:349-365.
- Topperwien, S., Behra, R., Xue, H. and Asigg, A. (2007). Cadmium accumulation in *scenedesmus vacuolatus* under freshwater conditions. *Journal of Environmental Science and Technology*, **41**: 5383–5388.
- Uddin, M. T., Islam, M. S. and Abedin, M. Z. (2007). Adsorption of phenol from aqueous solution by water hyacinth ash. *ARPN Journal of Engineering and Applied Sciences*, **2**:2.
- Umplebyli, R.J., Bode, M. and Shimizu, K.D. (2000). Measurement of the continuous distribution of binding sites in molecularly imprinted polymers. *Analyst*, **125**: 1261–1265.
- Umplebyli, R.J., Baxter, S.C., Bode, M., Berch, J.K., Shah, R.N. and Shimizu, K.D. (2001). Application of the Freundlich adsorption isotherm in the characterization of molecularly imprinted polymers. *Anal. Chim. Acta*, **435**: 35–42.
- Umplebyli, R.J., Baxter, S.C., Rampey, A.M.; Rushton, G.T., Chen, Y., Shimizu, K.D. (2004). Characterization of the heterogeneous binding site affinity distributions in molecularly imprinted polymers. *J. Chromatogr. B*, **804**: 141–149.
- United Nations (2008). The millennium development goals report. New York.
- Unuabonah, E.I. and Taubert, A. (2014). Clay–polymer nanocomposites (CPNs): Adsorbents of the future for water treatment, *Appl. Clay Sci*, **10**:1016.
- Vannela, R. and Verma, S.K. (2006). Cu²⁺ removal and recovery by Spi SORB: batch stirred and up-flow packed bed columnar reactor systems. *Bioprocess Biosyst. Eng.*, **29**: 7-17.
- Vijaya, Y. and Krishnaiah, A. (2009). Sorptive response profile of chitosan coated silica in the defluoridation of aqueous solution. *Journal of Chemistry*, **6**: 713–724.
- Vijaya, Y., Popuri, S.R., Reddy, A.S., and Krishnaiah, A. (2011). Synthesis and characterization of glutaraldehydecrosslinked calcium alginate for fluoride removal from aqueous solutions, *Journal of Applied Polymer Science*, **120**: 3443–3452.
- Viswanathan, N. and Meenakshi, S. (2008a). Enhanced fluoride sorption using La (III) incorporated carboxylated chitosan beads. *Journal of Colloid and Interface Science*, **322**: 375–383.

- Viswanathan, N. and Meenakshi, S. (2008b). Selective sorption of fluoride using Fe (III) loaded carboxylated chitosan beads. *Journal of Fluorine Chemistry*, **129**: 503–509.
- Viswanathan, N. and Meenakshi, S. (2010). Development of chitosan supported zirconium (IV) tungstophosphate composite for fluoride removal. *Journal of Hazardous Materials*, **176**: 459–465.
- Vlatakis, G., Andersson, L.I., Muller, R., and Mosbach, K. (1993). Drug assay using antibody mimics made by molecular imprinting. *Nature*, **361**: 645–647.
- Waghmare, S.S and Arfin,T. (2015). Fluoride Removal from Water by Aluminium Based Adsorption: A Review. *J. Biol. Chem. Chron*, **2**(1):01-11.
- Waheed, S., Attar, S. and Waghmare, M. (2009). Investigation on sorption of fluoride in water using rice husk as an adsorbent. *Nature Environment and Pollution technology*, **8**: 217-223.
- Wambu, E.W. and Muthakia, G.K. (2011). High fluoride water in the Gilgil area of Nakuru County, Kenya. *Research report*, **44** (1): 37–41.
- Wambu, E.W., Onindo, C.O., Willis J. A. and Muthakia, G.K. (2011). Fluoride Adsorption onto Acid-Treated Diatomaceous Mineral from Kenya. *Materials Sciences and Applications*, **2**: 1654-1660.
- Wambu, E.W. (2015). Fluoride levels in water sources of Gilgil area in Kenya. Defluoridation using locally available geomaterials, PHD. Thesis, Kenyatta University.
- Whitford, G.M. (1997). Determinants and mechanisms of enamel fluorosis. *Ciba Foundation Symposium*, **205**: 226–241.
- Williamson, M.M. (1953). Endemic dental fluorosis in Kenya. A preliminary report. *East African Medical Journal*, **30**: 217-233.
- Xu, X., Li, Q., Cui, R, Pang, J., An, H., Wang, W. and Zhai, J. (2012). Column-mode fluoride removal from aqueous solution by magnesia-loaded fly ash cenospheres. *Environ. Techno*, **33**:1409-1415.
- Xu, L., Chen, G. and Peng, C. (2017). Adsorptive removal of fluoride from drinking water using porous starch loaded with common metal ions. *Carbohydrate Polymers*, **160**: 82–89.
- Yakout, S. M. and Elsherif, E. (2010). Batch kinetics, isotherm and thermodynamic studies of adsorption of strontium from aqueous solutions onto low cost rice-straw based carbons. *Carbon Science and Technology*, **1** (2010): 144 – 153.
- Yamauchi, K., Yamauchi, A., Kusunoki, T., Kohda, A. and Konishi, Y. (1996). Preparation of stable aqueous solution of keratins, and physiochemical and biodegradational properties of films. *J. Biomed. Mater. Res. A*, **31**(4): 439-444.

- Yasinta, J., Victor, E. D. and Daniel, M. (2018). A Comparative Study on Removal of Hazardous Anions from Water by Adsorption: A Review. *International Journal of Chemical Engineering*, **10**:1155.
- Yinlin, L., Yunjie, L., Fei, C. and Lehe M. (2014). Sulfonation Process and Desalination Effect of Polystyrene/PVDF Semi-Interpenetrating Polymer Network Cation Exchange Membrane. *Polymers* **6**:1914-1928.
- Zazouli, M.Z, Mahvi, A.H., Dobaradaran, S., Barafrashtehpour, M., Mahdavi, Y., Davoud Balarake, D., Bushehr, S. T. and Iran, Z. (2014). Adsorption of fluoride from aqueous solution by modified azolla filiculoides. *Research report Fluoride*, **47**(4):349–358.
- Zhang, W.X., Yan, H., Li, H.J., Jiang, Z.W., Dong, L., Kan, X.W., Yang, H., Li, A.M. and Cheng, R.S. (2011). Removal of dyes from aqueous solutions by straw based adsorbents: Batch and column studies. *Chemical Engineering Journal*, **168**: 1120–21127.
- Zhang, W., Li, H., Kan, X., Dong, L., Yan, H., Jiang, Z., Yang, H., Li, A. and Cheng, R. (2012). Adsorption of anionic dyes from aqueous solutions using chemically modified straw. *Bioresource Technology*, **117**: 40–247.
- Zhang, J.; Chen, N.; Tang, Z.; Yu, Y.; Hu, Q. and Feng, C. (2015). A study of the mechanism of fluoride adsorption from aqueous solutions onto Fe-impregnated chitosan. *Physical Chemistry Chemical Physics*, **17**(18): 12041–12050.
- Zhao, J., Guo, H., Ma, J., and Shen, Z. (2015). Effect of fluoride on arsenic uptake from arsenic-contaminated groundwater using *Pteris vittata* L. *International Journal of Phytoremediation*, **17**:355–362.

APPENDICES

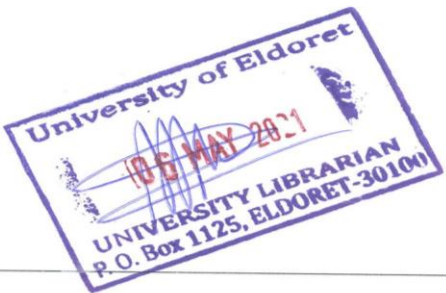
APPENDIX I: SIMILARITY REPORT

Document Viewer

Turnitin Originality Report

Processed on: 06-May-2021 12:49 EAT
 ID: 1579470119
 Word Count: 34052
 Submitted: 1

SC/PHD/003/15 By Roselyne Nasiebanda



Similarity Index	Similarity by Source
19%	Internet Sources: 12% Publications: 7% Student Papers: 7%

include quoted
 include bibliography
 excluding matches < 5 words
 mode:

<1% match () TABEKH, Hayat, Al KURDI, M. Hassan, AJJI, Zaki. "Sulphonation of expanded polystyrene waste with commercial sulphuric acid for potential use in removal of heavy metals from contaminated waters", Society of Plastics and Rubber Engineers, 2015	✕
<1% match () TABEKH, Hayat, Al KURDI, M. Hassan, AJJI, Zaki. "Sulphonation of expanded polystyrene waste with commercial sulphuric acid for potential use in removal of heavy metals from contaminated waters", Society of Plastics and Rubber Engineers	✕
<1% match (Internet from 27-Mar-2013) http://www.aelminingservices.com	✕
<1% match (Internet from 02-Sep-2012) http://water-observatory.net	✕
<1% match (Internet from 17-Feb-2021) https://profiles.uonbi.ac.ke/publications/ag/W?order=asc&page=6&sort=year	✕
<1% match (Internet from 16-Oct-2018) http://shodhganga.inflibnet.ac.in	✕
<1% match (student papers from 09-Jan-2019) Submitted to Pacific University on 2019-01-09	✕
<1% match (Internet from 31-Mar-2019) http://www.eresearchco.com	✕